Development of the Low Noise 500-GHz Heterodyne Receiver for Antarctic Telescopes

Development of the Low Noise 500-GHz Heterodyne Receiver for Antarctic Telescopes

Taketo Nagasaki

February 2014

Development of the Low Noise 500-GHz Heterodyne Receiver for Antarctic Telescopes

Taketo Nagasaki
Doctoral Program in Physics

Submitted to the Graduate School of
Pure and Applied Sciences
in Partial Fulfillment of the Requirements
for the Degree of Doctor of Philosophy in
Science

at the
University of Tsukuba

Abstract

This thesis presents development of a new 500 GHz heterodyne receiver for the transportable 30 cm submillimeter-wave telescope to operate at Dome Fuji station in Antarctica. The 30 cm telescope is designed to observe Milky Way in CO($J = 4 - 3$) at 461 GHz and [CI] ($^3P_1 - ^3P_0$) at 492 GHz. Dome Fuji is one of the most suitable site to observe submillimeter and terahertz-wave on the ground because of its high altitude of 3810-m and low average temperature of -55 degC. The new 500 GHz receiver covers the frequency range of 460-493 GHz in Single side band (SSB) mode with intermediate frequency (IF) of 4-8 GHz. The frequency resolution of the spectrometer is 61 kHz with 1 GHz bandwidth centered at 7.2 GHz of the IF. It is required to realize noise temperature less than 100 K in SSB using electric consumption less than 1.5 kW.

We adopted a sideband separating (2SB) mixer unit that has been developed for Atacama Large Millimeter/sub-millimeter Array (ALMA) band-8 receiver. The 2SB unit consists of a corrugated horn, a RF hybrid, two mixers and a IF hybrid. We place the 2SB mixer unit and two low noise amplifiers (LNAs) on the 3 K stage so as to minimize loss in the cables between the mixer and the LNAs. Local signal is injected at the input RF hybrid of the 2SB mixer unit though a waveguide that connects the RF hybrid and the local source placed outside of the cryo-receiver. The receiver is cooled to below 3.5 K with a two stage Gifford-Mcmahon cooled-cycle cooler. In design, total receiver noise temperature at 461 GHz is 70 K evaluated at input window of the cryo-receiver assuming loss in the windows of 0.63 dB, SIS mixer noise temperature of 30 K and HEMT noise of 7.4 K.

It is crucial to reduce physical temperature of the mixer unit for realizing this low receiver noise temperature of 70 K. We separated 3 K stage and the mixer unit as indepen-

dent components temperature points of the in thermal model. It is important to control the temperature of the mixer that is not always same as that of the 3 K stage. The most dominant heat load on the mixer is thermal condition through the waveguide. The heat load is reduced by controlling temperature gradient of the waveguide. We put thermal anchors on IF cables and waveguide from radiation shield stage. We selected the anchoring positions so that thermal load is minimum to the mixer by calculating thermal resistance of the anchor, waveguide and the IF cable. The multi layer insulator (MLI) is placed between the 60 K shielding and the inner surface of the cryostat that reduce the thermal load to the radiation shield stage. As the IR blocking filters, we selected Zitex G115 and inserted two IR filters between the windows and mixer horn. The thermal load was designed to be less than 54 mW and 1.3 W for 3 K stage and 60K radiation shield stage respectively. We demonstrated that the SIS mixer unit was cooled down to less than 3.5 K with electric power consumption of only 1.2 W.

The receiver noise could be further reduced by optimizing receiver parameters such as SIS voltage, intensity of magnetic field and local signal intensity. As a result of assessment in laboratory, receiver noise temperature in SSB at the front of RF window are less than 70 K and 90 K at 461 GHz and 492 GHz respectively. This result is most low receive noise temperature in the world for 500 GHz band receiver. Image Rejection Ratio is grater than 14 dB and allan variance τ is lager than 100 s.

New receiver was installed on the 30 cm telescope and operated at a site (4400 m altitude) in northern Chile from September 2012 to November 2012. After the first light toward Orion-KL in CO ($J = 4 - 3$) and CI ($^3P_1 -^3 P_0$) lines, we succeed in mapping Orion Molecular Cloud with CI ($^3P_1 -^3 P_0$) line.

Acknowledgement

I am most grateful to Naomasa Nakai, my superior. I have learned what is most important thing to study astronomy and also he taught the problem of this study. I am grateful to Masumichi Seta who has taught this study's problem to clear the challenging. And he had led me to achieve low noise receiver. I thank Makoto Nagai, Yusuke Miyamoto and Shun Ishii. They advised this thesis and had installed and operated 30-cm submillimeter-wave telescope at Chile with me. Shun Ishii has taught me about developing and measurement submillimeter-wave receiver.

I thank Hiroaki Imada, Kouta Saito and Kohichiro Doihata. They developed 30-cm telescope to operate in Antarctica, installed and demolish 30-cm telescope at Chile. Hiroki Imada developed alignment way between receiver and telescope optics. Kouta Saito refined telescope to operate at cold ambient like antarctica. Kohichiro Doihata simulated cooling action form cold wind in antarctica. I thank all the 30-cm telescope members. I thank Tom Nitta, he discussed about developing receiver and astronomy. He developed M-KID camera to install at large antarctic telescope and studied physics with me from under gradient student days.

I am grateful to Yutaro Sekimoto, who contributed ALMA band-8 mixer unit and discussed problem of this study. I thank engineers of ALMA in NAOJ. They researched state of the ALMA band-8 mixer unit and advised for measurement way in laboratory. I also thank to Yuichi Togashi of Oshima Prototype Engineering Co. for manufacturing of the receiver and 30-cm telescope. I appreciate Leonardo Bronfman, Mayir Leonel, people in Parinacota and CONAF in Lauca National Park are supported to operate 30-cm telescope in Parinacota, Chile. I am grateful to Mr. Kobayasi of the All Honda Sales for advice to operate the generator at high altitude.

I really appreciate the referees of this thesis, Masayuki Umemura and Hideo Ogawa for

discussions and suggestions.

Contents

List of Figures

List of Tables

1

Introduction

1.1 Interstellar Medium in the Milky Way

The galaxy is contained by large mass of interstellar medium and stars and these matters are continued generation and extinction. In a spiral galaxy, there are large fractions of the interstellar gas such as the giant molecular clouds (GMCs) like the Milky Way. This object size is 50-200pc and mass is $10^4-10^6 M_\odot$ and there are subsistent at spiral arms. These fundamental pictures of molecular gas are established by radio observation of the Milky Way in 1970s. In GMC, there are many dense cores and it is filed of stat formation. Main contents of molecular gas is H_2 and this molecular has not electric dipole moment. Physical temperature is about 10 K and density is n[H_2]¿10^2-10^3 in molecular gas, therefore these regions are not observed by optical-wave. Molecular cloud is observed by CO lines there are millimeter and submillimeter-wave generally.

The distribution and amount of molecular hydrogen was deduced from survey of galactic plan by CO ($J = 1 - 0$) observation(Burton. W. B. (1975), Scoville. N. Z (1975), Cohen. R. S (1977)), where J is the rotation quantum number. A large scale CO ($J = 0 - 1$) survey in the Milky Way is done by CfA 1.2-m telescope(T. M. DAME (2001)). This observation explained the distribution and movement of molecular clouds. In other frequency, the Portable 18 cm Submilimeter-wave Telescope (POST18) observed Galactic plane, the region is l = 300° - 345° and b = 0° in the 492 GHz fine-structure transition of neutral atomic carbon (C ^{0} $^3P_1$ -$^3P_0$; [C_I]) (Tomoharu Oka & Yamamoto (2005)). They calculated C^{circa}/CO abundance ratio in the galactic disk and dominated high ratio areas that are MGC and consisted in spiral arms.

1.2 Observation of Submillimeter-wave

In a general way, the wave that frequency is between 300 GHz and 3 THz is defined to submillimeter-wave. There are two components that are construct by radiation from thermal motion and emission line of especial molecule or atom for astronomy. In especial, emission line is the most important to identify physical condition in molecular gas. Table 1.1 is showed typical spectrums in submillimeter-wave range and explained condition that molecular is spawned.

However, it is very difficult to observe submillimeter-wave emission line on the ground.

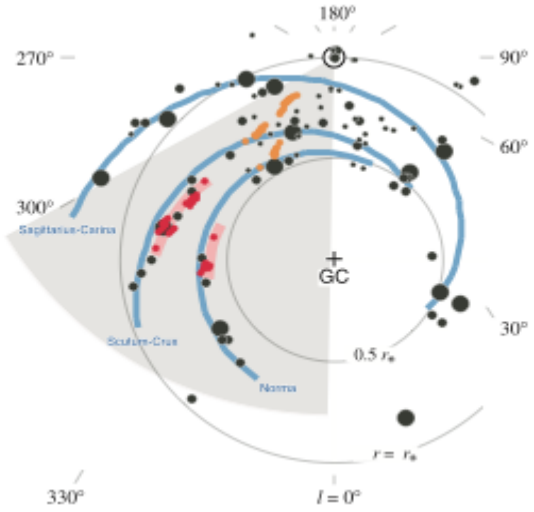

Figure 1.1: Three spiral arms of our Galaxy (blue solid lines) and high [CI]/CO ratio areas (red and orange filled circles).

Table 1.1: Major Lines in Submillimeter and Terahertz region

Frequency[GHz]	line	condition
461.0	CO($J = 4 - 3$)	warm and dense gas
492.2	[CI]($^3P_1 - ^3P_0$)	diffuse gas
806.7	CO($J = 7 - 6$)	hot and dense core
809.3	[CI]($^3P_2 - ^3P_1$)	diffuse gas
1463	[NII]($^3P_1 - ^3P_0$)	diffuse ionized gas

Be cause of submillimeter-wave is absorbed by oxygen molecular and water molecular in ambient. And there are no receivers to observe with low noise and high sensitivity, it is confined to develop the low noise receiver at this frequency. It is necessary to operate telescope in high altitude and low atmosphere pressure site like top of Mt. Mauna Kea in Hawaii (Pardo et al. (2001)) and Atacama desert in Chile (Tomoya et al. (1998)).

It could derive physical condition of molecular clouds such as density and temperature by direct comparison of the intensity of CO($J = 4 - 3$) with the that of CO($J = 1 - 0$) dataDAMA et al. (1987). The CO($J = 4 - 3$) line was first detected toward Orion BN-KL by Kuiper Airborne observatory (phillips et al. (1980)). Today, receiver noise temperature in 500 GHz is less than 200 K in SSB (SATOU et al. (2008)) and the system noise temperature of the submillimeter-wave telescope is limited by atmosphere.

1.3 Observation at the Antarctica

Because of submillimeter-wave absorption by atmosphere, we must to operate telescope at determinate area like high altitude place. The Antarctica is most good site to observe submillimeter-wave and Terahertz-wave at the ground. In the Antarctica, there are several telescopes like South Pole Telescope (SPT) and Antarctica Submillimeter telescope and Remote Observatory (AST/RO). SPT is installed in NSF South pole research station and the largest telescope in Antarctica, Main refractor's diameter is 10-m and Offset-Cassegrain telescope. This telescope was designed to observe high-z galaxy cluster using the Sunyaev-Zel'dovic Effect and Cosmic Microwave Background Radiation (CMB). The receiver is installed 960-element bolometer array of superconducting transition edge sensors of 95, 150 and 200 GHz. AST/RO telescope is 1.7-m diameter telescope that installed and operated at South Pole. The receiver was installed a 230 GHz SIS receiver, 450-495 GHz SIS receivers and 800-820 GHz SIS receiver that required about 20 liters of liquid helium per day. This telescope observed central reason of the Milky Way of CO($J = 1 - 0$), ^{13}CO($J = 1 - 0$), CS($J = 2 - 1$), CO($J = 4 - 3$), [CI] and CO($J = 7 - 6$). However this telescope operation was end and there is only SPT of sub millimeter-wave telescope in 2013.

1.3.1 Dome Fuji

Dome Fuji station is located center of the Antarctic Continent and stay aloof from seacoast. There is Japanese bace that we can stay all season and Altitude is 3800-m. Average temperature is about -55 degrees C and minimum temperature is -80 degree C. Therefore, contained amount of water vapor in atmosphere is very low and it is expected high transmission of submillimeter-wave and terahertz-wave. It is high advantage to observe large area.

We measured atmospheric-transparency of 220 GHz at the Dome Fuji station. This frequency's transparency has relations with sub millimeter-wave transparency and it is able to calculate 500-GHz atmospheric-transparency. The atmospheric-transparency at zenith was measured tipping radiometer with tipping way from 18 December 2006 to 14 January 2007. The mean optical depth was 0.045 ± 0.007 and optical depth is less than 0.06 during 98% of this period. Figure1.3 is showed result of 200 GHz optical depth in Dome

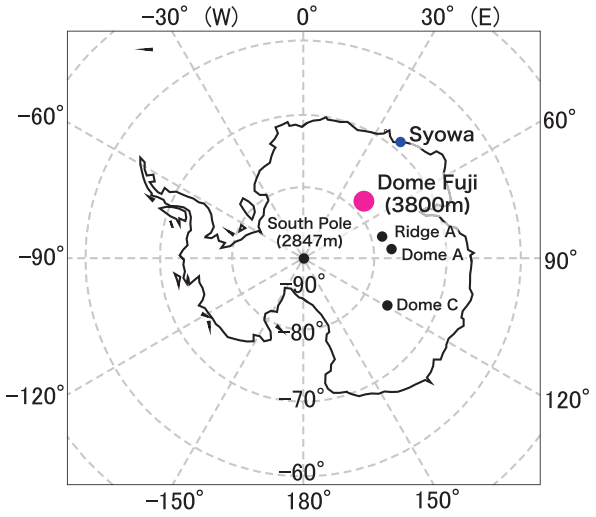

Figure 1.2: The antarctic map and Dome Fuji location

Fuji and Atacama desert. In this result, Optical depth in Dome Fuji in summer is lower than in Atacama in summer and is equal to Atacama in winter. In a general way, optical depth in winter is higher than in summer and it is counted that optical depth in Dome Fuji in winter is higher than Atacama winter. Figure1.4 is showed simulated spectrum of the atmospheric-transparency in Dome Fuji in best condition. The precipitable water vapor (PWV) is expected to 50-um, because such a loos PWV has been recorded hat the South Pole. This result is showed there is able to observe submillimeter-wave and terahertz-wave in Dome Fuji in winter.

1.4 The 30 cm submillimeter-wave telescope

Few years ago, we developed Tsukuba 30 cm submillimeter-wave telescope (Ishii et al. (2011)). This telescope is installed 500 GHz heterodyne receiver and main miller is 30 cm. This telescope is prototype of Antarctic telescope. To operate in Antarctica, there are especial provisions to absorb circumstances. This telescope is portable that all unit's weight are less than 60 kg and cubic volume is less than 1-m^3. Therefore, we are able to install telescope at Antarctica only few persons. Science target is Milky way survey of 500 GHz that emission of high excitation carbon monoxide (^{12}CO[$J = 4-3$]) and neutral

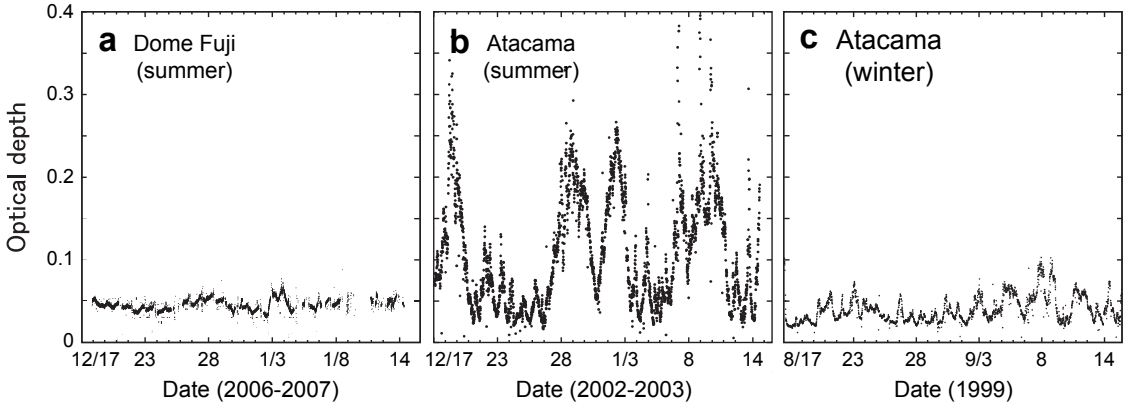

Figure 1.3: Optical depth of 200 GHz in Dome Fuji and Atacama desert

carbon (CI[$^3P_1 - ^3P_0$]) with 9 minutes spatial resolution. Old receiver is contained 1-pixel SIS heterodyne mixer at 4 K stage and one IF amplify is installed at 60 K stage. This receiver is able to observe in SSB signal that RF signal is separated to SSB by SSB filter at the front of receiver.

1.4.1 Debatable points at 30 cm telescope

We had operated 30 cm telescope with old receiver in 2009, 2010 and 2011. Therefore, there are several problems for this telescope to operate with high sensitivity observation at the Antarctica. At first, receiver noise temperature is high and it takes long time to observe large area like Milky Way. This telescope is prototype of antarctic telescope and it is necessary that receiver noise temperature is as low as possible. In especially, 30 cm telescope is designed to observe the Milky Way and high noise receiver takes long time to observe large area directory. Second, Alignment of receive is difficult and it takes long

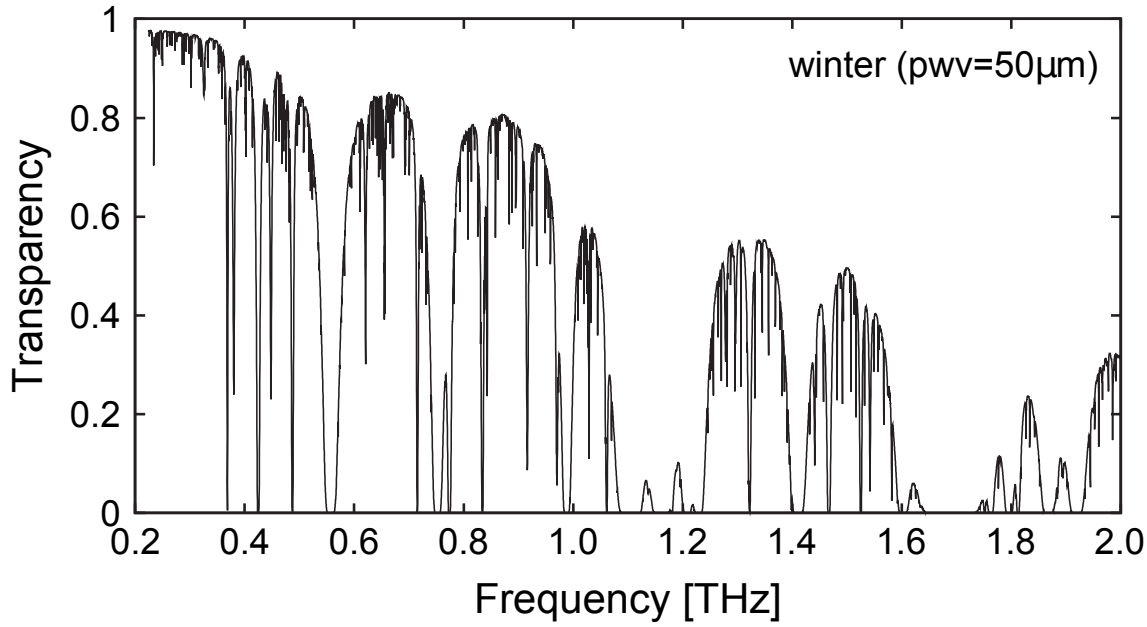

Figure 1.4: Simulated spectrum of the atmospheric-transparency in Dome Fuji with PWV is expected 50-um.

time to start observation. This receiver is installed FPS and we must make an adjustment of two hones that RF window and terminated signal of Local to decide the receiver position. To operate in Dome Fuji in summer, we must set up and operate telescope in only one month. Therefore, we set up telescope and receiver only few days to observe in Dome Fuji in summer.

Therefore, it is necessary to develop new 500 GHz receiver system.

1.4.2 Goals and Structure of this Thesis

In this thesis, the primary goal is developing low noise 500 GHz receiver and operating with 30 cm telescope. The list of several goals is following

- Design of 500 GHz low receiver noise temperature and low thermal load cryostat(Chapter3).

Figure 1.5: Tsukuba 30 cm submillimeter-wave telescope

- Determine receiver parameters and confirm receiver performance in laboratory(Chapter3)
- Confirm the performance of new 500 GHz receiver with operation of 30 cm sub millimeter-wave telescope (Chapter4).

In chapter 2, we report principle of heterodyne observation and sideband-separate(2SB). receiver. In chapter 3, we design new 500 GHz receiver. This receiver is operated with low cooling capacity at 3 K stage and it is necessary thermal load of 3 K stage is low. And receiver noise temperature is requested about 3 times of quantum noise. At new receiver, there are several parameters and we define them to operate low noise receiver. In chapter 4, we present result of new 500 GHz receiver experimental operation with 30 cm submillimeter-wave at Parinacota in northern Chile from September 2012 to October 2012. Finally, we summarize of the thesis in Chapter 5.

2

Receiver for submillimeter

2.1 Receiver

At radio telescope, there are two types receiver that one is coherent receiver like heterodyne and the other is incoherent receiver like bolometer. Heterodyne receiver is able to observe information of intensity and phase. At millimeter and submillimeter-wave range which are over 100 GHz, there is not low noise amplify and spectrometer. Therefore, RF signal is down-converted to 4-8 GHz or 1 GHz to observed by low noise receiver. RF signal is focused by main mirror and transported by optical system to receiver. In a receiver, feed horn changes RF signal to electric signal and mixer down-converts to few GHz. The mixer is contained by element of non-line shape attribute between current and voltage. It is applied semiconductor diode, Schottky diode or Superconductor/Insulator/Superconductor (SIS) for element. Principle of down-convert is written in Appendix 2.

2.2 SIS mixer

Superconductor/Insulator/Superconductor (SIS) is a mixer that operated by quasi-particle tunnel effect. SIS mixer is configured thin insulator (thickness is about 1-um) sandwiched by two superconductor plates. This principle is propounded by Tucker (Tucker (1985)) and it has high non-line shape attribute that is able to achieve low noise mixer.

2.3 Sideband Separate (2SB) Receiver

For 30 cm submillimeter-wave telescope, we selected mixer units of sideband separate (2SB) receiver for Atacama Large millimeter/submillimeter Array (ALMA) band-8 was developed by National Astronomy Observatory of Japan(NAOJ). ALMA band-8 receiver is configured two horns, two hybrid units, four mixers and four low noise amplifies. Receiver noise temperature at the front of cryostat window is less than 290 K between 385 GHz and 500 GHz. 2SB receiver is one of the coherent receiver that is able to observe with two SSB signal all together. This is high advantage that two signal are not different observation position. Two signal is occurred by phase control using path length and Hybrid.

At new 500 GHz receiver, we setup one 2SB units that is one horn, one RF hybrid, two

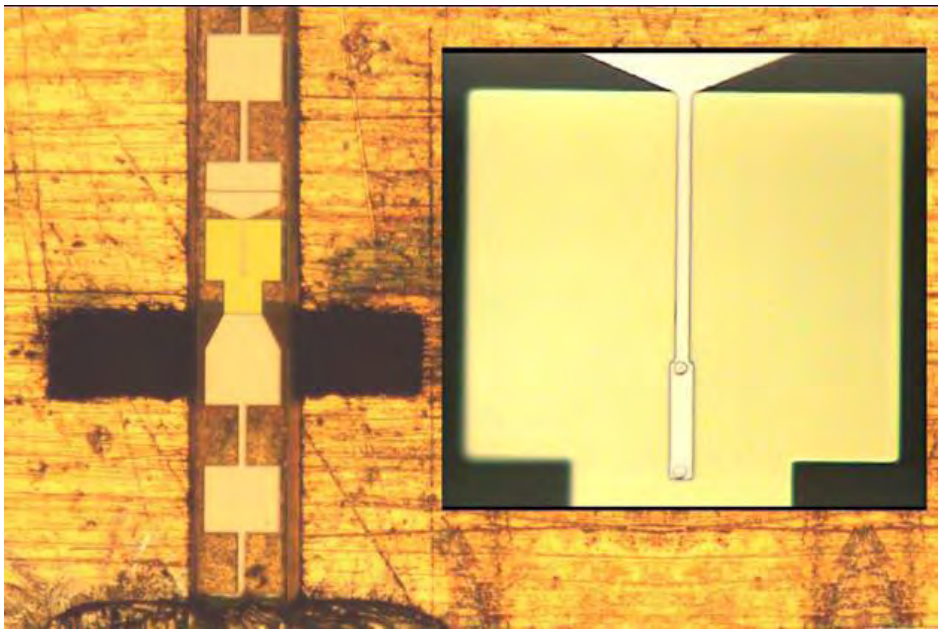

Figure 2.1: ALMA band-8 SIS mixer (Wenlei Shan & Sekimoto (2005)).

mixers, one IF Hybrid and two HEMTs. Therefore, output signals are LSB signal and USB signal. Feed horn is corrugate horn and chances radio signal to electric signal. RF signal is separated to two signals that one signal is added phase lag at RF hybrid and mixed local signal. Local signal's coupler is -20dB coupler and

2.3.1 Fundamental of 2SB receiver

At RF signal, there are two signal components that USB and LSB. Signal is showed by voltage, V_{int} is input signal, V_{upper} is USB component and V_{lower} is LSB component.

$$\begin{aligned} V_{int} &= V_{upper} + V_{lower} \\ &= V_{U0}\cos(2\pi\nu_U t) + V_{L0}\cos(2\pi\nu_L t) \end{aligned} \tag{2.1}$$

At RF Hybrid, V_{int} is separate two signals. And one side signal band is added phase

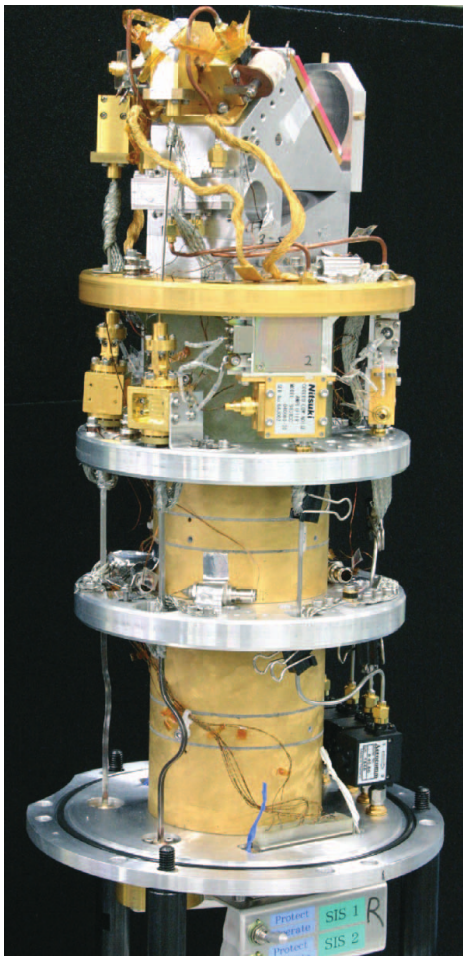

Figure 2.2: ALMA band-8 QM receiver

lag that $\pi/2$ compare with the other.

$$V_+ = \frac{1}{2}\left(V_{U0}\cos\left(2\pi\nu_U t\right) + V_{L0}\cos\left(2\pi\nu_L t\right)\right) \tag{2.2}$$

$$V_- = \frac{1}{2}\left(V_{U0}\cos\left(2\pi\nu_U t - \pi/2\right) + V_{L0}\cos\left(2\pi\nu_L t - \pi/2\right)\right) \tag{2.3}$$

V_+ is signal that non phase lag and V_- is phase lag signal. These signals are given fre-

quency conversion at each mixers.

$$V_{IF,+} = \frac{1}{2}\left(V_{U0}\cos\left(2\pi\nu_U t - 2\pi\nu_{Local}t\right) + V_{L0}\cos\left(2\pi\nu_L t - 2\pi\nu_{Local}t\right)\right) \tag{2.4}$$

$$\begin{aligned} V_{IF,-} &= \frac{1}{2}\left(V_{U0}\cos\left(2\pi\nu_U t - \pi/2 - 2\pi\nu_{Local}t\right) + V_{L0}\cos\left(2\pi\nu_L t - \pi/2 - 2\pi\nu_{Local}t\right)\right) \\ &= \frac{1}{2}\left(V_{U0}\sin\left(2\pi\nu_U t - 2\pi\nu_{Local}t\right) - V_{L0}\sin\left(2\pi\nu_{Local}t - 2\pi\nu_L t\right)\right) \end{aligned} \tag{2.5}$$

These signal are input IF Hybrid, V_+ is through and V_- is added phase lag at output port1.

$$\begin{aligned} V_{PORT-1} &= \frac{1}{2}\left(V_{U0}\cos\left(2\pi\nu_U t - 2\pi\nu_{Local}t - \pi/2\right) + V_{L0}\cos\left(2\pi\nu_L t - 2\pi\nu_{Local}t - \pi/2\right)\right) \\ &\quad + \frac{1}{2}\left(V_{U0}\sin\left(2\pi\nu_U t - 2\pi\nu_{Local}t\right) - V_{L0}\sin\left(2\pi\nu_{Local}t - 2\pi\nu_L t\right)\right) \\ &= \frac{1}{2}\left(V_{U0}\sin\left(2\pi\nu_U t - 2\pi\nu_{Local}t\right) + V_{L0}\sin\left(2\pi\nu_{Local}t - 2\pi\nu_L t\right)\right) \\ &\quad + \frac{1}{2}\left(V_{U0}\sin\left(2\pi\nu_U t - 2\pi\nu_{Local}t\right) - V_{L0}\sin\left(2\pi\nu_{Local}t - 2\pi\nu_L t\right)\right) \\ &= V_{U0}\sin\left(2\pi\nu_U t - 2\pi\nu_{Local}t\right) \end{aligned} \tag{2.6}$$

$$\tag{2.7}$$

Therefore, port1 is output only USB signal without the need to use SSB filters. And LSB signal is output at port2 that V_+ is added phase lag and V_- is through.

$$\begin{aligned} V_{PORT-2} &= \frac{1}{2}\left(V_{U0}\cos\left(2\pi\nu_U t - 2\pi\nu_{Local}t\right) + V_{L0}\cos\left(2\pi\nu_L t - 2\pi\nu_{Local}t\right)\right) \\ &\quad + \frac{1}{2}\left(V_{U0}\sin\left(2\pi\nu_U t - 2\pi\nu_{Local}t - \pi/2\right) - V_{L0}\sin\left(2\pi\nu_{Local}t - 2\pi\nu_L t - \pi/2\right)\right) \\ &= \frac{1}{2}\left(V_{U0}\cos\left(2\pi\nu_U t - 2\pi\nu_{Local}t\right) + V_{L0}\cos\left(2\pi\nu_L t - 2\pi\nu_{Local}t\right)\right) \\ &\quad + \frac{1}{2}\left(-V_{U0}\cos\left(2\pi\nu_U t - 2\pi\nu_{Local}t\right) + V_{L0}\cos\left(2\pi\nu_{Local}t - 2\pi\nu_L t\right)\right) \\ &= V_{L0}\cos\left(2\pi\nu_{Local}t - 2\pi\nu_L t\right) \end{aligned} \tag{2.8}$$

2.3.2 Phase lag

2SB receiver is output two SSB signals using phase control at waveguide. Therefore, it is very important to compose hybrid and IF cable with supposing phase. If there is phase accident error, receiver noise temperature is rising and LSB signal is outputted at USB port. We calculated effect of phase error at IF cable and hybrid that after down-

conversion. When phase error is declare by angular frequency ω, output signal at USB port is written as

$$\begin{aligned} V_{port-3} &= \frac{V_{U0}}{2}\sin 2\pi\left(\nu_U-\nu_{Local}\right)t \\ &+\frac{V_{U0}}{4}\{\sin 2\pi\left(\nu_U-\nu_{Local}\right)t+\sin\left(2\pi\nu_U t-2\pi\nu_{Local}t+2\omega\right)\}\frac{1}{\cos\left(-\omega\right)} \\ &+V_{L0}\sin\left(-\frac{\omega}{2}\right)\cos\left(2\pi\nu_{Local}t-2\pi\nu_L t+\frac{\omega}{2}\right) \end{aligned} \tag{2.9}$$

And output signal at LSB port is written as

$$\begin{aligned} V_{port-4} &= \frac{V_{L0}}{2}\cos 2\pi\left(\nu_{Local}-\nu_L\right)t \\ &+\frac{V_{L0}}{4}\{\cos 2\pi\left(\nu_{Local}-\nu_L\right)t+\cos\left(2\pi\nu_{Local}t-2\pi\nu_L t+2\omega\right)\}\frac{1}{\cos\left(-\omega\right)} \\ &-V_{U0}\sin\left(-\frac{\omega}{2}\right)\sin\left(2\pi\nu_U t-2\pi\nu_{Local}t+\frac{\omega}{2}\right) \end{aligned} \tag{2.10}$$

In law (2.9), first term is USB signal and second term is negative component for USB signal. 3-rd term is LSB signal component at USB port. When ω is zero, receiver is ideal and V_{port-3} is only V_{U0}. However ω is not zero, LSB signal is outputted at USB signal and USB signal is decayed.

We calculated signal loss of 461 GHz at several phase errors. To observe 461 GHz at USB port, local signal frequency is 455 GHz and LSB signal is 449 GHz. Table2.3.2 is showed loss of LSB signal and loss of output signal at phase error is 0, 5, 7, 10, 15, 20 and 45 degree. From this result, t is necessary phase error is less than few degree to develop low noise 2SB receiver.

2.3.3 Noise temperature

2SB receiver has two mixers and noise temperature is depended on deference of gain and conversion loss of mixers. Therefore, low of noise temperature is very complexity. Figure (2.3) is showed block diagram of new 500 GHz 2SB receiver. There are one horn, one RF hybrid, two mixers, two coordinate phase IF cables, one IF hybrid, two ISOs, two HEMTs and four IF cables. Signal from object is transmitted through horn, RF Hybrid, mixer,

Table 2.1: Relationship of phase error to signal loss

Phase error	G_{L0}	G_{output}	G_{output} [dB]
0 °	1	1	0
5 °	0.9945	0.9886	0.04969
7 °	0.9889	0.9778	0.09754
10 °	0.9773	0.9551	0.1997
15 °	0.9492	0.9009	0.4530
20 °	0.9105	0.8289	0.8148
45 °	0.5830	0.3398	4.687

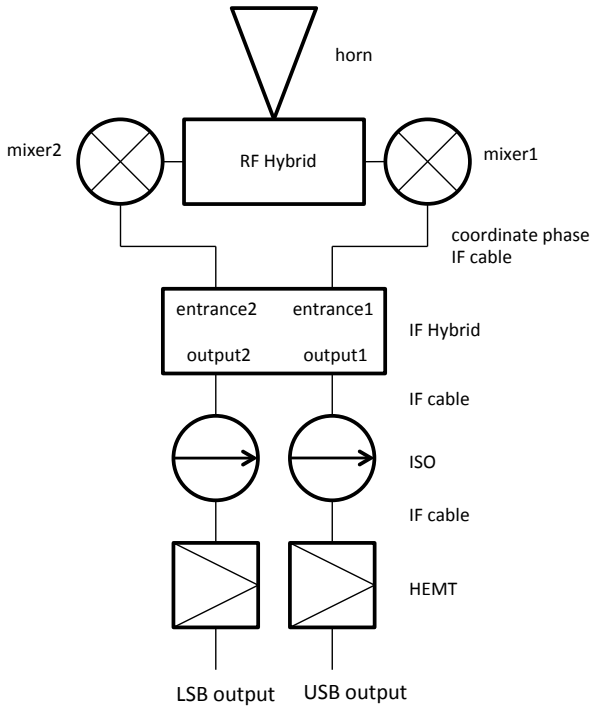

Figure 2.3: Block diagram of new 500 GHz 2SB receiver

coordinate phase IF cable, IF Hybrid, ISO and HEMT to outside. At this calculation, we decided 2SB unit from RF Hybrid to IF Hybrid to simplicity.

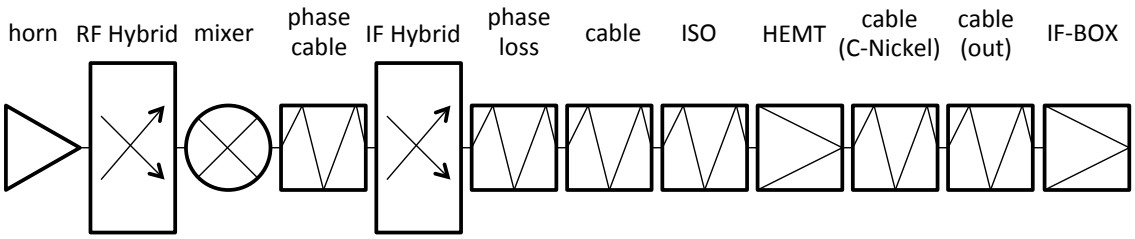

Figure 2.4: Block diagram for USB signal

Noise temperature at 2SB unit

In this section, we describe noise temperature at output of USB. At the mixer1, there is through USB signal and LSB signal. Figure (2.4) is showed block diagram for SSB signal.

Output signal is written

$$\begin{aligned}&\left[\{(T_{\mathrm{DSB}-1}+T_{3.5-\mathrm{K}}G_{\mathrm{RF}-\mathrm{hy}})G_{1\mathrm{u}}+T_{\mathrm{IF}-1}\}G_{\mathrm{IF}-1}+T_{\mathrm{IF}-\mathrm{hy}}\right]G_{11\mathrm{u}}\\&+\left[\{(T_{\mathrm{DSB}-1}+T_{3.5\mathrm{K}}G_{\mathrm{RF}-\mathrm{hy}}+T_{\mathrm{RF}-\mathrm{hy}})G_{1\mathrm{l}}+T_{\mathrm{IF}-1}\}G_{\mathrm{IF}-1}+T_{\mathrm{IF}-\mathrm{hy}}\right]G_{11\mathrm{l}}\\&=T_{1\mathrm{USB}}\end{aligned}\tag{2.11}$$

T_{DSB-1} is noise accrued at mixer1, $T_{3.5-K}$ is signal from RF Hybrid terminater, G_{RF-hy}

is gain at RF Hybrid, G_{1u} is gain at mixer1 at USB signal, T_{IF-1} is noise temperature at coordinate phase cable, T_{IF-hy} is noise temperature at IF Hybrid, G_{11u} is gain at USB signal through entrance1 and exit1. 2nd term is descried LSB noise. G_{1l} is gain at mixer1 for LSB signal and G_{11l} is gain at LSB signal through entrance1 and exit1

In a similar way, Output signal at LSB is written

$$\begin{aligned}
&\big[\{(T_{\mathrm{DSB-2}} + T_{3.5\mathrm{K}} G_{\mathrm{RF-hy}} + T_{\mathrm{RF-hy}}) G_{2\mathrm{u}} + T_{\mathrm{IF-2}}\} G_{\mathrm{IF-2}} + T_{\mathrm{IF-hy}}\big] G_{21\mathrm{u}} \\
&+\big[\{(T_{\mathrm{DSB-2}} + T_{3.5\mathrm{K}} G_{\mathrm{RF-hy}} + T_{\mathrm{RF-hy}}) G_{2\mathrm{l}} + T_{\mathrm{IF-2}}\} G_{\mathrm{IF-2}} + T_{\mathrm{IF-hy}}\big] G_{21\mathrm{l}} \\
&= T_{2\mathrm{USB}}
\end{aligned} \tag{2.12}$$

G_{21u} is gain at USB signal through entrance2 and exit2 and G_{21l} is gain at LSB signal through entrance2 and exit2.

Therefore, signal at USB output is written with (2.11) and (2.12)

$$\begin{aligned}
T_{\mathrm{USB-2SB}} &= T_{1\mathrm{USB}} + T_{2\mathrm{USB}} \\
&= \big[\{(T_{\mathrm{DSB-1}} + T_{3.5\mathrm{K}} G_{\mathrm{RF-hy}} + T_{\mathrm{RF-hy}}) G_{1\mathrm{u}} + T_{\mathrm{IF-1}}\} G_{\mathrm{IF-1}} + T_{\mathrm{IF-hy}}\big] G_{11\mathrm{u}} \\
&\quad +\big[\{(T_{\mathrm{DSB-1}} + T_{3.5\mathrm{K}} G_{\mathrm{RF-hy}} + T_{\mathrm{RF-hy}}) G_{1\mathrm{l}} + T_{\mathrm{IF-2}}\} G_{\mathrm{IF-1}} + T_{\mathrm{IF-hy}}\big] G_{11\mathrm{l}} \\
&\quad +\big[\{(T_{\mathrm{DSB-2}} + T_{3.5\mathrm{K}} G_{\mathrm{RF-hy}} + T_{\mathrm{RF-hy}}) G_{2\mathrm{u}} + T_{\mathrm{IF-2}}\} G_{\mathrm{IF-2}} + T_{\mathrm{IF-hy}}\big] G_{21\mathrm{u}} \\
&\quad +\big[\{(T_{\mathrm{DSB-2}} + T_{3.5\mathrm{K}} G_{\mathrm{RF-hy}} + T_{\mathrm{RF-hy}}) G_{2\mathrm{l}} + T_{\mathrm{IF-2}}\} G_{\mathrm{IF-2}} + T_{\mathrm{IF-hy}}\big] G_{21l}
\end{aligned} \tag{2.13}$$

Next, we descried noise temperature at input conversion. We decide total input conversion noise and gain

$$\{T_{2\mathrm{SB-USB}} G_{2\mathrm{SB-u}} + T_{2\mathrm{SB-LSB}} G_{2\mathrm{SB-l}}\} \quad = \quad (2.13) \tag{2.14}$$

When $G_{2\mathrm{SB-u}} = G_{1\mathrm{u}} G_{\mathrm{IF-1}} G_{11\mathrm{u}}$, $G_{2\mathrm{SB-l}} = G_{1\mathrm{l}} G_{\mathrm{IF-1}} G_{11\mathrm{l}}$, $G_{2\mathrm{SB-l}} = G_{2\mathrm{SB-u}}$ and $T_{2\mathrm{SB-LSB}} = T_{2\mathrm{SB-USB}}$, (2.14) is written

$$2 \times T_{2\mathrm{SB-USB}} G_{2\mathrm{SB-u}} \quad = \quad (2.13) \tag{2.15}$$

From (2.15), noise temperature at USB output is written

$$\begin{aligned} T_{\mathrm{2SB-USB}} &= \frac{1}{2G_{\mathrm{1u}}G_{\mathrm{IF-1}}G_{\mathrm{11u}}}\Big(\big[\{(T_{\mathrm{DSB-1}}+T_{\mathrm{3.5K}}G_{\mathrm{RF-hy}}+T_{\mathrm{RF-hy}})G_{\mathrm{1u}}+T_{\mathrm{IF-1}}\}G_{\mathrm{IF-1}}+T_{\mathrm{IF-hy}}\big]G_{\mathrm{11u}} \\ &\quad +\big[\{(T_{\mathrm{DSB-2}}+T_{\mathrm{3.5K}}G_{\mathrm{RF-hy}}+T_{\mathrm{RF-hy}})G_{\mathrm{2u}}+T_{\mathrm{IF-2}}\}G_{\mathrm{IF-2}}+T_{\mathrm{IF-hy}}\big]G_{\mathrm{21u}}\Big) \end{aligned} \tag{2.16}$$

And noise temperature of LSB signal at USB output is written

$$\begin{aligned} T_{\mathrm{2SB-LSB}} &= \frac{1}{2G_{\mathrm{1u}}G_{\mathrm{IF-1}}G_{\mathrm{11u}}}\Big(\{(T_{\mathrm{DSB-1}}+T_{\mathrm{3.5K}}G_{\mathrm{RF-hy}}+T_{\mathrm{RF-hy}})G_{\mathrm{1l}}+T_{\mathrm{IF-2}}\}G_{\mathrm{IF-1}}+T_{\mathrm{IF-hy}}\big]G_{\mathrm{11}l} \\ &\quad +\big[\{(T_{\mathrm{DSB-2}}+T_{\mathrm{3.5K}}G_{\mathrm{RF-hy}}+T_{\mathrm{RF-hy}})G_{\mathrm{2l}}+T_{\mathrm{IF-2}}\}G_{\mathrm{IF-2}}+T_{\mathrm{IF-hy}}\Big)G_{\mathrm{21}l} \end{aligned} \tag{2.17}$$

Therefore, total noise temperature at USB output is written with $T_{\mathrm{2SB}}(\mathrm{USB}) = T_{\mathrm{2SB-USB}} + T_{\mathrm{2SB-LSB}}$

$$\begin{aligned} T_{2SB}(\mathrm{USB}) &= \frac{1}{2G_{\mathrm{1u}}G_{\mathrm{IF-1}}G_{\mathrm{11u}}}\Big(\big[\{(T_{\mathrm{DSB-1}}+T_{\mathrm{3.5K}}G_{\mathrm{RF-hy}}+T_{\mathrm{RF-hy}})G_{\mathrm{1u}}+T_{\mathrm{IF-1}}\}G_{\mathrm{IF-1}}+T_{\mathrm{IF-hy}}\big]G_{\mathrm{11u}} \\ &\quad +\big[\{(T_{\mathrm{DSB-2}}+T_{\mathrm{3.5K}}G_{\mathrm{RF-hy}}+T_{\mathrm{RF-hy}})G_{\mathrm{2u}}+T_{\mathrm{IF-2}}\}G_{\mathrm{IF-2}}+T_{\mathrm{IF-hy}}\big]G_{\mathrm{21u}}\Big) \\ &\quad +\frac{1}{2G_{1u}G_{IF-1}G_{11u}}\Big(\{(T_{\mathrm{DSB-1}}+T_{\mathrm{3.5K}}G_{\mathrm{RF-hy}}+T_{\mathrm{RF-hy}})G_{\mathrm{1l}}+T_{\mathrm{IF-1}}\}G_{\mathrm{IF-1}}+T_{\mathrm{IF-hy}}\big]G_{\mathrm{11l}} \\ &\quad +\big[\{(T_{\mathrm{DSB-2}}+T_{\mathrm{3.5K}}G_{\mathrm{RF-hy}}+T_{\mathrm{RF-hy}})G_{\mathrm{2l}}+T_{\mathrm{IF-2}}\}G_{\mathrm{IF-2}}+T_{\mathrm{IF-hy}}\Big)G_{\mathrm{21}l} \end{aligned} \tag{2.18}$$

In a similar way, noise temperature at LSB output is

$$\begin{aligned} T_{2SB}(\mathrm{LSB}) &= \frac{1}{2G_{\mathrm{2l}}G_{\mathrm{IF-2}}G_{\mathrm{22l}}}\Big(\big[\{(T_{\mathrm{DSB-1}}+T_{\mathrm{3.5K}}G_{\mathrm{RF-hy}}+T_{\mathrm{RF-hy}})G_{\mathrm{1l}}+T_{\mathrm{IF-1}}\}G_{\mathrm{IF-1}}+T_{\mathrm{IF-hy}}\big]G_{\mathrm{12l}} \\ &\quad +\big[\{(T_{\mathrm{DSB-2}}+T_{\mathrm{3.5K}}G_{\mathrm{RF-hy}}+T_{\mathrm{RF-hy}})G_{\mathrm{2l}}+T_{\mathrm{IF-2}}\}G_{\mathrm{IF-2}}+T_{\mathrm{IF-hy}}\big]G_{\mathrm{22l}}\Big) \\ &\quad +\frac{1}{G_{2l}G_{IF-2}G_{22l}}\Big(\{(T_{\mathrm{DSB-1}}+T_{\mathrm{3.5K}}G_{\mathrm{RF-hy}}+T_{\mathrm{RF-hy}})G_{\mathrm{1u}}+T_{\mathrm{IF-1}}\}G_{\mathrm{IF-1}}+T_{\mathrm{IF-hy}}\big]G_{\mathrm{12u}} \\ &\quad +\big[\{(T_{\mathrm{DSB-2}}+T_{\mathrm{3.5K}}G_{\mathrm{RF-hy}}+T_{\mathrm{RF-hy}})G_{\mathrm{2u}}+T_{\mathrm{IF-2}}\}G_{\mathrm{IF-2}}+T_{\mathrm{IF-hy}}\Big)G_{22u} \end{aligned} \tag{2.19}$$

In these laws, T_{DSB} is DSB mixer noise at the front of mixer. Relationship between T_{DSB} and T_{SSB} is writhed in

$$T_{DSB} \times (G_s + Gi) = T_{SSB} \times G_s \tag{2.20}$$

Where G_s is conversion factor of main signal and G_i is conversion factor of image signal. At the calculation, we insert quantum noise at T_{SSB} as 23-K at 461GHz and 26-K at 492GHz.

Therefore, noise temperature referred at mixer input is written as

$$\begin{aligned} T_{2SB}(\mathrm{USB}) &= \frac{1}{2G_{1\mathrm{u}}G_{\mathrm{IF}-1}G_{11\mathrm{u}}} \\ &\Big[\Big(\big[\{(T_{\mathrm{SSB}-1}\frac{G_s}{(G_s+G_i)}+T_{3.5\mathrm{K}}G_{\mathrm{RF}-\mathrm{hy}}+T_{\mathrm{RF}-\mathrm{hy}})G_{1\mathrm{u}} \\ &+T_{\mathrm{IF}-1}\}G_{\mathrm{IF}-1}+T_{\mathrm{IF}-\mathrm{hy}}\big]G_{11\mathrm{u}} \\ &+\big[\{(T_{\mathrm{SSB}-2}\frac{G_s}{(G_s+G_i)}+T_{3.5\mathrm{K}}G_{\mathrm{RF}-\mathrm{hy}}+T_{\mathrm{RF}-\mathrm{hy}})G_{2\mathrm{u}} \\ &+T_{\mathrm{IF}-2}\}G_{\mathrm{IF}-2}+T_{\mathrm{IF}-\mathrm{hy}}\big]G_{21\mathrm{u}}\Big) \\ &+\Big(\{(T_{\mathrm{SSB}-1}\frac{G_s}{(G_s+G_i)}+T_{3.5\mathrm{K}}G_{\mathrm{RF}-\mathrm{hy}}+T_{\mathrm{RF}-\mathrm{hy}})G_{1\mathrm{l}} \\ &+T_{\mathrm{IF}-1}\}G_{\mathrm{IF}-1}+T_{\mathrm{IF}-\mathrm{hy}}\big]G_{11\mathrm{l}} \\ &+\big[\{(T_{\mathrm{SSB}-2}\frac{G_s}{(G_s+G_i)}+T_{3.5\mathrm{K}}G_{\mathrm{RF}-\mathrm{hy}}+T_{\mathrm{RF}-\mathrm{hy}})G_{2\mathrm{l}} \\ &+T_{\mathrm{IF}-2}\}G_{\mathrm{IF}-2}+T_{\mathrm{IF}-\mathrm{hy}}\Big)G_{21l}\Big] \end{aligned} \tag{2.21}$$

Noise temperature referred at the front of window input conversion

Receiver noise temperature T_{RX} referred at the front of cryostat window is written as follow.

$$\begin{aligned} T_{\mathrm{RX}} &= T_{\mathrm{window}}+\frac{T_{\mathrm{horn}}}{G_{\mathrm{window}}}+\frac{T_{\mathrm{RF}-\mathrm{hy}}}{G_{\mathrm{window}}G_{\mathrm{horn}}}+\frac{T_{2\mathrm{SB}}}{G_{\mathrm{window}}G_{\mathrm{horn}}G_{\mathrm{RF}-\mathrm{hy}}} \\ &+\frac{T_{\mathrm{IF}-2}}{G_{\mathrm{window}}G_{\mathrm{horn}}G_{\mathrm{RF}-\mathrm{hy}}G_{2\mathrm{SB}}}+\frac{T_{\mathrm{ISO}}}{G_{\mathrm{window}}G_{\mathrm{horn}}G_{\mathrm{RF}-\mathrm{hy}}G_{2\mathrm{SB}}G_{\mathrm{IF}-2}} \\ &+\frac{T_{\mathrm{HEMTfollow}}}{G_{\mathrm{window}}G_{\mathrm{horn}}G_{\mathrm{RF}-\mathrm{hy}}G_{2\mathrm{SB}}G_{\mathrm{IF}-2}G_{\mathrm{ISO}}} \end{aligned} \tag{2.22}$$

2.4 2SB Receiver of Millimeter/Submillimeter-wave

In millimeter-wave and sub millimeter-wave range, Several 2SB receivers were developed and using to observation at the world. There are famous 2SB receiver written as follow

- 60-cm Radio Survey Telescope

  There is 200 GHz band 2SB receiver to observe CO (J=2-1: 230.538 GHz) at USB and ^{13P}CO(J=2-1: 220.398 GHz) at LSB (Taku. NAKAJIMA & NOGUCHI (2007)) at Nobeyama, Japan. Over the RF frequency range is 205-240 GHz and singe-sideband receiver noise temperature is 40-100 K at the 4.0-8.0 GHz IF frequency band. The image rejection ratio is greater than 10 dB. Spectrometer is AOS that bandwidth is 250 MHz$\times$ 2 and resolution is 230 kHz.

- 45-m radio telescope

  The waveguide-type dual-porlarizatio sideband-separating SIS receiver system of 100-GHz band receiver is installed in this telescope at the Nobeyama Radio Observatory, Japan (Taku. NAKAJIMA & KAWABE (2008)). This receive observes over the range of 80-120 GHz, single-sideband receiver noise temperature is 50-100 K and image rejection ratio is greater than 10 dB.

- 1.85-m mm-submm Telescope

  The 230-GHz band 2SB receiver is installed in this telescope to observe ^{12}CO, ^{13}CO and C^{18}O ($J = 2 - 1$) lines at once in Nobeyama (Toshikazu ONISHI & KUNO (2013)). Receiver noise temperature is 75-100 K and image rejection ratio is about 15 dB.

- The Atacama Pathfinder Experiment (APEX)

  This is a radio telescope using a12-m ALMA prototype antenna operating at the Atacama Desert on the Chilean Andes at about 5100-m altitude. In this telescope, there are three types 2SB receiver band1 (211-275 GHZ), band2 (275-370 GHz) and band3(385-500 GHz). The receiver noise temperature is 170 800-K and image rejection ration is 7-20 dB(R. R. Monje & Dochev (2008)). The receiver is installed 4.2 K stage and Local signal is transported by beam from outside of cryostat to receiver.

- Atacama Large Milimeter/submillimeter Array(ALMA)

  ALMA is large scale interferometer with an international collaboration between Janan, Europe and North America. There are six 2SB receivers (band3:84-116 GHz, band4:125-163 GHz, band5:163-211 GHz, band6:211-275 GHz, band7:275-373 GHz and band8:385 500-GHz) and all receivers are designed to have a top performance

each bands. Especially, band8 2SB receiver's SSB signal noise temperature is 75-270 K and image rejection ratio is grater than 10 dB in almost range.

3

Design

3.1 New 500 GHz Receiver

The new cryo-receiver replaces the old cryo-receiver of the 30-cm telescope while keeping the basic specifications of the telescope such as beam size of 9′.4 at 461 GHz, very low power consumption of the system (2.5 kW) and a 1-GHz wide spectrometer. We adopted the ALMA band-8 2SB mixer unit to the new receiver. We showed the schematic view of the new 30-cm telescope in Fig3.2. The 30-cm main reflector and a sub-reflector construct an offset-Cassegrain antenna system. The local signal (LO) is injected by the coupler in the mixer unit in the new receiver, while it was quasi-optically coupled in the old receiver. We modified the transmission optical system to the new receiver and table 3.5 shows the new beam parameters. The beam parameter is designed to be frequency independent at sub-reflector and the horn aperture. We set the edge taper of mirrors after sub-reflector to 40 dB. The edge clearance of the beam to space in the telescope is set to 50 dB.

To apply effective of submillimeter-wave's high transmission sky at Dome Fuji, it is necessary receiver noise is very low. Today, ALMA band 8 receivers are operating with a large three stages cryo-cooler in ALMA, APEX and experiment dewar of ALMA, NAOJ (R. R. Monje & Dochev (2008) and Sozo YOKOGAWA & NARASAKI (2003)). It was designed to work for thermal load of 1 W, 10 W, and 70 W for 4 K, 12 K, and 70 K stages respectively. To operate in Antarctica, we must accommodate this ALMA band-8 mixers for our small 2-stage GM cooler that operates at small power consumption of 1.3 kW. Because of there is electric consumption limit to operate the telescope at the Dome Fuji. It is less than 3 kW for total power and less than 2 kW at receiver system. The most high consumption system is cooling system for cryostat. Therefore, it is important to use low consumption cooler for the antarctic telescope receiver. And it requires improved thermal load design for the new receiver. We purpose to design the 500 GHz receiver that performance is likely to ALMA spec using low cooling power unit.

3.1.1 Configuration of new Receiver

The mixer blocks are directly connected with 3 K stage. This configuration is minimum number of components and thermal resistance between cold head and mixer blocks.
In the radio telescope receivers, signal loss in front of 1st amp is ascendant for noise tem-

perature. It is important to reduce signal loss between the mixer and 1st amp as low as possible. Therefore, we placed two SIS mixers very close to the cold head of the cooler and CLNAs near SIS mixer in new receiver. There are only two cables, IF hybrid and Isolator. These two cables are shortest configuration and Isolator connects to AMPs directory.

Local signal generator is located at out of the flange and signal is transported by waveguide from bottom of 300 K france to the receiver. This signal is split at RF hybrid and transmitted to each mixer. Attenuator at out of 300 K flange controls signal power and we are able to choice best power for mixer. Local signal's frequency is about 500 GHz and waveguide is used WR-6. waveguide's material are selected Copper or Stainless steel to reduce thermal load.

Figure 3.3 shows block diagram of the components at the new cryo-receiver. Receiver noise temperature is directly depended on physical temperature of mixer. Therefore, it is more efficient way to reduce mixer temperature for achieving low receiver noise temperature.

3.2 Noise and Gain

New 500 GHz receiver is must be low noise temperature to operate at high transmission sky like the Antarctica. Therefore, it is important to design of signal loss. From the attribute of radio telescope receiver, the low loss is necessary at the front of receiver.

3.2.1 Noise Design

Table 3.1 and Table 3.2 shows noise budget for cryo-receiver and optics. Noise temperature is proceed from individual object. Contribution for T_{sys} is showed noise level for system noise temperature that front of main miller. The receiver noise is calculated by equation (2.21) and (2.22). At RF window, there are one Capton film, two IR filters and these signal losses are calculated by multi-layer film loss using film parameters (Lamb et al. (2001)).

Table 3.3 and table 3.4 shows noise budget for receiver noise temperature referred at the front of 300 K RF window.

Table 3.1: Noise Design of 461 GHz

Object	Gain(linear)	Gain(dB)	Noise temp[K]	Contribution for T_{sys}[K]
Optics	0.87	-0.61	44.2	44.2
Filters	0.86	-0.63	26.9	27.5
receiver			42.0	52.5
Total				124

Table 3.2: Noise Design of 492 GHz

Object	Gain(linear)	Gain(dB)	Noise temp[K]	Contribution for T_{sys}[K]
Optics	0.86	-0.64	46.5	46.5
Filters	0.87	-0.62	28.1	28.7
receiver			51.2	63.9
Total				139

Table 3.3: Receiver Noise Design of 461 GHz

Object	Gain(linear)	Gain(dB)	Noise temp[K]	Contribution for T_{RX}[K]
Filter	0.86	-0.63		27.5
Horn	0.98	-0.10	0.08	0.09
1st Hybrid	0.49	-0.1	3.7	4.3
mixer	0.95	-0.1	23	
IF-cable	0.98	-0.1	0.08	
2nd Hybrid	0.98	-0.1	0.08	
receiver			24.3	29.5
Phase error	0.98	-0.1	0.08	0.11
IF cable	0.95	-0.2	0.16	0.22
ISO	0.93	-0.3	0.25	0.35
HEMT		32	7.4	11.0
IF cable		-1.9	82.3	0.08
IF cable(out)		-0.7	50.9	0.07
IF system		51	320	0.54
Total				69

Gain design

The signal from star, it is too low power to observe signal directory. Therefore, RF signal is amplified by few AMPs and controlled intensity for spectrometer. RF signal is down converted at mixer to 4-8 GHz frequency and transported by two coaxial cables from each CLNAs to bottom of 300 K flange. And IF signal is down-converted to 0-1 GHz at IF BOX to analyzed at spectrometer. Figure (3.1) is showed level diagram of new 500 GHz

Table 3.4: Receiver Noise Design of 492 GHz

Object	Gain(linear)	Gain(dB)	Noise temp[K]	Contribution for T_{RX}[K]
Filter	0.87	-0.62		28.7
Horn	1.03	-0.12	0.1	0.11
1st Hybrid	0.49	-0.2	0.16	0.2
mixer	0.95	-0.8	26	
IF-cable	0.98	-0.2	0.16	
2nd Hybrid	0.98	-0.2	0.16	
receiver			27.6	34.4
Phase error	0.98	-0.1	0.08	0.11
IF cable	0.95	-0.3	0.25	0.42
ISO	0.93	-0.4	0.34	0.61
HEMT		32	7.4	11.0
IF cable		-1.9	82.3	0.08
IF cable(out)		-0.7	50.9	0.07
IF system		51	320	0.54
Total				80

receiver between horn and spectrometer. There are one CLNAs and two AMPs to control output signal power is -6 dBm/1GHz.

3.3 Optics Design

The signal from star is focused by main miller and transmitted by optics. New receiver's horn has different parameter to receive RF signal and we designed new optical system for the new 500 GHz receiver. The conditions of new optical system are showed following requirement;

- Frequency independent matching between sub reflector and the feed horn.
- Beam edge is over -40 dB.
- Beam clearance is over -50 dB.
- Loss is less than -0.8 dB.

Table 3.5 is showed beam parameters of optical system at 461 GHz. There are two ellipsoidal mirrors and three plane mirrors from sub-reflector.

Figure 3.1: New 500 GHz receiver's level diagram of 461 GHz.

Table 3.5: Beam parameters of optical system at 461.04 GHz

Element	z^a (mm)	$w(z)^b$ (mm)	D(z)^c (mm)	$R(z)^d$ (mm)
Main reflector	−252.75	–	300.00	–
Subreflector	0.00	19.73	60.40	306.80
Plane mirror 1 (PM1)	171.58	8.88	76.22	145.97
Plane mirror 2 (PM2)	234.38	5.27	45.22	101.40
Elipsoidal mirror1 (EM1)	524.38	14.93	64.10	234.38 112.24
Plane mirror 3 (PM3)	743.73	12.21	52.40	100.24
Elipsoidal mirror 2 (EM2)	799.73	19.05	81.78	155.61 146.91
Window of the cryostat	900.31	6.10	26.18	67.80
Feed horn	929.73	2.57	–	24.43

^{a} Distance from the position of the subreflector.
The positive direction is taken to the feed horn.
^{b} Beam radius.
^{c} Diameter of a mirror (−40 / −17 dB) or clearance for space (−50 dB).
^{d} Radius of curvature.

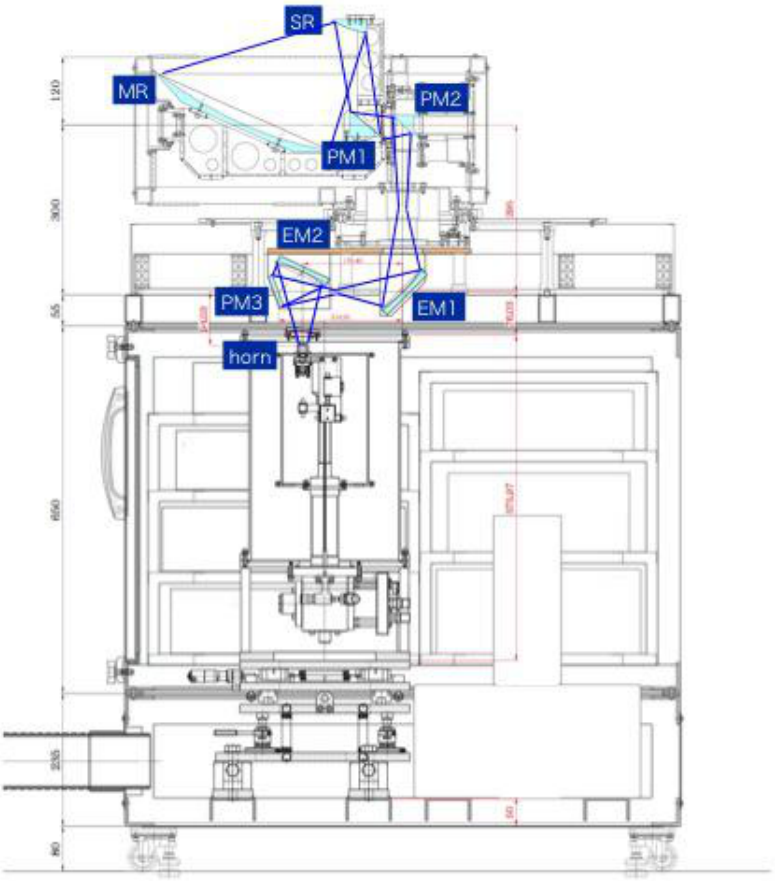

Figure 3.2: Schematic drawing of the new receiver system in the 30-cm telescope.

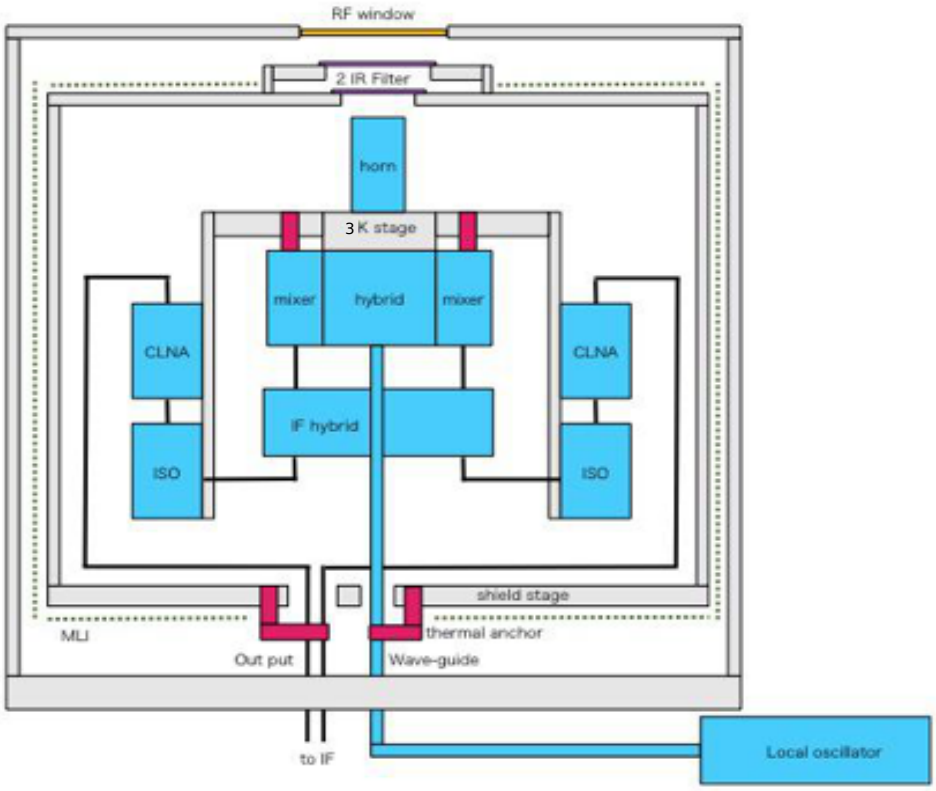

Figure 3.3: Configuration of new 500 GHz 2SB cryo-receiver system.

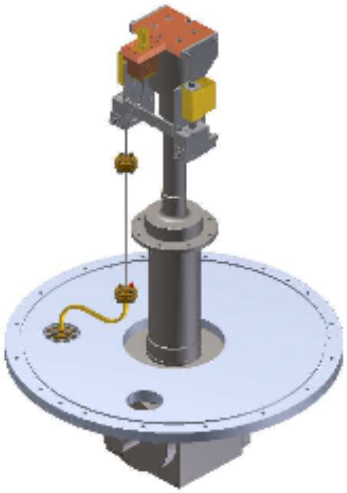

Figure 3.4: New 500 GHz cryo-receiver design.

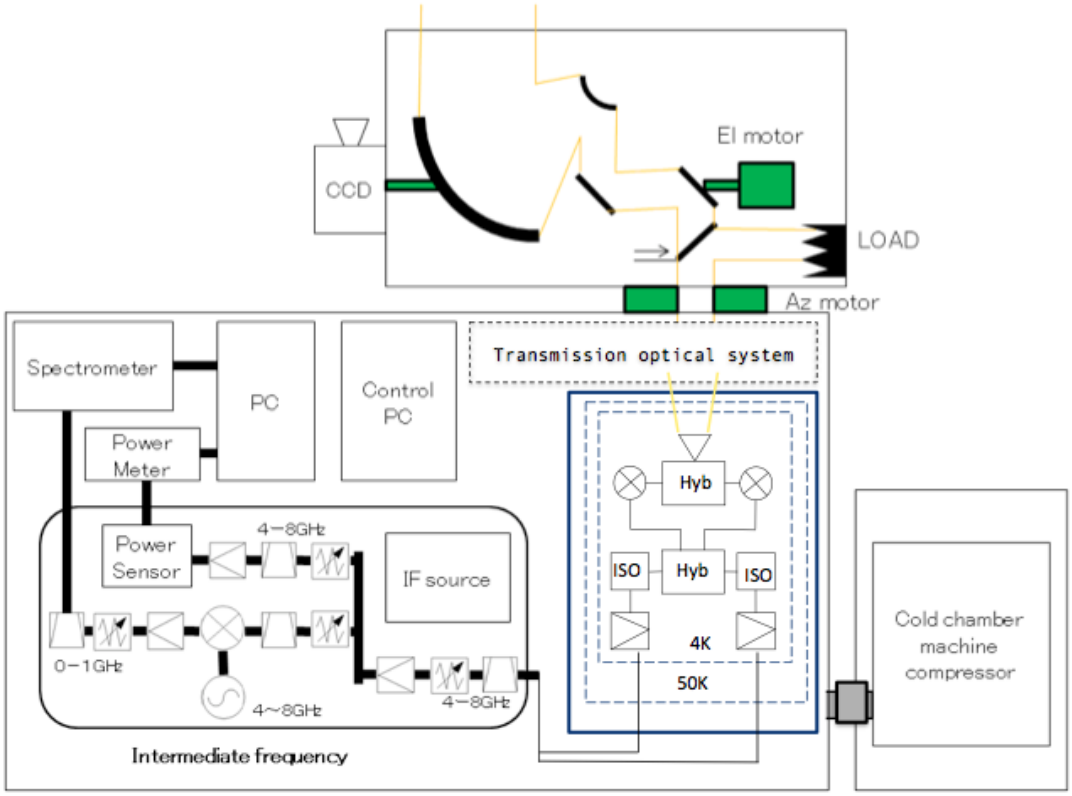

Figure 3.5: Diagram of 30 cm telescope and new 500 GHz receiver.

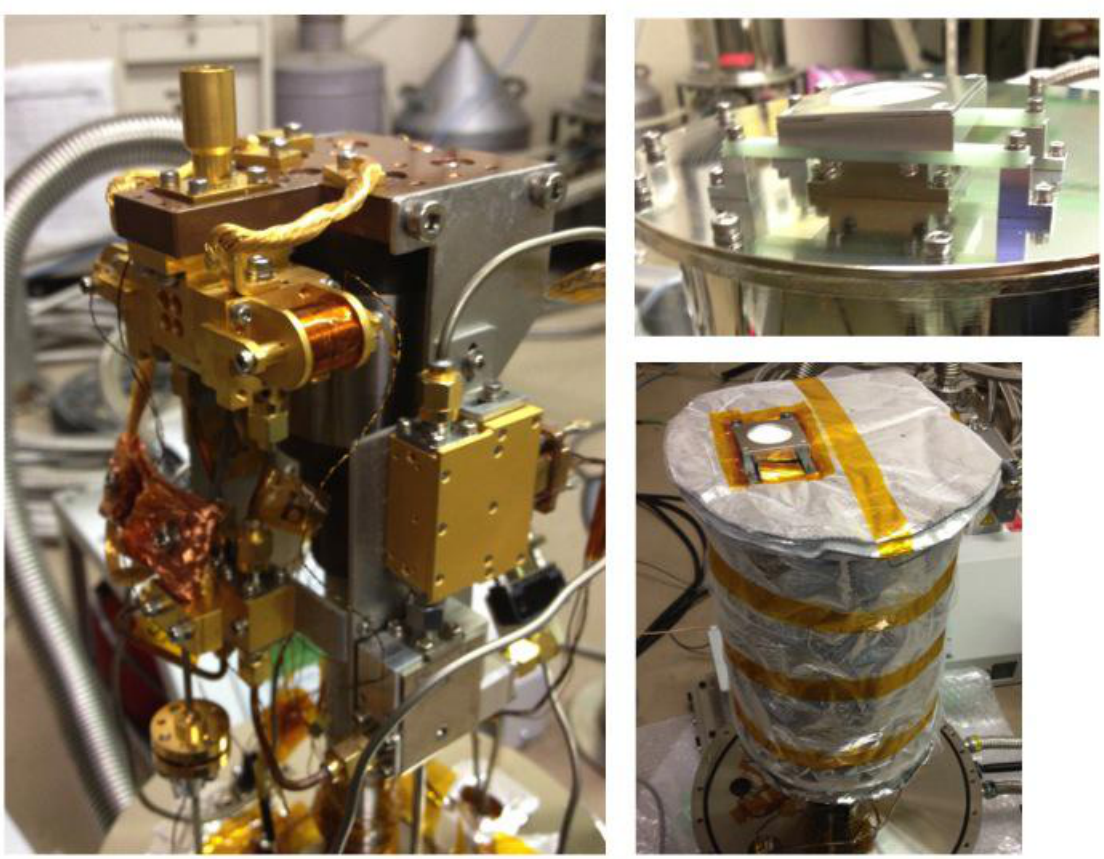

Figure 3.6: New 500 GHz receiver(left), Distribution of IR filters(right top) and MLI is placed out of thermal radiation shield(right bottom).

3.4 Thermal Design

Thermal design is a most important point for the Antarctic telescope receiver. At orbit receiver, The Herschel's cryostat of thermal load to receiver is reduce very low and is less than 47.2 mW (R. Hohn & Jewell (2004)). Operating temperature of SSB mixer is directly linked to receiver performance. To achieve the receiver noise temperature, it is necessary to cold the SIS mixer temperature less than 3.5 K. To reduce the mixer temperature, points of design are following;

- Separation of temperature for mixer block and 3 K head in thermal design.
- Reduction of thermal resistance between the SIS mixer block and 3 K cold head.
- Control thermal inflow route using thermal anchor.

3.4.1 Thermal contact resistance

In the thermal design, to clear up thermal resistance is important. If thermal resistance is obvious thing, we are able to evaluate difference of temperature between certain point. Thermal resistance is configured contact resistance and conductivity resistance. It is difficult to expect contact resistance, because the resistance is depend to material, temperature, pressure and roughness. There is no theoretical equation therefore it is only empirical equation. We confirmed thermal contact resistance lead an experiment. At the supposition of contact resistance, we used following formulas that was advocated TatibanaTatibana (1952). This model is simplified like figure 3.7.

$$R = (\frac{\delta_0 + \delta_1}{\lambda_1} + \frac{\delta_0 + \delta_2}{\lambda_2})\frac{H_B}{cP} \tag{3.1}$$

where δ is contact roughness, H_B is Brinell hardness, c is constant as 0.6 and P is pressure between materials.

We confirmed applicability of this expression by experiment at small system. We controlled quantity of thermal load by only one heater and measured difference of temperature between only one contact. Thermal resistance is calculated by thermal load and difference of temperature like dT = R$\times$W. This system is put in cryostat and pressure is

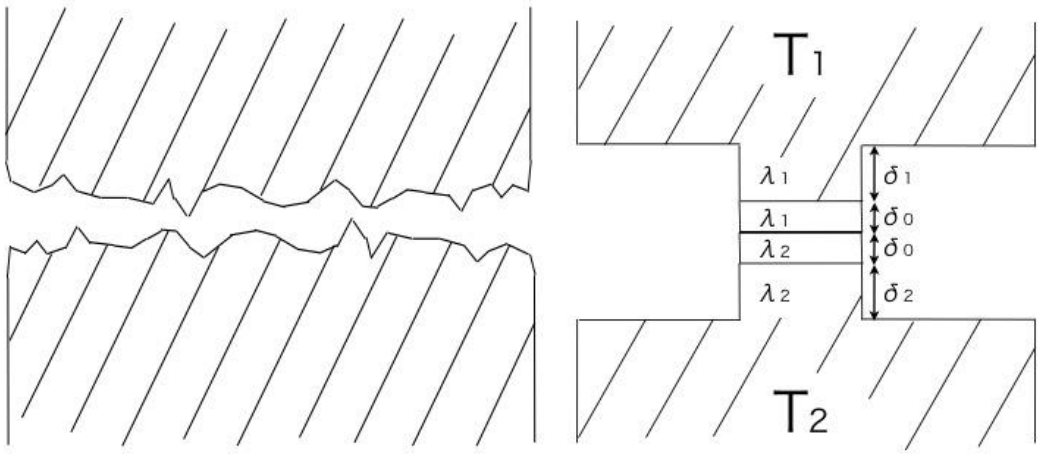

Figure 3.7: Model of thermal contact resistance. Microscopic model (left) and simplification model (right).

less than 10^{-2} [Pa] that is enough to ignore heat exchanges by gas. We measured deference of temperature at contact point of flange. This is made by copper and coated with Nickel. Flange's cross section is 4.7×10^{-4}[m^2] and height is 0.23-m. We measured two situation that thermal load is 0.58 W and 1.59 W. Table 3.6 is showed results of experiment. Both thermal resistances are fitted to calculated value and confirmed applicability. Therefore, we conformed this law is able to design thermal contact resistance.

We designed contact resistance about 4 components that between 3 K stage and mixer, 3 K waveguide thermal anchor, shield stage waveguide thermal anchor and shield stage waveguide thermal anchor with this law.

Table 3.6: Confirmation of thermal contact resistance

thermal load [W]	T_{high}	T_{low}	dT	thermal resistance [K/W]
0.58	299.77	299.69	0.08	0.14 ± 0.03
1.59	311.62	311.46	0.16	0.10 ± 0.01
Calculation				0.11

3.4.2 Thermal load

The thermal load from conduction and radiation are calculated by following formulas.

$$\text{Conduction}$$
$$W(T) = \frac{S}{L}\int_{T_{high}}^{T_{low}} \lambda(T)dt \tag{3.2}$$
$$\text{Radiation}$$
$$W(T) = 5.67 \times 10^6 \times \left(\frac{T_h^4 - T_l^4}{\frac{\epsilon_h}{(1-\epsilon_h)S_h} + \frac{\epsilon_l}{(1-\epsilon_l)S_l} + \frac{1}{S_l}}\right) \tag{3.3}$$

where S is cross-section [m^2], λ is thermal conductivity, L is distance [m] and ϵ is emissivity. We separated 3 K stage and mixer unit for independent components and designed thermal load each quantities. It is necessary to reduce thermal load to the SIS mixer. We install mixer blocks at the position that close to cooler head. The number of contact between cold head to receiver is only two. Therefore, thermal resistance of this area is very low as 1.1 [K/W]. At the all component, we design as such as small cross section to reduce inflow quantity from radiation. Radiation shield is a cylinder with diameter of 170-mm and height of 230-mm. This shield is made by Cu to reduce the difference of temperature between top and bottom. Out of shield, we installed twenty layers of Multi-layer insulation. Two IR filters (Zitex G115) are placed in at the RF window. One filter is fixed at shield window and the other is inserted at more high temperature place between 300 K window and shield window with hold by glass epoxy from top of radiation shield. 1st IR filter reduces the thermal load in radiation by 6 mW that corresponds to reduction of 0.15 K at mixer temperature and 1.3 K at shield stage.

we used thermal anchor at the IF cable and waveguide connect to shield stage. In addition, waveguide is connected to cold stage at the front of receiver to absorb thermal load before into mixer unit. IF cables are used coaxial cable that is made CuNi coved by

Ag(center), PTFE(middle) and CuNi(outer). That is direct connected between 3 K and 300 K stage. The waveguide is used WR-6 type and material is SUS and Cu. SUS waveguide is task for anti-conduction guide. Several waveguides are covered by Au to reduce the loss of transmission signal. We operated signal generator of 500 GHz at the out of cryostat. This distribution have advantage about correspond to breakdown. However, the signal of transmit is high frequency and signal loss is very high. The distribution of waveguide in this receiver is selected to most short length in cryostat. And to reduce thermal load, we distribute thermal anchor at waveguide. The anchors is connected to shield stage and 3 K stage. The bias cable is using Manganin line that cross-section is small. Bias cable and sensor cable are connected to shield stage to control temperature distribution.

3.4.3 Thermal anchor and contact resistance

It is general way to reduce physical temperature that thermal anchor is installed between cold material to object. At this receiver, we installed thermal anchor at IF cable, waveguide and mixer blocks. These anchors were made by copper and coated by gold. Main cable is aggregate of hundred thin copper cables that cross-section is 5.31×10^{-7}-m^2. Anchors at mixer blocks are installed to reduce thermal resistance between 3-K stage and mixer block. These thermal anchors at IF cable and wave-guide are able to change position of connecting place. At IF cable, anchor is connected from 60 K stage. At waveguide, there are two anchors that one is connected from 3 K stage and the other is connected from 60 K stage. There is only one position that mixer temperature is minimum. When the distance from receiver is close, thermal resistance of anchor is not large enough compare with resistance of anchor. On the other hand, long length between receiver and position is meaning waveguide length is short. Therefore, thermal inflow quantity is increase. However, it is necessary to learn contact resistance at anchor connecting position to decide the anchor position. Thermal resistance is defined to coefficient of temperature difference and thermal load. The model of around anchor is confirmed model accuracy. This model is means that we are able to ignore the efficacy of connecting jig of thermal anchor. At the connecting jig, thin is 10-mm and cross section is 5.3×10^{-6} [m^2]. T_{center} is temperature of wave-guide at connecting position to anchor.

anchor position of IF-cable

IF-cables are installed in receiver to output signal between HEMT and 300 K stage directly. This cable is designed to install low temperature situation and length is 0.85-m. This cable is configured by several materials that is cupronickel, non-dielectric is Teflon and center is nickel. The physical quantities of material are showed figure (3.11) and (3.12).

At IF-cable, there is one anchor cable from 60 K stage. This cable is installed to reduce thermal load to the mixer and there is one position that mixer temperature is minimum. Thermal anchor is connected by clincher at 60 K stage and IF-cable and length is 0.075-m. Thermal resistance of anchor is showed table 3.7. These resistances are lined on straight and total thermal resistance is calculated by law of series configuration. Figure (3.8) is

Table 3.7: Thermal resistance of 60 K IF cable anchor

component	surface (60-K stage - anchor)
cross section [m^2]	6.4×10^{-5}
material	Cu-Cu
thermal conductance(T_{high}) [W/(m K)]	8.33×10^{2}
thermal conductance(T_{low}) [W/(m K)]	8.33×10^{2}
Pressure[N/m^2]	$4\ .28\times10^{6}$
δ_{high} [m]	1.00×10^{-5}
δ_{low} [m]	1.00×10^{-5}
resistance [K/W]	15.88×10^{-1}
component	surface (anchor - IF cable)
cross section [m^2]	3.01×10^{-5}
material	Cu-CuNi
thermal conductance(T_{high})	8.33×10^{2}
thermal conductance(T_{low})	9.94
Pressure[N/m^2]	9.09×10^{5}
δ_{high}[m]	1.00×10^{-5}
δ_{low}[m]	1.00×10^{-4}
resistance [K/W]	3.72×10^{2}
component	anchor cable
cross section [m^2]	5.31×10^{-6}
material	Cu-Cu
length[m]	0.075
thermal conductance [W/(m K)]	$5.09\ 10^{2}$
resistance [K/W]	3.02×10^{1}
total resistance [K/W]	4.03×10^{2}

showed calculation of relationship between anchor's position and mixer temperature. Therefore, the minimum position is 0.2-m from 300 K stage and thermal load is 4.4 mW to receiver from 60 K stage. Thermal load is 0.59 W to 60 K stage from 300 K stage.

thermal resistance of wave-guide anchor

At wave-guide, there are two thermal anchors that one is connected from 3 K stage and the other is connected from 60 K stage. waveguide is connected between 300-K stage and RF Hybrid. Therefore, thermal load to mixer block increases mixer temperature. To reduce mixer temperature, we installed thermal anchor from 3 K stage at waveguide around mixer block. Thermal resistance of anchor is less than waveguide and thermal load passes on anchor. Thermal load quantity is determined by thermal resistance ratio of anchor to waveguide between mixer block and anchor position. 60 K anchor is installed

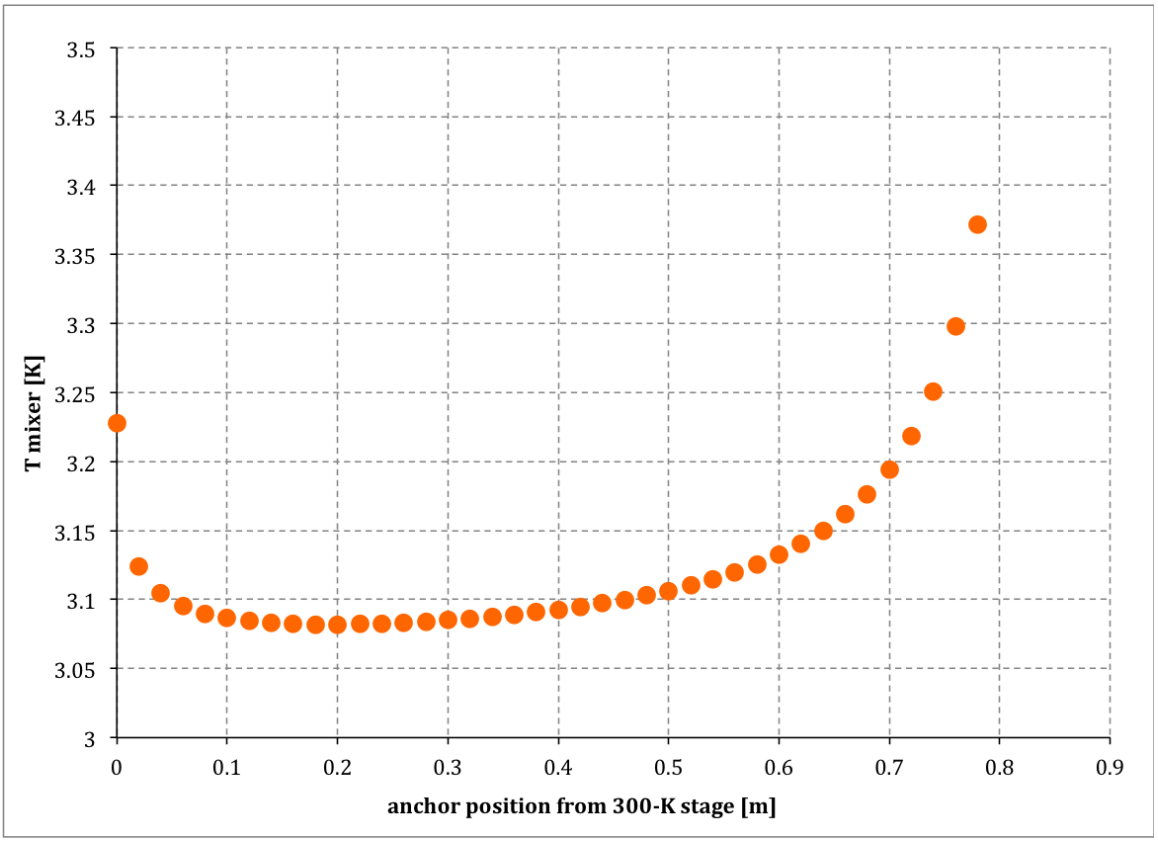

Figure 3.8: Relationship of anchor position and mixer temperature at IF-cable.

to select the situation that thermal load to mixer block is minimum.

Thermal resistance of anchors are showed table 3.8 and table 3.9. We calculated thermal anchors position that mixer temperature is minimum. There are two parameters that 60 K anchor's position and 3 K anchor's position. waveguide is WR-6 and configured three guides. 300 K side guide is made by copper and coated with Au. Guide configuration is sigmoidal type and length is 0.141-m. Middle guide is straight and material is SUS coated with Au. Length is 0.15-m. Receiver side guide is sigmoidal type and length is 0.11-m. Guide's material is SUS and there is no Au coat only. We describe two anchors position that distance from connection point between 300 K guide and middle guide on middle guide for 60 K anchor and distance from receiver on receiver side guide for 3 K anchor. Figure (3.9) is showed relationship between mixer temperature and anchors position. X-axis is a 60 K anchor position scale and Y-axis is a 3 K anchor position scale. Contour levels for the mixer temperature are set at arbitrary intervals, 3.195, 3.200, 3.205, 3.210,

Table 3.8: Thermal resistance of 3 K anchor for wave-guide

component	surface (3 K stage - anchor)
cross section [m^2]	6.09×10^{-5}
material	Cu-Cu
thermal conductance(T_{high}) [W/(m K)]	4.00×10^{2}
thermal conductance(T_{low}) [W/(m K)]	4.00×10^{2}
Pressure[N/m^2]	4.50×10^{6}
δ_{high} [m]	1.00×10^{-5}
δ_{low} [m]	1.00×10^{-5}
resistance [K/W]	5.59×10^{-1}
component	surface (anchor - waveguide)
cross section [m^2]	4.00×10^{-5}
material	Cu-TeCu
thermal conductance(T_{high})	4.00×10^{2}
thermal conductance(T_{low})	3.68×10^{2}
Pressure[N/m^2]	6.85×10^{6}
δ_{high}[m]	1.00×10^{-5}
δ_{low}[m]	1.00×10^{-4}
resistance [K/W]	5.80×10^{2}
component	anchor cable
cross section [m^2]	5.31×10^{-6}
material	Cu
length[m]	0.0435
thermal conductance [W/(m K)]	$5.09\ 10^{2}$
resistance [K/W]	2.16×10^{1}
total resistance [K/W]	1.12×10^{2}

3.215, 3.220, 3.225, 3.230, 3.235 and 3.240 K. It is minimum position when 60-K anchor is connected at 0.03-m and 3 K anchor is connected at 0.095-m.

For next stage, we discussed the way to reduce mixer temperature. When we chance connect way for weld at waveguide, thermal resistance of anchor is down. Figure 3.10 is showed relationship at this inquest. Contour levels for the mixer temperature are set at arbitrary intervals, 3.155, 3.160, 3.165, 3.170, 3.175, 3.18, 3.185, 3.190, 3.195 and 3.200 K. Minimum point of mixer temperature is reduce to 3.154-K.

Table 3.9: Thermal resistance of 60 K anchor for wave-guide

component	surface (60 K stage - anchor)
cross section [m^2]	6.40×10^{-5}
material	Cu-Cu
thermal conductance(T_{high}) [W/(m K)]	8.33×10^{2}
thermal conductance(T_{low}) [W/(m K)]	8.33×10^{2}
Pressure[N/m^2]	4.28×10^{6}
δ_{high} [m]	1.00×10^{-5}
δ_{low} [m]	1.00×10^{-5}
resistance [K/W]	3.03×10^{-1}
component	surface (anchor - waveguide)
cross section [m^2]	1.20×10^{-5}
material	Cu-SUS
thermal conductance(T_{high})	8.33×10^{2}
thermal conductance(T_{low})	5.78
Pressure[N/m^2]	2.74×10^{6}
δ_{high}[m]	1.00×10^{-5}
δ_{low}[m]	8.00×10^{-4}
resistance [K/W]	4.44×10^{2}
component	anchor cable
cross section [m^2]	5.31×10^{-6}
material	Cu
length[m]	0.17
thermal conductance [W/(m K)]	$3.85\ 10^{2}$
resistance [K/W]	2.16×10^{1}
total resistance [K/W]	4.83×10^{2}

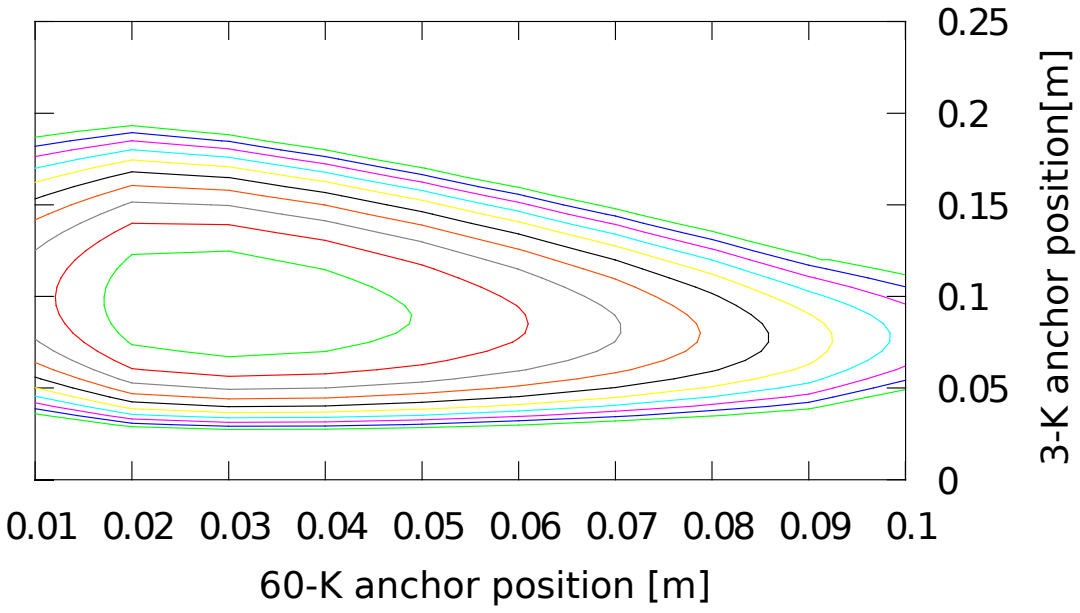

Figure 3.9: Relationship between variable anchors position and mixer temperatuer

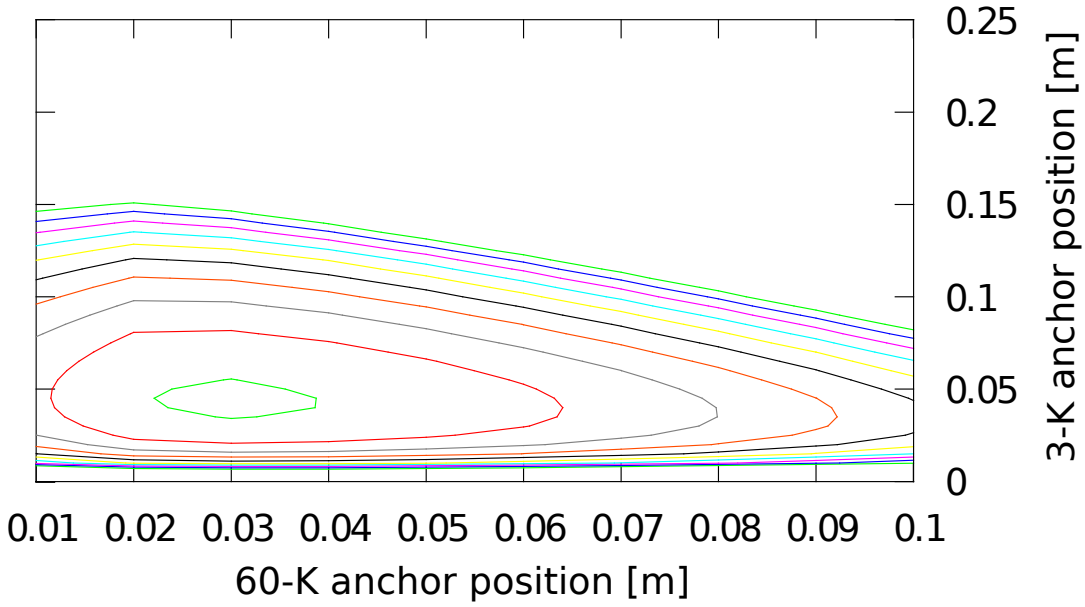

Figure 3.10: Relationship between fixed anchors position and mixer temperatuer

Table 3.10: Thermal load

component	quantity
to cold stage	
IF cable	3 mW
waveguide (mixer)	0.2 mW
waveguide (3 K stage)	2 mW
bias cable	1 mW
temperature sensor	0.1 mW
HEMT	8 mW
RF window	2 mW
Radiation from shield	1 mW
total	53 mW
to shield stage	
IF cable	0.05 W
waveguide	0.08 W
bias cable	0.03 W
temperature sensor	0.01 W
1st IR filter leg	0.1 W
RF window	0.04 W
Radiation(MLI)	0.9 W
Radiation(non-MLI)	0.1 W
total	1.3 W

3.4.4 Result of thermal design

The result of thermal design is showed table 3.10 and thermal load diagram is showed at figure 3.11. For each stage, components of thermal load from conductance are showed table3.11 and 3.12. The total thermal load is less than 60 mW at cold stage and 1.5 W at shield stage.

In one instance, We describe thermal load of waveguide at 3 K stage from conduction. The waveguide distribution is showed at figure 3.4 that is connected between 300 K stage and RF hybrid directory. Thermal load of parameter in design is showed in table 3.11. T_{high} is 59.9 K, T_{low} is 48.9 K, length is 0.07 m, cross section is 9.0×10^{-7} m^2 and conductivity is 9.34 $Wm^{-1}K^{-1}$. The quantity is calculated by equation (3.2) and list of thermal load to each stage is showed at table 3.10 as 2 mW. And thermal load is measured at laboratory in next section.

We have developed low thermal inflow cooling receiver system that mixer temperature is less than 3.5 K.

Table 3.11: 3 K stage Thermal design parameter

	quantity
IF cable	
number	2
T_{high}	54.7 K
T_{low}	17.9 K
length	0.55 m
cross section(center)	2.04×10^{-7} m^2
cross section(middle)	1.99×10^{-6} m^2
cross section(outer)	1.58×10^{-6} m^2
conductivity(center)	20.7 $Wm^{-1}K^{-1}$
conductivity(middle)	0.24 $Wm^{-1}K^{-1}$
conductivity(outer)	9.27 $Wm^{-1}K^{-1}$
waveguide	
number	1
T_{high}	59.9 K
T_{low}	48.9 K
length	0.07 m
cross section	9.0×10^{-7} m^2
conductivity(center)	9.34 $Wm^{-1}K^{-1}$
bias cable	
number	32
T_{high}	42.0 K
T_{low}	3.0 K
length	0.3 m
cross section	5.1×10^{-8} m^2
conductivity(center)	4.38 $Wm^{-1}K^{-1}$
thermal sensor cable	
number	12
T_{high}	42.0 K
T_{low}	3.0 K
length	0.3 m
cross section	1.3×10^{-8} m^2
conductivity(center)	4.38 $Wm^{-1}K^{-1}$
waveguide(to mixer)	
number	1
T_{high}	11.4 K
T_{low}	3.0 K
length	0.035 m
cross section	9.0×10^{-7} m^2
conductivity(center)	0.32 $Wm^{-1}K^{-1}$

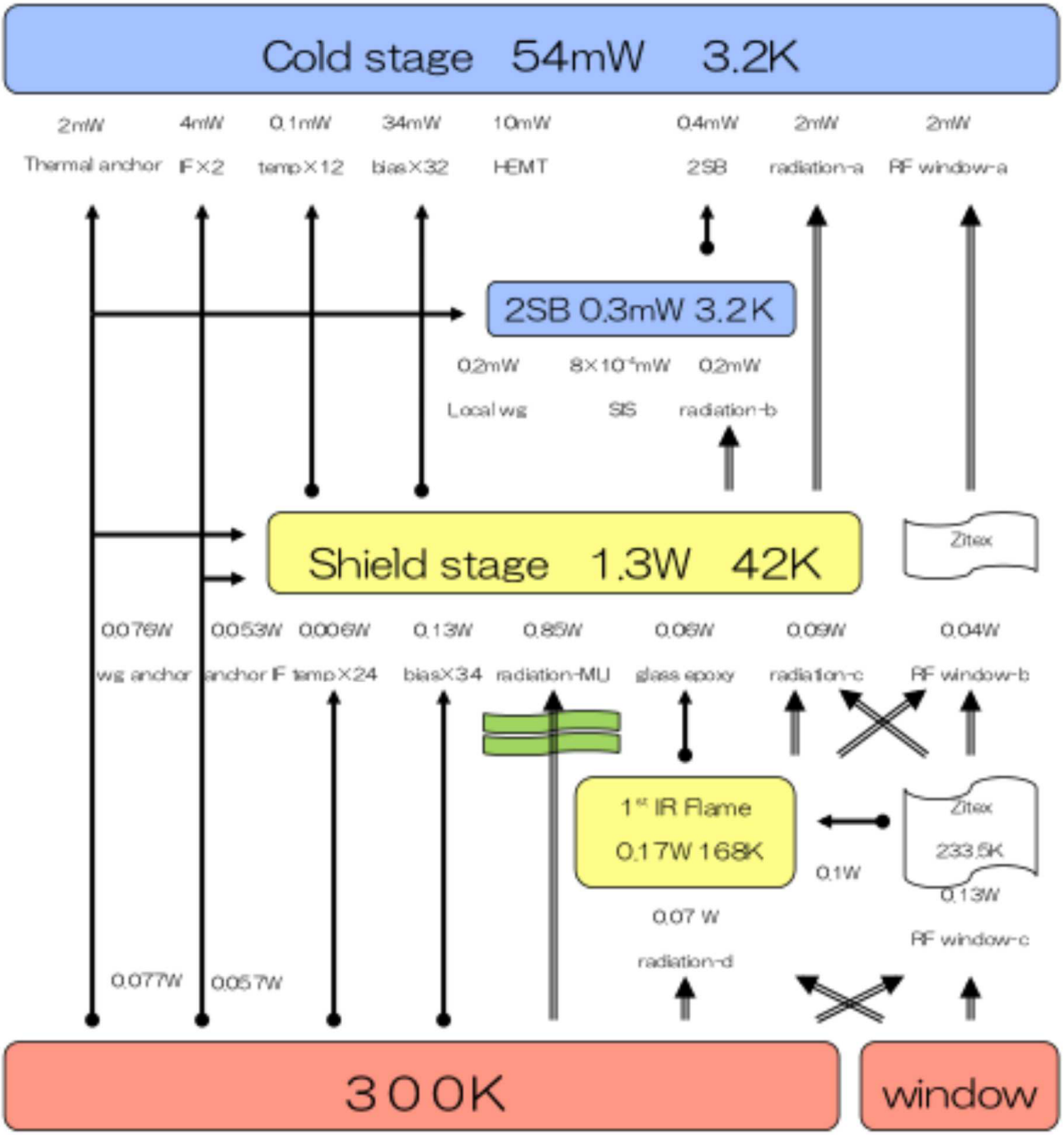

Figure 3.11: Thermal load diagram. Single line intends pathway from conductance and double line intendes from radiation.

Table 3.12: 42 K stage Thermal design parameter

	quantity
IF cable	
number	2
T_{high}	300 K
T_{low}	79.7 K
length	0.2 m
cross section(center)	2.04×10^{-7} m^2
cross section(middle)	1.99×10^{-6} m^2
cross section(outer)	1.58×10^{-6} m^2
conductivity(center)	16.5 $Wm^{-1}K^{-1}$
conductivity(middle)	0.24 $Wm^{-1}K^{-1}$
conductivity(outer)	13.7 $Wm^{-1}K^{-1}$
waveguide	
number	1
T_{high}	300 K
T_{low}	162.6 K
length	0.025 m
cross section(SUS)	9.0×10^{-7} m^2
cross section(Cu)	2.35×10^{-6} m^2
conductivity(SUS)	16.44 $Wm^{-1}K^{-1}$
conductivity(Cu)	399.5 $Wm^{-1}K^{-1}$
bias cable	
number	34
T_{high}	300 K
T_{low}	42 K
length	0.2 m
cross section	5.1×10^{-8} m^2
conductivity(center)	15.3 $Wm^{-1}K^{-1}$
thermal sensor cable	
number	24
T_{high}	300 K
T_{low}	42 K
length	0.2 m
cross section	1.3×10^{-8} m^2
conductivity(center)	15.3 $Wm^{-1}K^{-1}$

4

Receiver Parformance

4.1 Cooling capacity

This receiver's cryo-cooler is 2 stages GM cooler made by Sumitomo Heavy Industries, Ltd. This cooler system is configured Cold Head Unit (RDK - 101E) and Compressor Unit (CNA -11C). Cooing capacity of catalog is 3.0 W at 60K 1st stage and 0.1 W at 4.2 K at 2nd stage with 50Hz frequency. Power consumption of compressor is 1.5 kW at steady situation. Compressor unit's cooling system is Air cooler and weight is 75 kg. Therefore, this cooing system is able to operate at the center of Antarctica with only few human.

We measured cooling capacity when total thermal inflow quantity is changed with few step. Two heaters are put in each stage and choice thermal load quantity that controlled by current. Thermal inflow quantity when no-thermal load is 3 mW at cold stage and 0.85 W at shield stage. The cold stage heater was chanced thermal quantity between from 10 to 100 mW with maximum load is 200 mW. The shield stageAntarctica heater was changed to 2 W. The result is showed figure 4.1 that X-axis is shield stage temperature and Y-axis is cold stage temperature. The most low temperate is 2.4 K at cold stage and 41 K at shield stage. To be less than 3.5 K at mixer temperature, it is necessary that total thermal load is less than 103-mW at 3 K stage and 1.35W at 60 K stage. Therefore, this cooler is able to cool the mixer at the Antarctica.

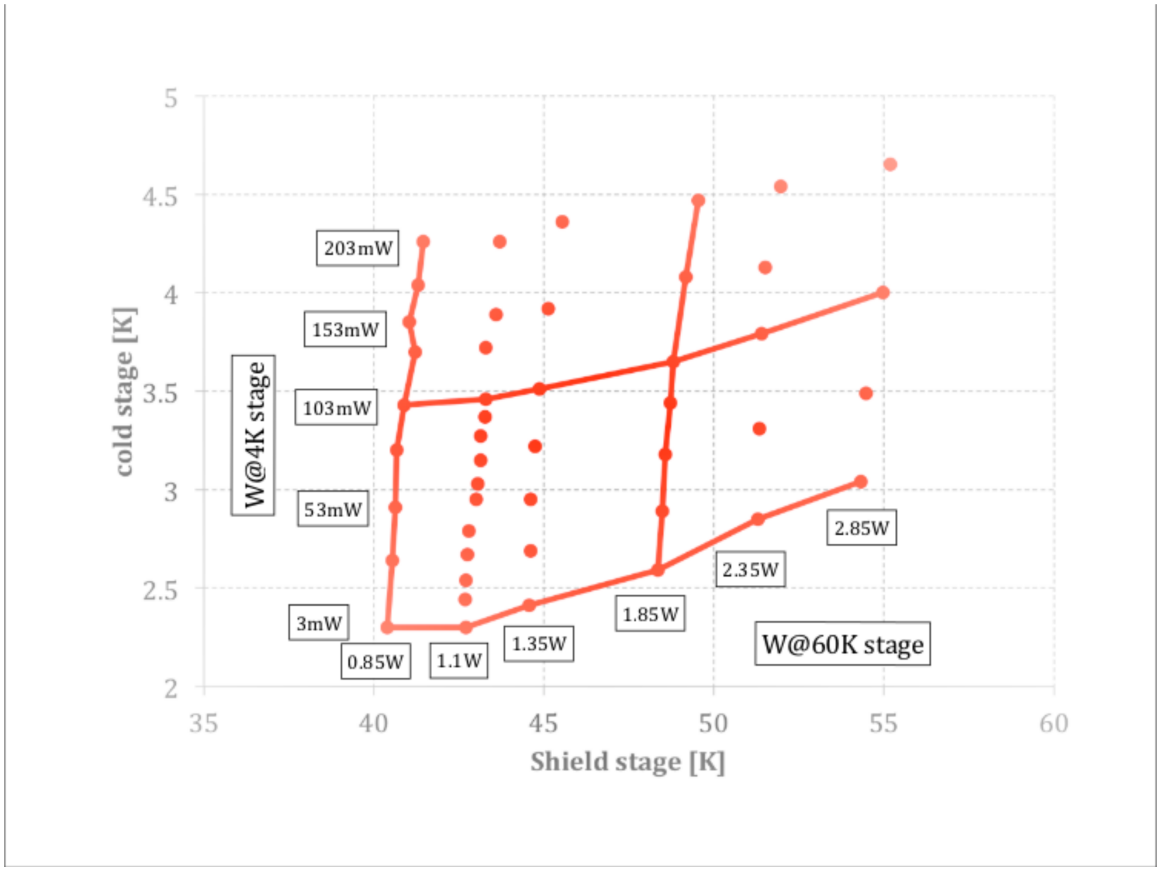

Figure 4.1: Cooling power of cryo-cooler

4.2 confirmation of thermal load

4.2.1 Determine thermal load quantities

The heat flow quantity is estimated by the difference of transmitted quantity from 300 K side (W_a) and outflow (W_b) in the waveguide. W_a-W_b is thermal road conduct in thermal anchor. To estimate difference in temperature, we measured temperatures that before and after anchor on waveguide (T_a and T_b) and the anchor jig to fix. The result of comparison, we confirmed theoretic thermal contact resistance is in agreement in the range with error. We determined the thermal anchor position at the waveguide anchor that mixer temperature is minimum. Thermal quantity is determined by the result of cooling capacity to compare difference of temperature. The result is showed table 4.1 . IR Filter load is difference of load when 1st IR filter is removed. In this situation, 3 K load is increase and shield stage load is decrease. IR filter is selected Zitex G115 that thin is 400-um and cross section is $7.8\times10^{-6}[m^2]$. Thermal load is determined 5.9 mW at 3 K stage and 0.14 W at shield stage. MLI is located out of Radiation Shield that 20-layers sandwich structure of thin film is covered by aluminum and unit-thermal conductance material. When MLI is established, thermal load to shield stage is determined to 0.87 W. However, the calculation of thermal inflow cut is 2.1 W and there is big discrepancy. The reason of this problem is that MLI is not selected ideal environment. Therefore, thermal cutting efficiency was drop away. HEMT load is only one HEMT generation quantity and determined to less than 10 mW at 3 K stage. Wave-guide load is determined by comparison with or without. Thermal inflow quantity is 5 mW at 3 K stage and 0.04 W at shield stage. Base on there result, We confirmed validity of thermal design of conduction and radiation.

The cooing temperature of both stage are less than 3.5 K at mixer block and 42 K at shield stage. We have constructed low temperature receiver with low cooling power cryo-cooler.

Table 4.1: Determination of thermal load

component	design	experiment
3 K stage		
Radiation	3.1 mW	3.0 mW
HEMT	8 mW	10 mW
waveguide)	2.2 mW	3.3 mW
IF cables	3 mW	2 mW
bias cable	39 mW	39 mW
60 K stage		
waveguide	0.08 W	0.04 W
IF cables	0.05 W	0.13 W
Radiation(MLI)	0.85 W	0.85 W
RF window	0.03 W	0.03 W

4.3 Signal loss of Zitex G115

We selected Zitex G115 for IR Filter to reduce thermal inflow quantity from RF window. RF window's diameter is 30 mm and thermal load is high. It is necessary to locate IR filter at RF window. However, signal loss of IR filter is occasion to increase receiver noise temperature. It is high-impact that signal loss is located at the front of 1st AMP. Thermal cut off quantity and receiver noise temperature are relationship of trade off. Therefore, we measured signal gain of Zitex G115 at 461GHz. The thickness of Zitex is 400 um. The gain of zitex is calculated by output of signal with or without and loss is determined to $\mathrm{G} = -0.18 \pm 0.02$ dB. This result is equal to expectation by calculation of dielectric loss and we confirmed the accuracy of it. And we confirmed two IR filters are installed at RF window is better.

4.4 Receiver performance

4.4.1 Parameters of 2SB receiver

At new 500 GHz receiver, there are 5 parameters and it is necessary to determine to operate with low receiver noise temperature. These parameters are written as follow

- Voltage at mixer.
- Intensity of magnetic field.
- Intensity of local signal.

Voltage is controlled by source meter (KEITHKEY 2600-sereise) with micro-volt order using four-wires system at each mixers.

At SIS mixer, there is Josephson effect that spoils the response of current when light into receiver from object. Josephson effect generates current that called Josephson-current if there is no deference of voltage at Superconductor/Insulator/Superconductor array and this current is noise for SIS miser. Josephson-current is suppressed with parallel magnetic field to connecting plane. Intensity of current is written as follow

$$I = I_c \left| \sin \frac{\sin \pi\Phi/\Phi_0}{\pi\Phi/\Phi_0} \right| \tag{4.1}$$

where Φ is intensity of magnetic field and relationship of current to magnetic field is absolute of sin. Therefore, we are able to suppress the Josephson-current with especial magnetic field. Magnetic field is generated by Superconducting-coil with 0.125-mm diameter NbTi covered Cu wire that total number of winding is about 4000. Intensity is controlled with current generated by source-meter at each mixer. Intensity of local signal is controlled by waveguide attenuator at out of cryostat.

We determined parameters at Tsukuba university laboratory. Conditions to decide parameters are written as follow

- Noise temperature is low.
- Image rejection ratio is more than 14 dB.
- Allan variance is more than 80 s.

When decision of parameters, it is most important receiver noise temperature is low. At high transmission sky, it is better that receiver noise temperature is as low as possible. Image Rejection Ratio (IRR) is a quantity to intend intensity of leakage signal to the other output port. To observe at SSB to determine physical condition, it is necessary IRR is lager than 10-dB at least. IRR limit is 14 dB at output port for new 500 GHz receiver. Receiver stability is estimated by Allan variance at spectrometer signal. 80 s is necessary to execute multi on-off observation that integration time is 20 s at one point. The parameter to observe at Antarctica, it is necessary to clear all limits.

4.4.2 deflux of magnetic field

2SB receiver is sensitive for magnetic field and it is important control magnetic field to operate at low noise receiver every time. When SIS mixer changes to superconductive transition state, mixer catches background magnetic field. This trop accrues Josephson current and influences to receiver noise. We execute release of magnetic field using magnetic coil when mixer is cooled less than 8 K at all times. This proceeding is written al follow

1. Change a magnetic field narrow down to zero, alternate plus and minus.

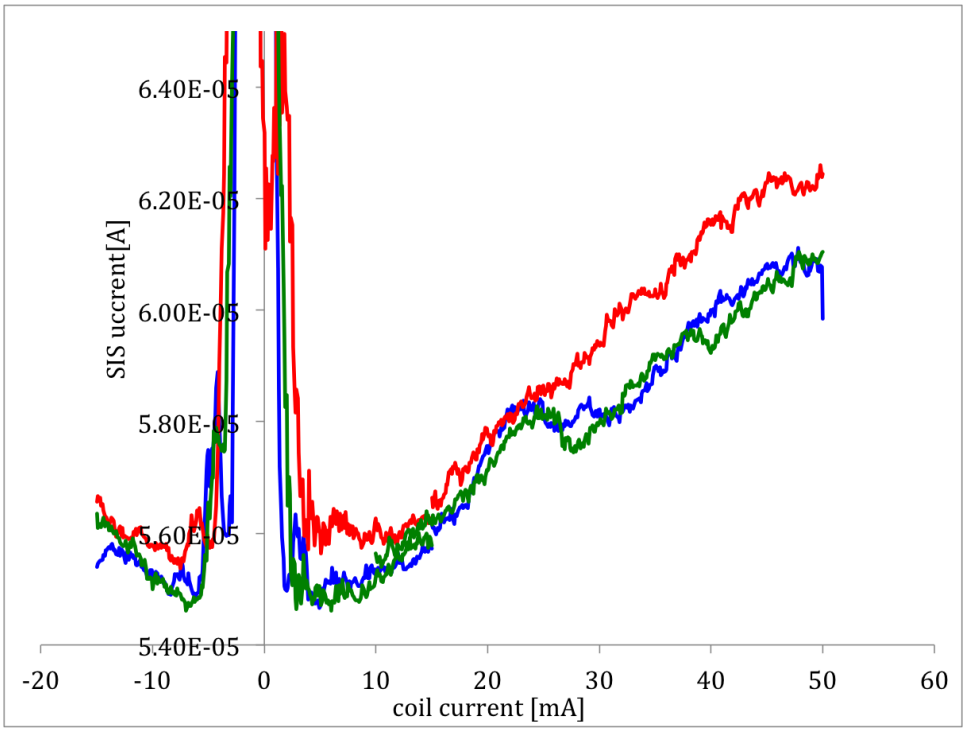

Figure 4.2: Josephson current at mixer2. X-axis is current of superconducting coil proportional to magnetic field. Red line is non-deflux condition, blue is effect of deflux operation and green is deflux effect at another day.

2. Rise mixer temperature over 12 K.

3. Cool mixer to operation temperature.

4. Conform Josephson current.

Figure4.2 is showed typical Josephson current at mixer2 that red line is non-deflux condition and blue is effect of deflux operation at mixer temperature is 3.2 K. There are apparent difference of Josephson current at 4-12 uA and over 25 uA.

parameter using DSB noise temperature

We executed two another approach to determine 2SB receiver parameters. The one way is calibrate mixer parameters at DBS signal independently and couple two DBS signals to observe SSB signal. Therefore, this method coordinates at only DSB signal and do not think relationship of two mixers. We defined name of this way as ”DSB turning” for descriptive purposes. Adjustment method is written as follow

1. Measure Y-factor when change SIS voltage and coil current independently.
2. Measure Y-factor when change coil current finely, SIS voltage is fix.
3. Measure by same method at the other mixer.
4. Measure Y-factor, IRR and Allan variance at SSB signal.

We measured these dependence at each frequencies. Figure 4.28 is showed Y-factor map when SIS voltage and magnetic field are changed and figure 4.4 is root mean square (r.m.s.) of Y-factor. At this measurement, we decided SIS voltage is 1.1 mV. Secondly, we measured relationship Y-factor and finely coil current when SIS voltage is 1.1 mV. This result is showed figure 4.32 that green points are Y-factor and red line is r.m.s.. At this result, when coil current is 9.2 mA Y-factor is better and r.m.s. is stable to observe. Table 4.2 is showed all parameters of each frequencies.

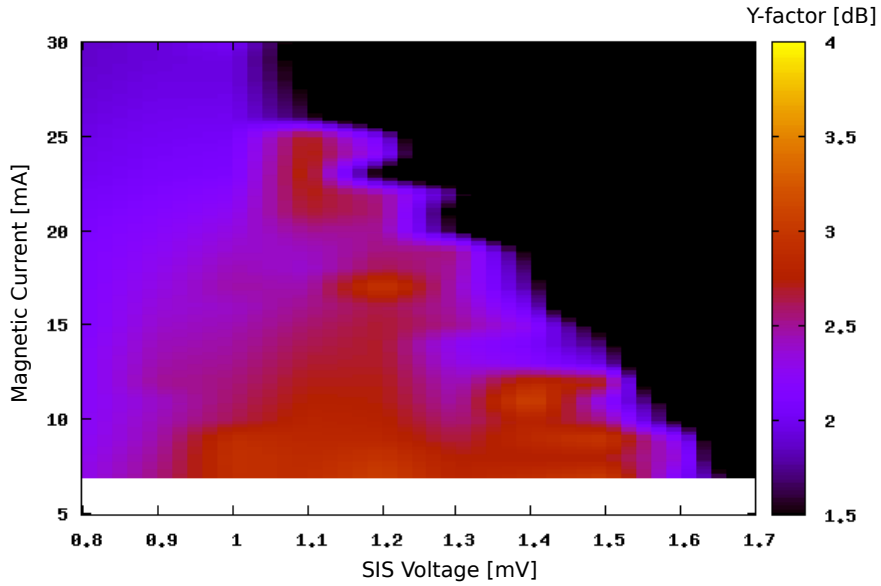

Figure 4.3: Relationship at mixer-1 between DSB noise temperature and parameters of 461 GHz

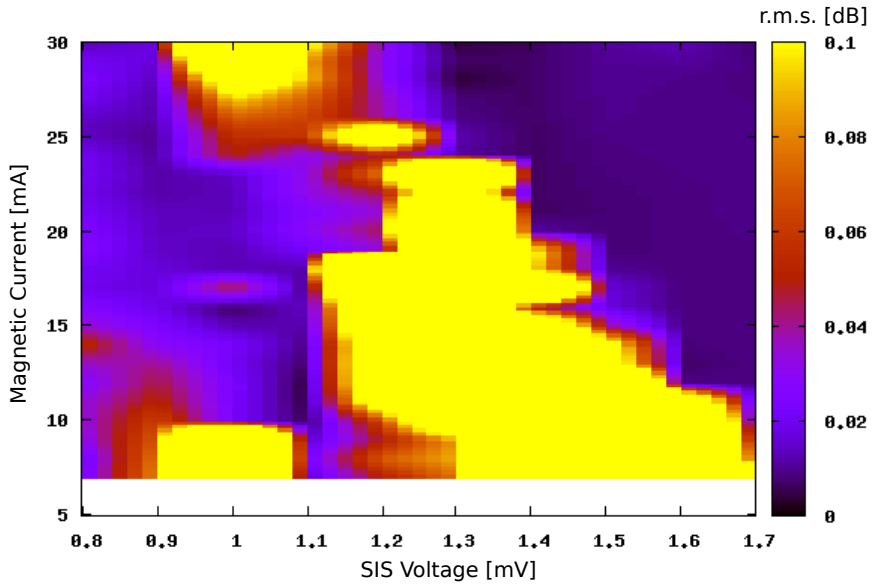

Figure 4.4: Relationship at mixer-1 between DSB noise temperature r.m.s. and parameters of 461 GHz

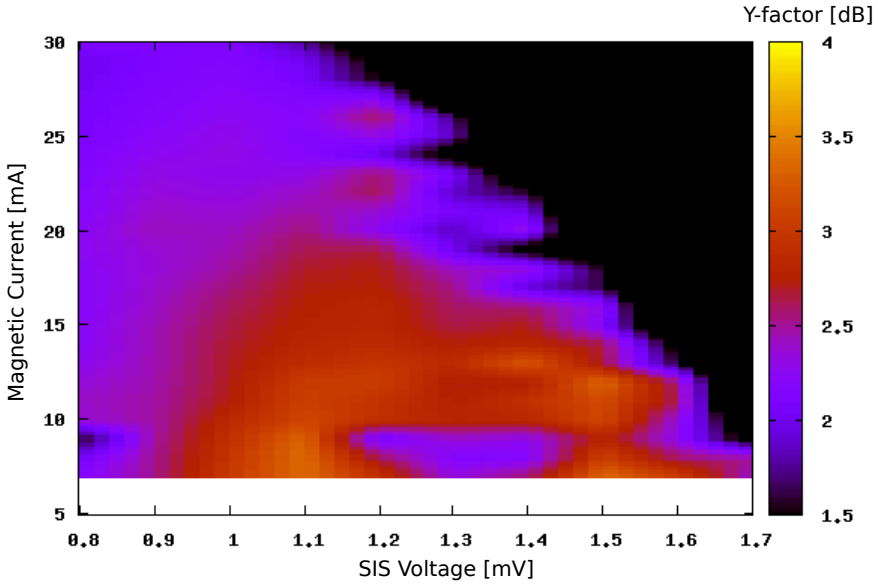

Figure 4.5: Relationship at mixer-2 between DSB noise temperature and parameters of 461 GHz

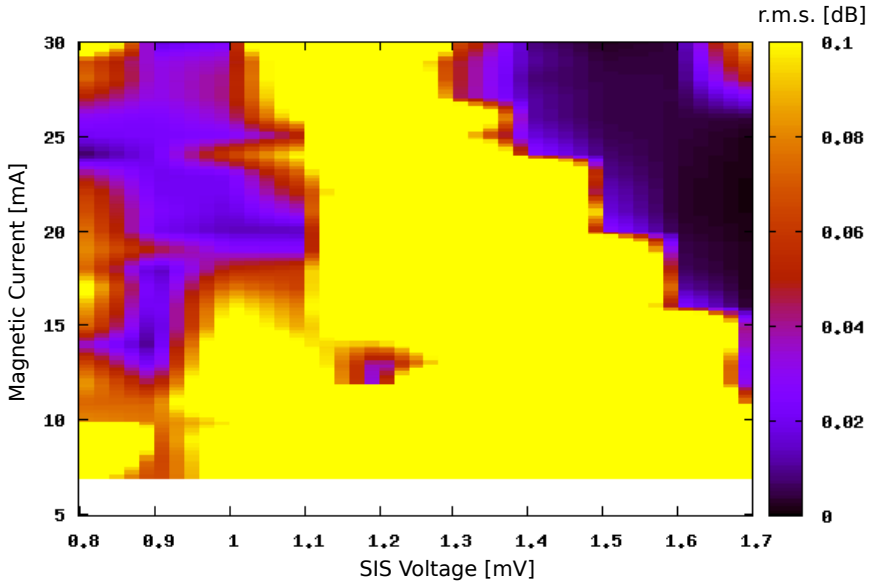

Figure 4.6: Relationship at mixer-1 between DSB noise temperature r.m.s. and parameters of 461 GHz

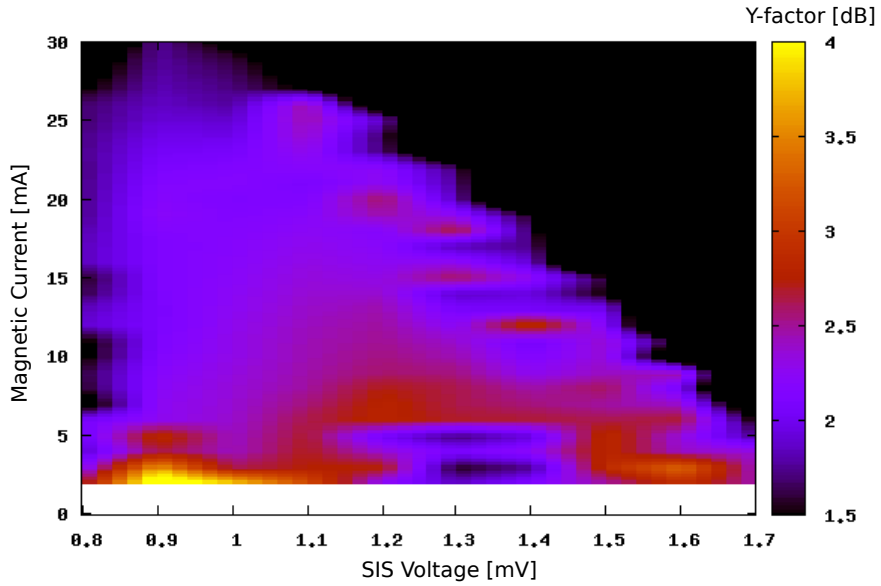

Figure 4.7: Relationship at mixer-1 between DSB noise temperature and parameters of 492 GHz

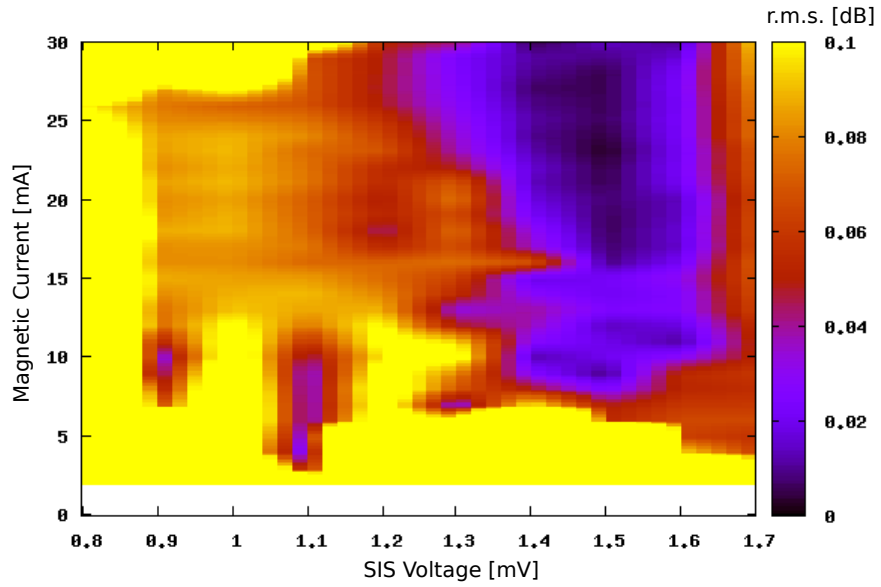

Figure 4.8: Relationship at mixer-1 between DSB noise temperature r.m.s. and parameters of 492 GHz

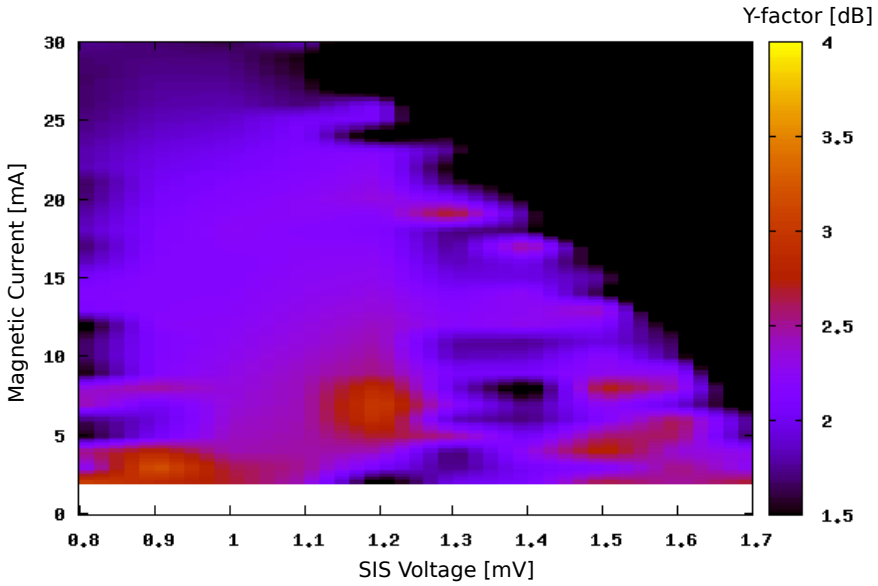

Figure 4.9: Relationship at mixer-2 between DSB noise temperature and parameters of 492 GHz

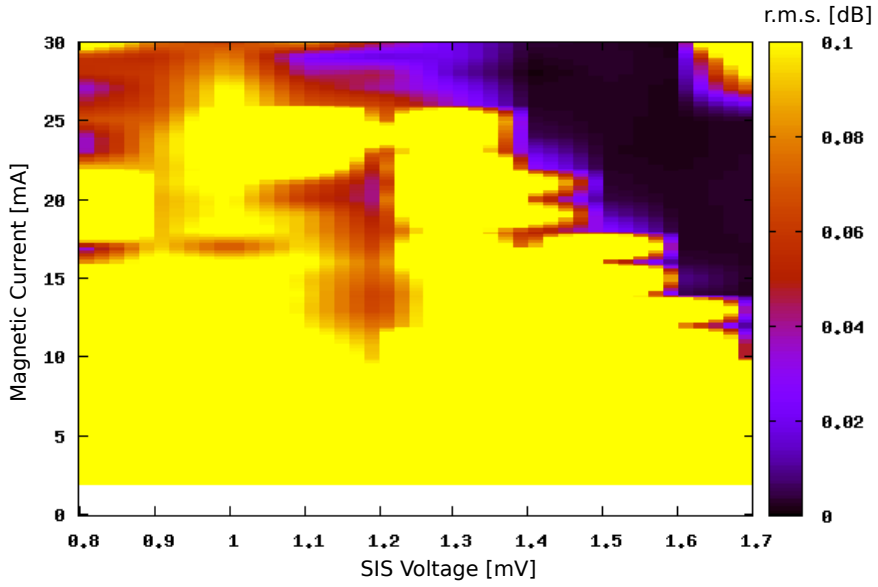

Figure 4.10: Relationship at mixer-2 between DSB noise temperature r.m.s. and parameters of 492 GHz

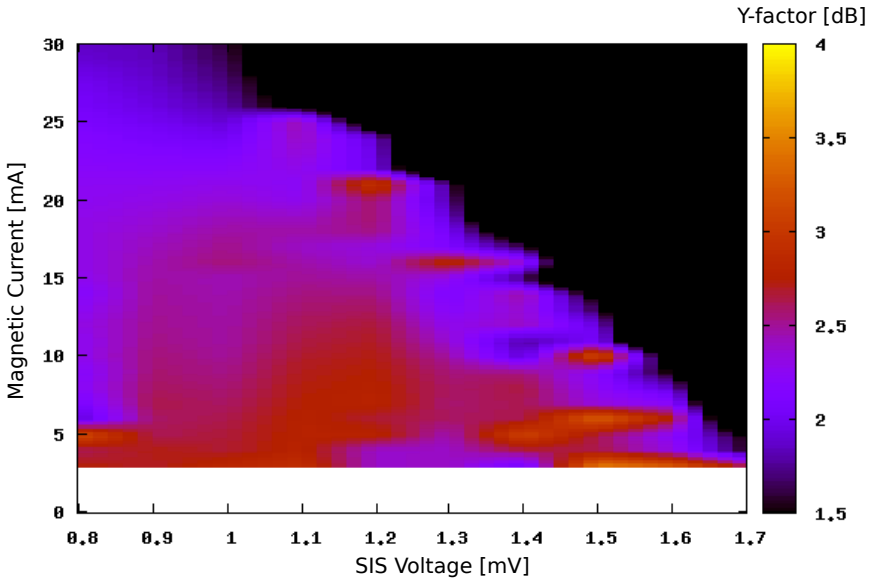

Figure 4.11: Relationship at mixer-1 between DSB noise temperature and parameters of 475 GHz

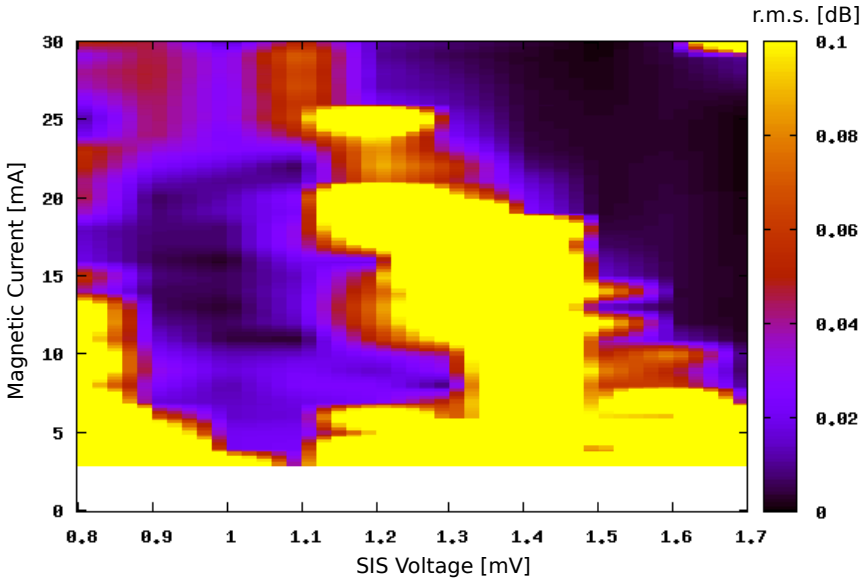

Figure 4.12: Relationship at mixer-1 between DSB noise temperature r.m.s. and parameters of 475 GHz

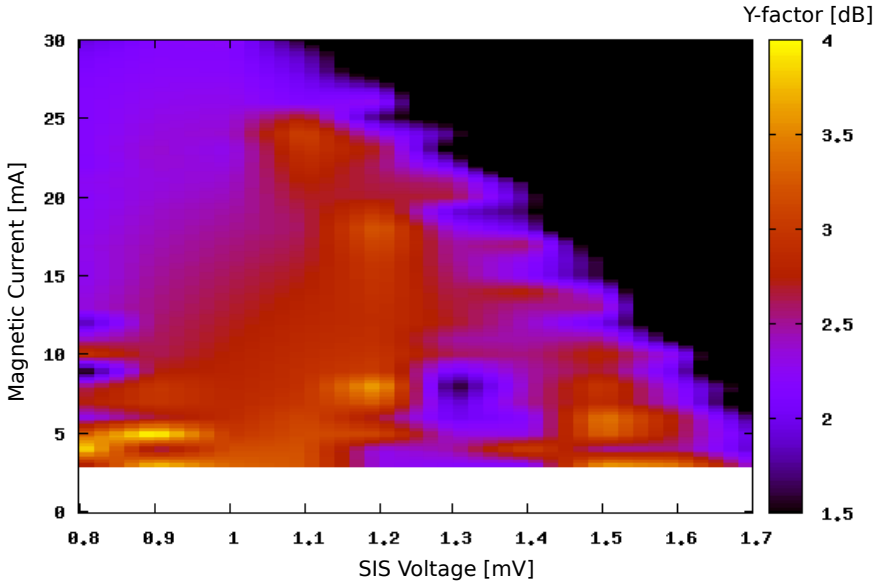

Figure 4.13: Relationship at mixer-2 between DSB noise temperature and parameters of 475 GHz

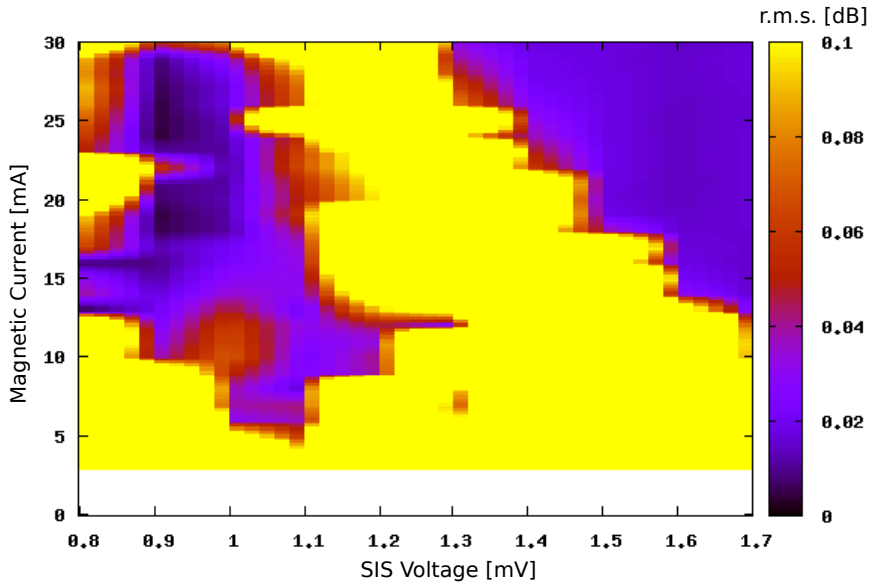

Figure 4.14: Relationship at mixer-2 between DSB noise temperature r.m.s. and parameters of 475 GHz

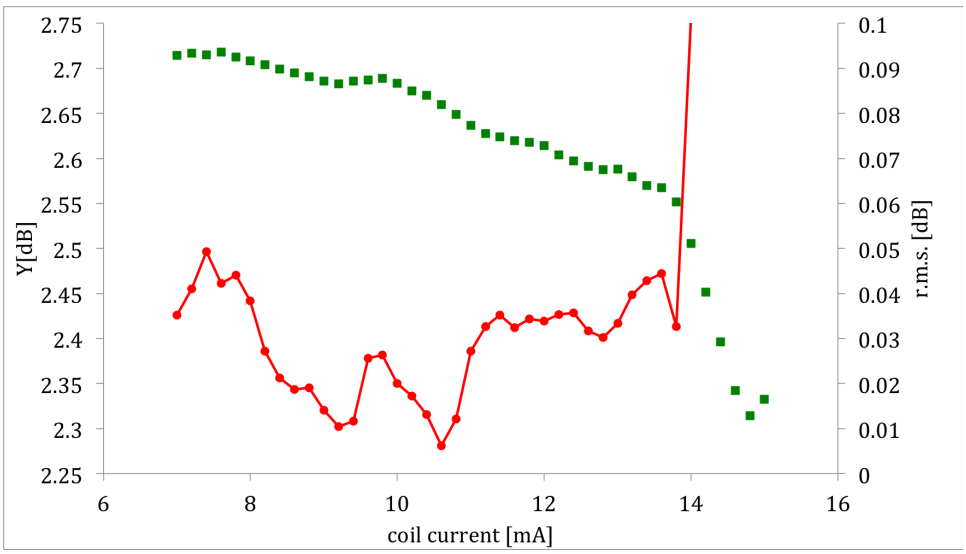

Figure 4.15: coil dependance of 461 GHz Y-factor and r.m.s. at mixer1

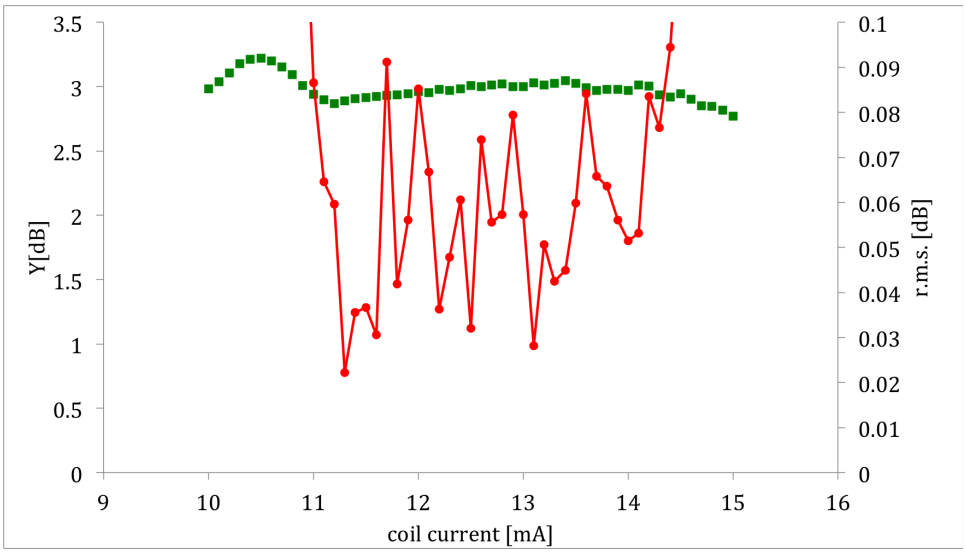

Figure 4.16: coil dependance of 461-GHz Y-factor and r.m.s. at mixer2

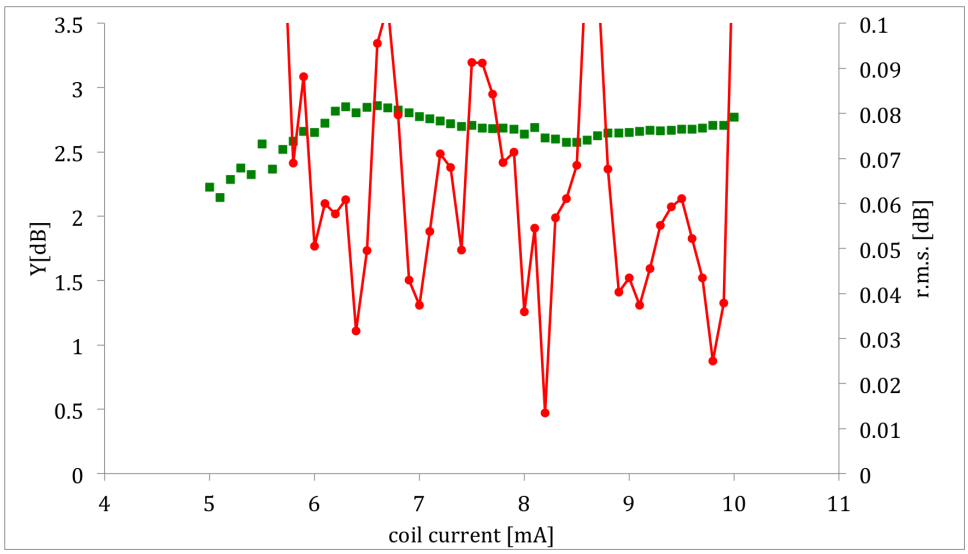

Figure 4.17: coil dependance of 492 GHz Y-factor and r.m.s. at mixer1

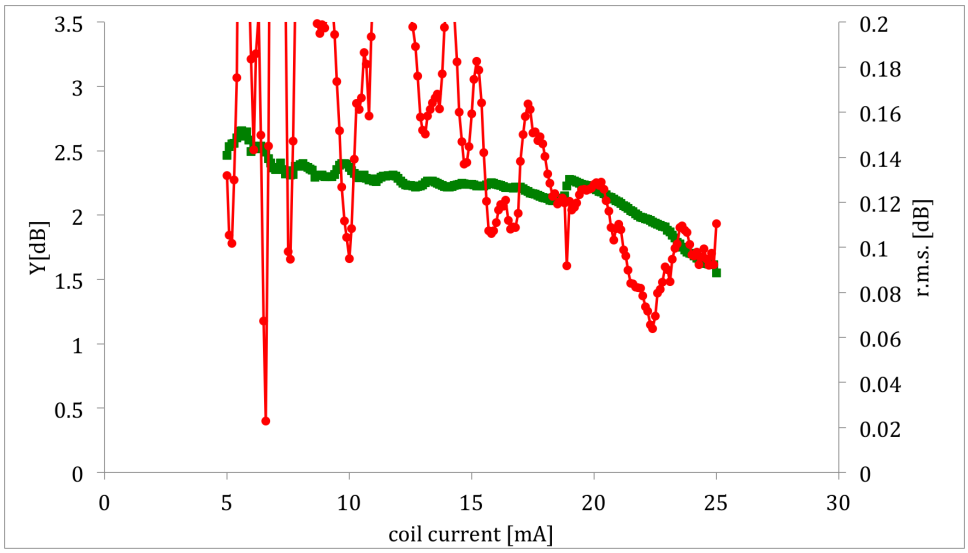

Figure 4.18: coil dependance of 492 GHz Y-factor and r.m.s. at mixer1

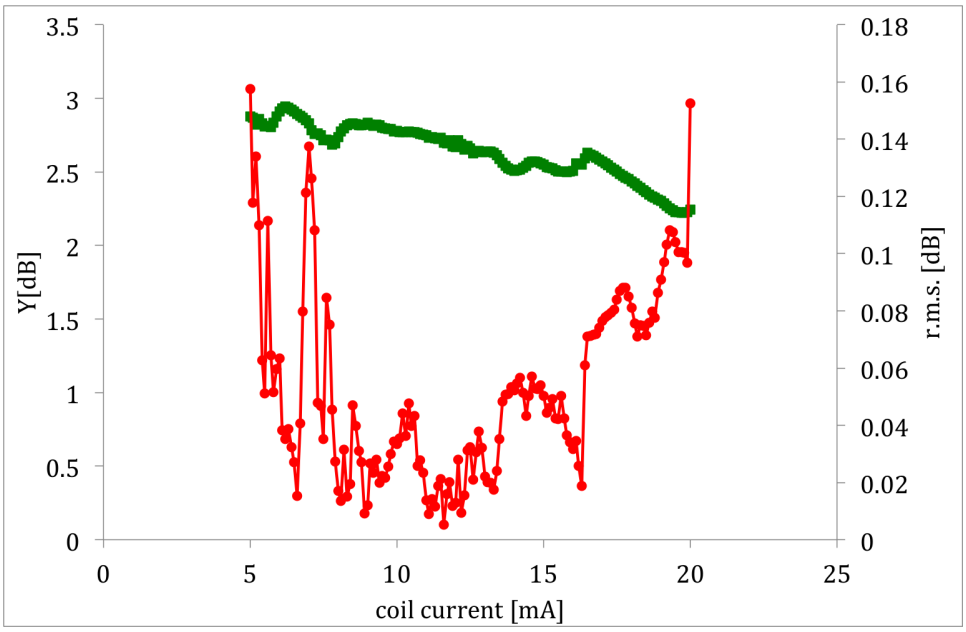

Figure 4.19: coil dependance of 475 GHz Y-factor and r.m.s. at mixer1

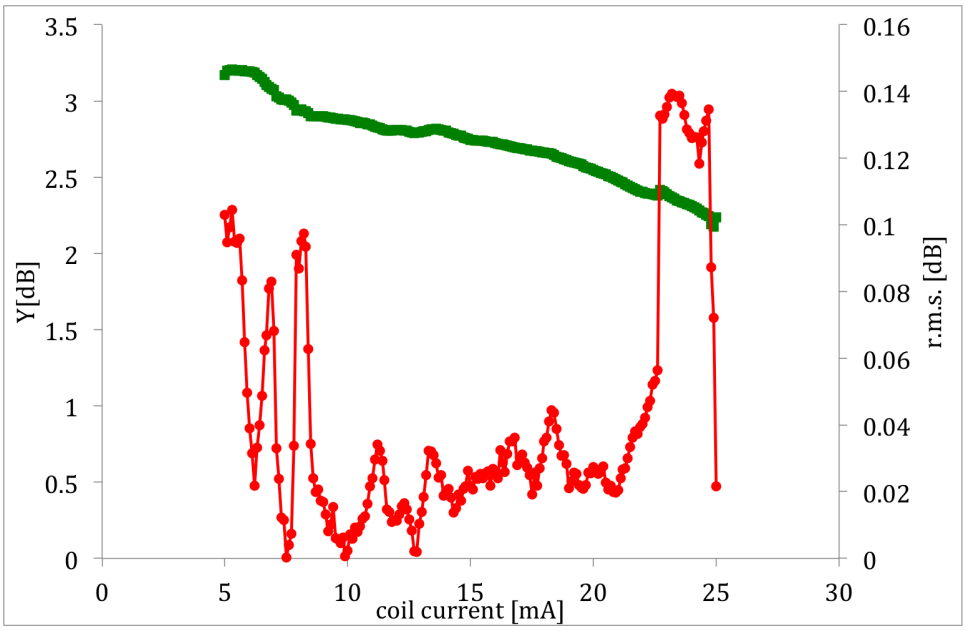

Figure 4.20: coil dependance of 475 GHz Y-factor and r.m.s. at mixer2

parameter using SSB noise temperature

As we described in the previous section, 2SB receiver has two mixer and standard adjustment is determine by DBS temperature. In this section, we advance new adjustment that considers couple of mixers and waveguide characteristics. This method is written as follow

1. Measure Y-factor when change SIS voltage and coil current independently at mixer1 when mixer2 is normal conducting stage.
2. Measure Y-factor when change coil current finely, SIS voltage is fix at mixer1.
3. Measure Y-factor when change SIS voltage and coil current independently at mixer2 when mixer1 is best parameter of DBS turning.
4. Measure Y-factor when change coil current finely, SIS voltage is fix at mixer2.
5. Measure Y-factor, IRR and Allan variance at SSB signal.

This method is adjust mixer2's parameters to mixer1 and parameters are selected to adjust SSB signal. Figure 4.21 is showed Y-factor and figure 4.22 is r.m.s. at SSB signal adjust mixer1 to mixer2. Same method is conducted at mixer1 to adjust mixer2.

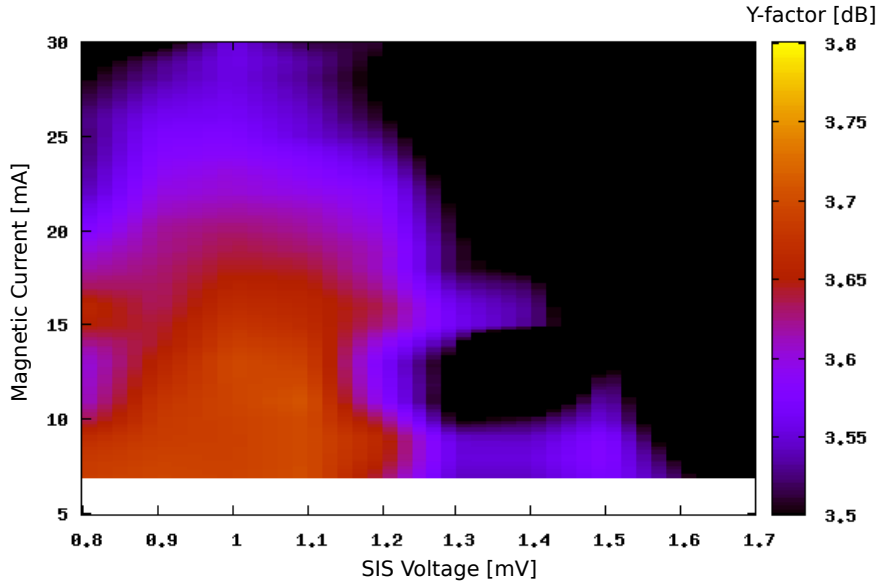

Figure 4.21: Relationship at mixer-1 between SSB noise temperature and parameters of 461 GHz

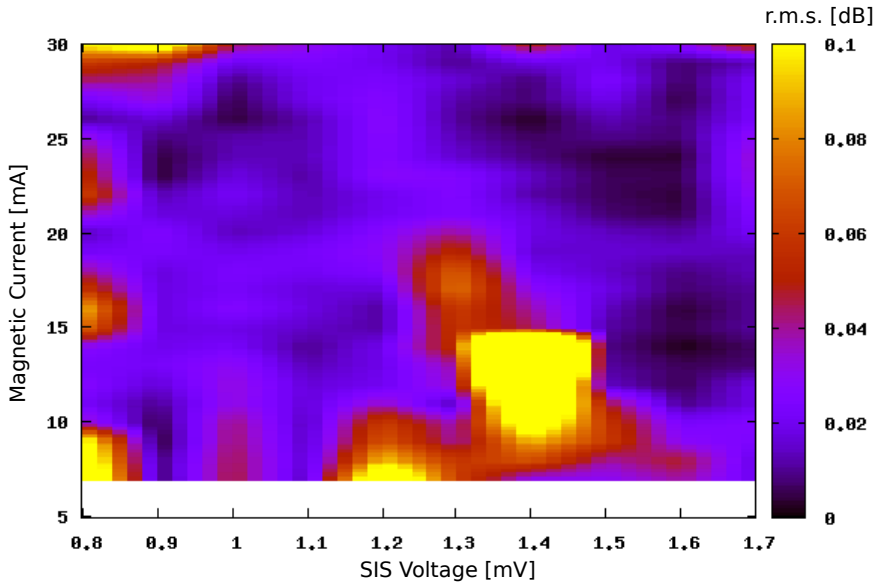

Figure 4.22: Relationship at mixer-1 between SSB noise temperature r.m.s. and parameters of 461 GHz

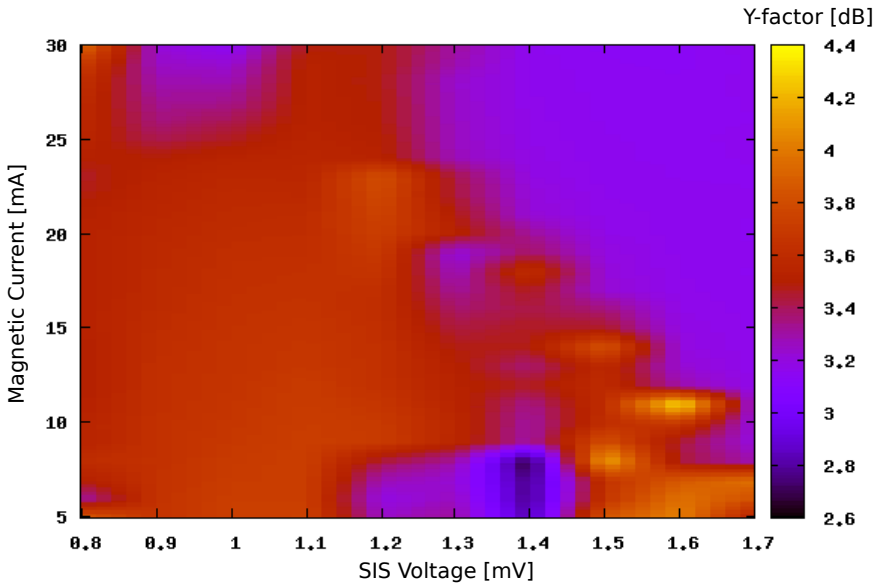

Figure 4.23: Relationship at mixer-2 between SSB noise temperature and parameters of 461 GHz

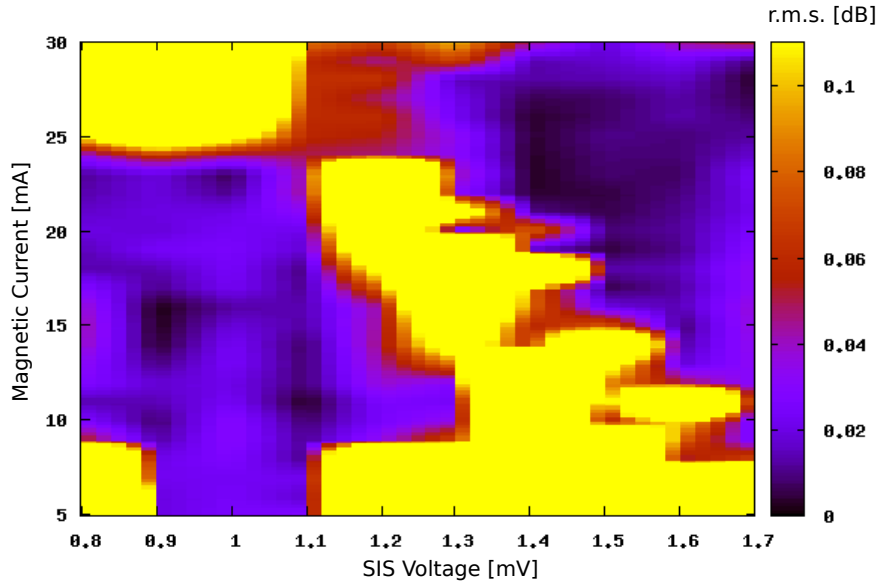

Figure 4.24: Relationship at mixer-1 between SSB noise temperature r.m.s. and parameters of 461 GHz

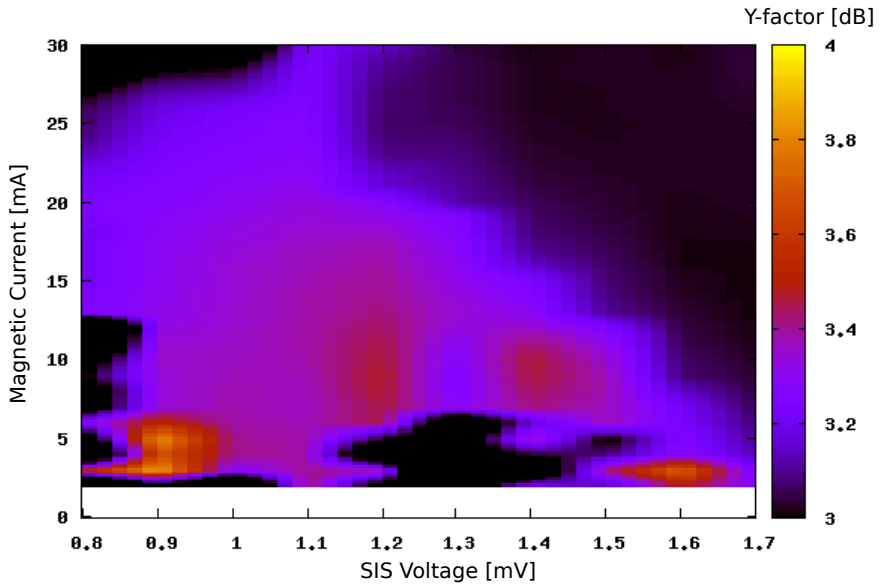

Figure 4.25: Relationship at mixer-1 between SSB noise temperature and parameters of 492 GHz

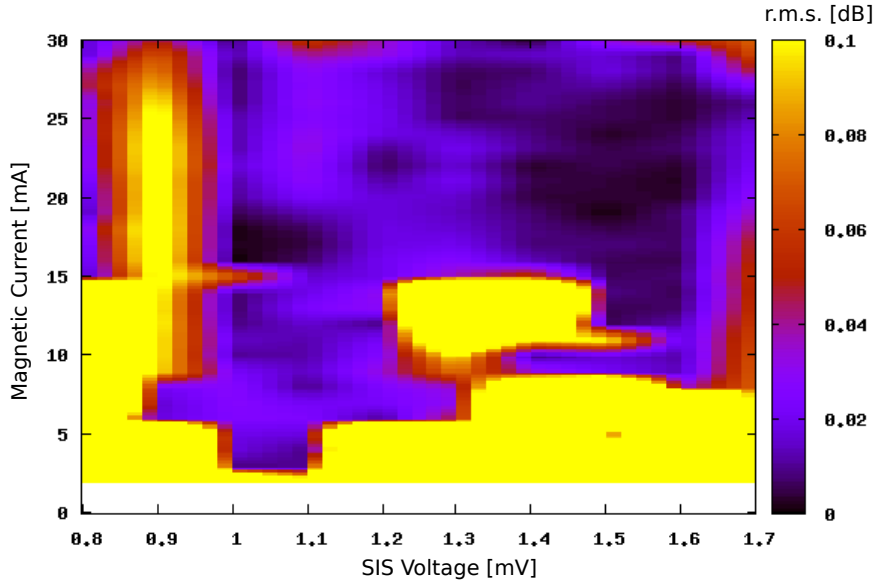

Figure 4.26: Relationship at mixer-1 between SSB noise temperature r.m.s. and parameters of 492 GHz

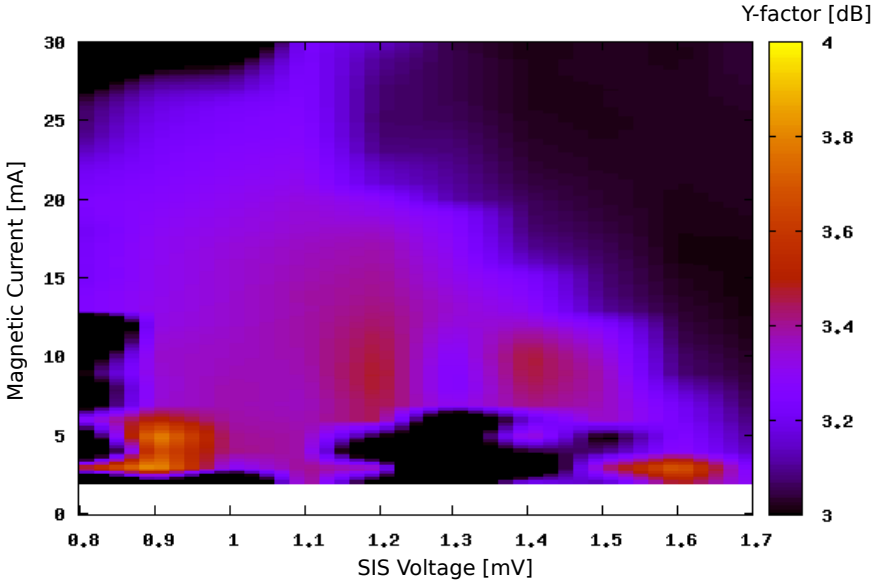

Figure 4.27: Relationship at mixer-2 between SSB noise temperature and parameters of 492 GHz

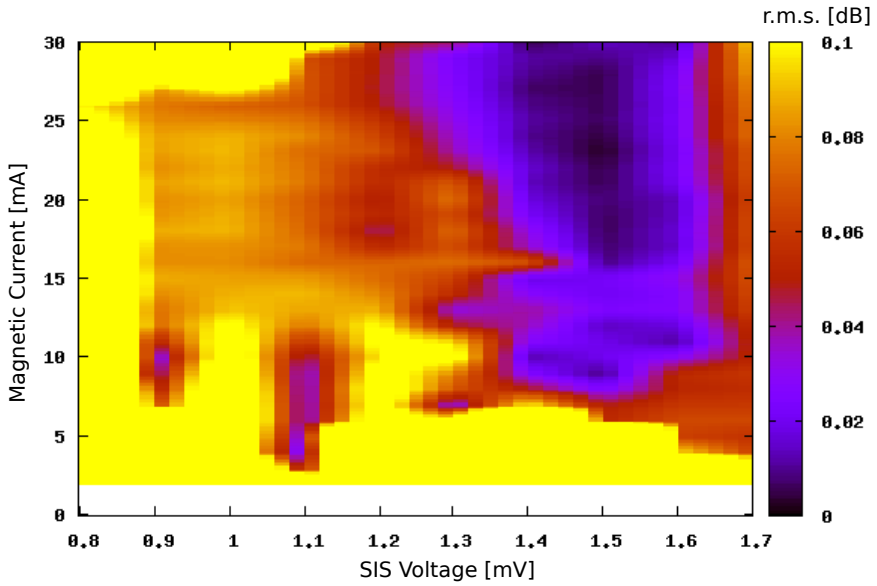

Figure 4.28: Relationship at mixer-2 between SSB noise temperature r.m.s. and parameters of 492 GHz

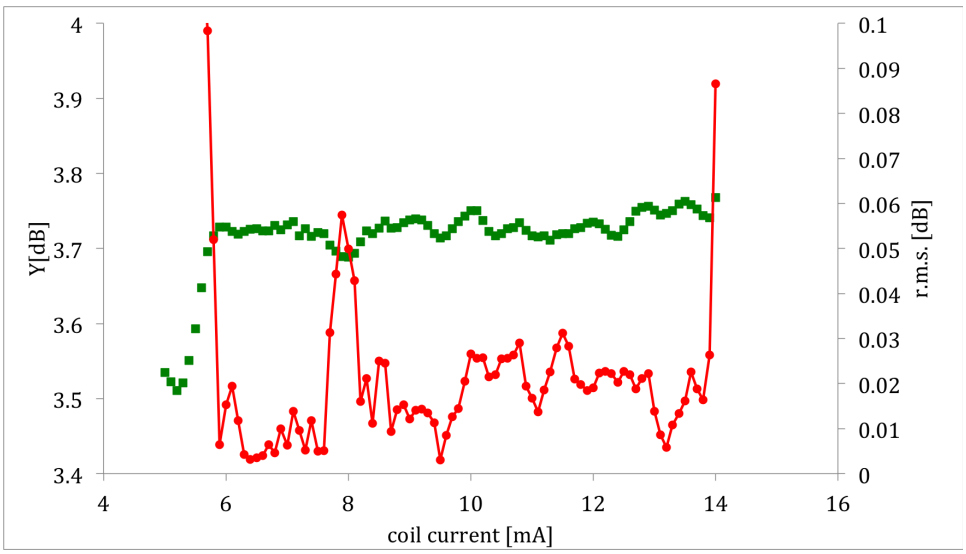

Figure 4.29: coil dependance of 461 GHz Y-factor and r.m.s. at mixer1

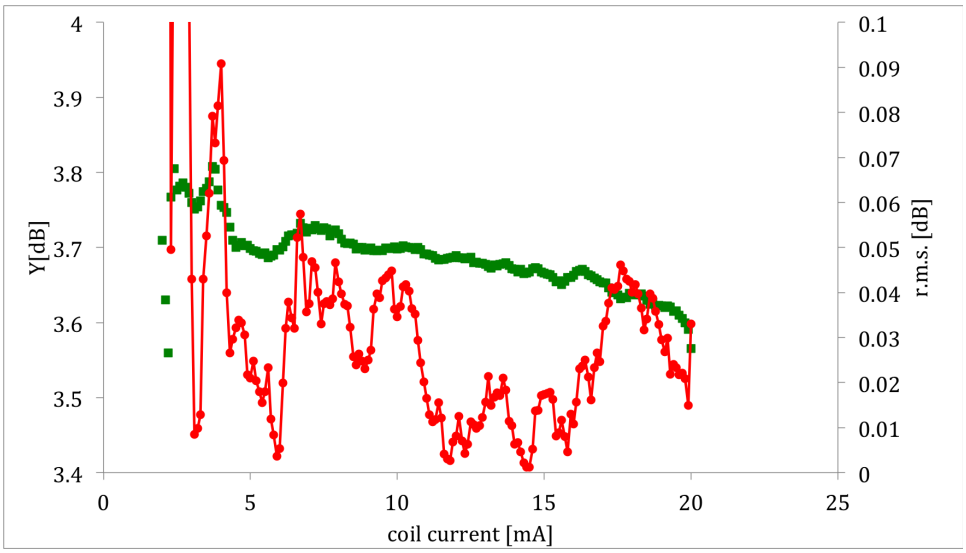

Figure 4.30: coil dependance of 461 GHz Y-factor and r.m.s. at mixer2

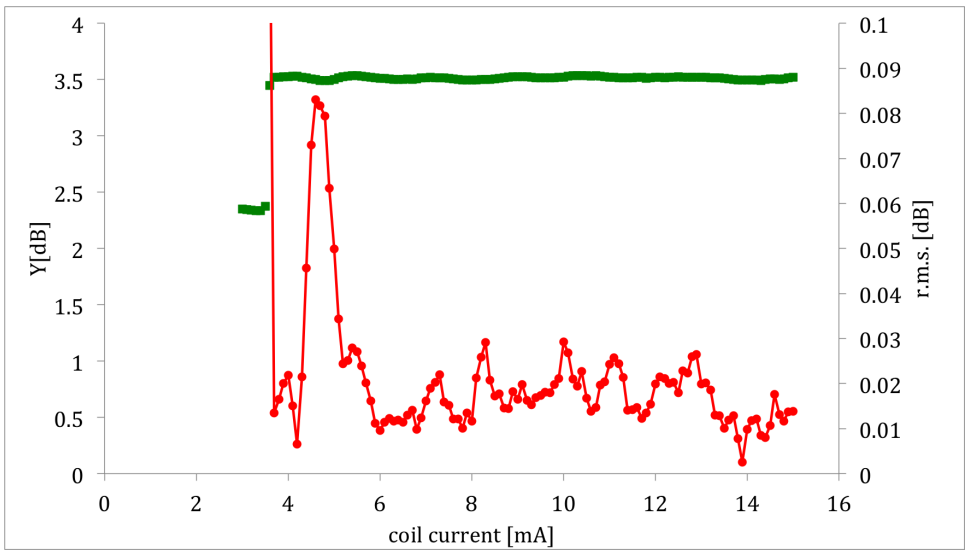

Figure 4.31: coil dependance of 492 GHz Y-factor and r.m.s. at mixer1

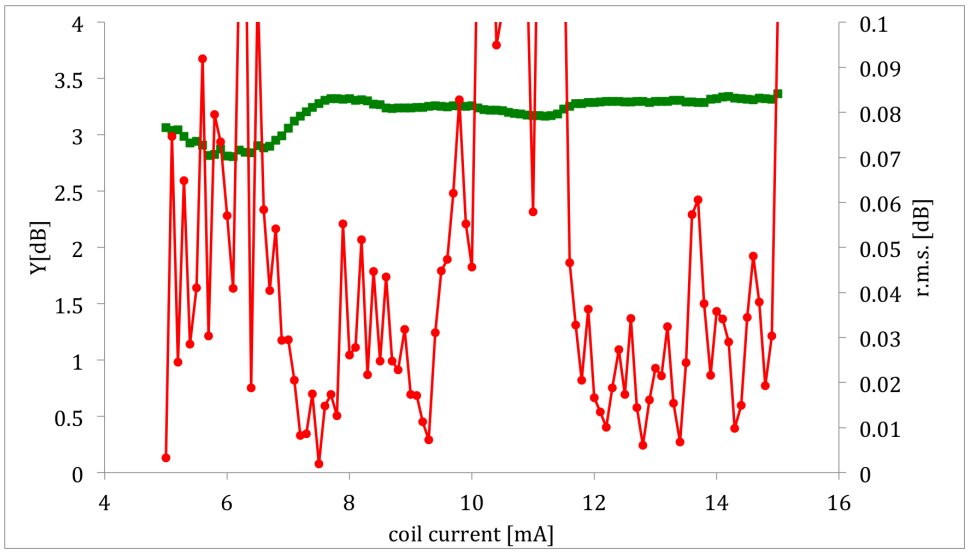

Figure 4.32: coil dependance of 492 GHz Y-factor and r.m.s. at mixer1

Table 4.2: Receiver parameter

parameter	V1 [mV]	V2 [mV]	I1[mA]	I2 [mA]
CO				
DSB turning	1.1	1.2	7.6	13.4
SSB turning for mixer2	1.1	1.28	7.6	13.4
SSB turning for mixer1	1.18	1.1	7.6	12.0
CI				
DSB turning	1.1	1.28	9.7	10.0
SSB turning for mixer2	1.1	1.28	10.5	10.0
SSB turning for mixer1	1.1	1.48	9.7	14.2
475 GHz				
DSB turning	1.2	1.18	9.4	9.9

4.4.3 Receiver performance

We measured receiver cooling temperature and performance at laboratory. At the observation state, we confirmed mixer temperature is 3.2 K. The receiver performance was checked with noise temperature, Image Rejection Ratio (IRR) and stability. Receiver noise temperature was measured Y-factor way at the front of the RF window. Figure 4.33 shows I-V curves of SIS mixer and noise temperature of 461 GHz at DSB. The blue line is SIS current without local signal, red line is SIS current with local signal and green line is showed noise temperature.

Image Rejection Ratio

Sideband separate (2SB) receiver is able to observe SSB signal that individual LSB and USB signals at once. However, DBS signal is separated by difference of pass length and LSB signal is outputted at USB signal output port. The reason is phase error and difference of signal loss for two signals load. This signal leakage is block to estimate physical condition from signal intensity. Therefore, it is necessary signal leakage is enough less than main signal. This quantity is estimated by ratio of main signal to image signal. The ratio is called IRR and it is necessary to be over 14 dB.

We measured IRR of each frequencies at spectrometer by compared of signal output (A. R. Kerr (2001) and Nakajima et al. (2010)). The measurement system is showed figure (4.35) and input 500 GHz signal is proceed by Gunn oscillator, followed by few multiplier. Table 4.3 is showed IRR and there are good parameters that IRR is more than 14 dB

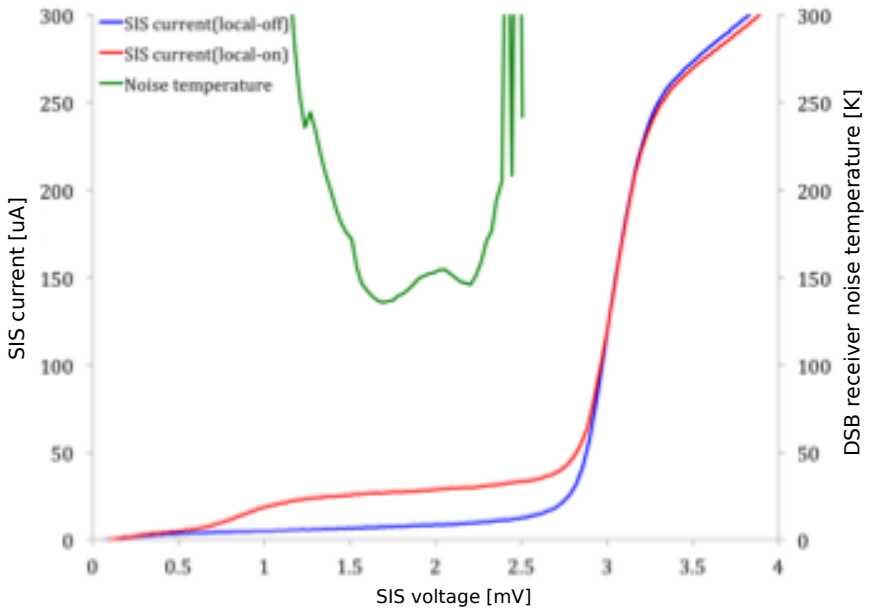

Figure 4.33: I-V curves and receiver noise temperature of DSB mixer in 461 GHz.

each frequencies.

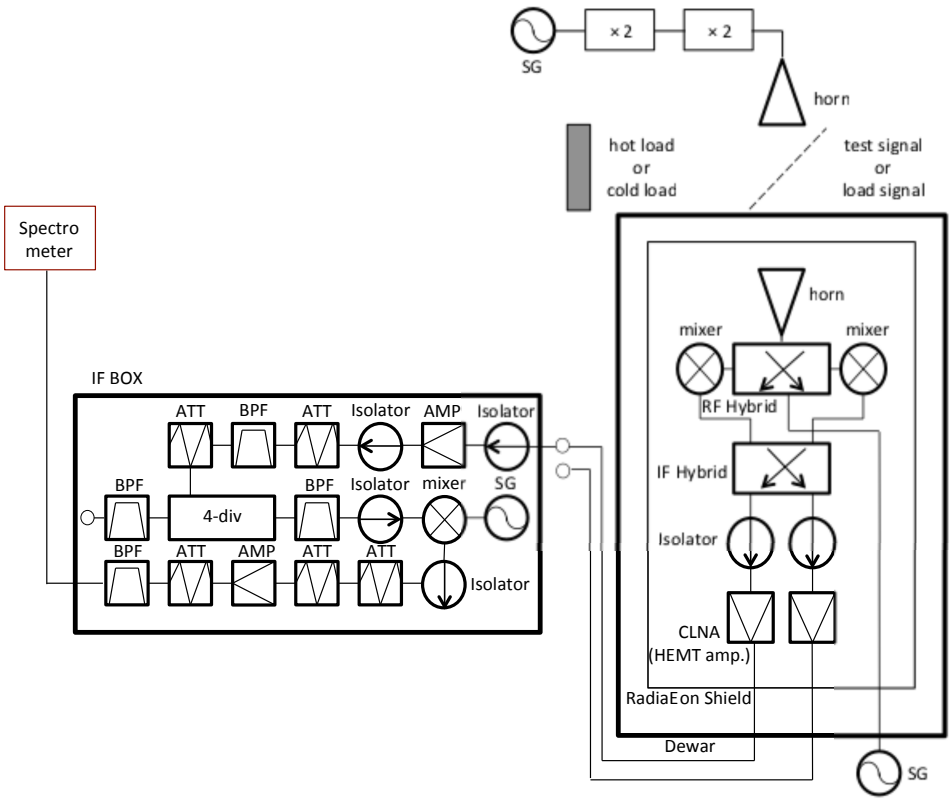

Figure 4.34: Block diagram of IRR measurement system

Table 4.3: Result of IIR

Turning	T_{RX} [K]	IRR [dB]	Allan variance [s]
461-GHz			
DSB turning	76.4± 0.1	16.1	126
SSB turning for mixer2	72.5±0.6	14.0	21
SSB turning for mixer1	65.6±0.1	17.3	126
475-GHz			
DSB turning	87.6±0.1	14.4	126
492-GHz			
DSB turning	82.8±0.8	15.7	100
SSB turning for mixer1	83.0±0.5	17.5	10
SSB turning for mixer2	100.6±2.1	17.3	40

The Allan-Variance

A stability of receiver is estimated by Allan variance. Measured signal is 1 GHz width and channel number is about 16000. We measured Allan variance of 461, 475 and 492 GHz at laboratory. Input signal is terminated signal by 300-K black body set at the front of cryostat 300 K window. Figure 4.36, 4.37 and 4.38 are showed Allan variance of 461-GHz each turning way and channel number are 2424, 3434, 4545, 5656, 6767, 7878, 8989, 9999, 11231,12145, 13451 and 14258. At 461 GHz, Allan variance of DSB turning and SSB turning for mixer2 are over 126 s. SSB turning for mixer1's τ is less than 80 s. At 492 GHz, the longest Allan variance is DSB turning and τ is 100-s. SSB turning way for mixer1's τ is 20 s and turning for miser2's is 40 s. 475 GHz Allan variance is only measured at DSB turning and τ is 126 s. Therefor, each frequencies have good parameters that Allan variance is over 100 s.

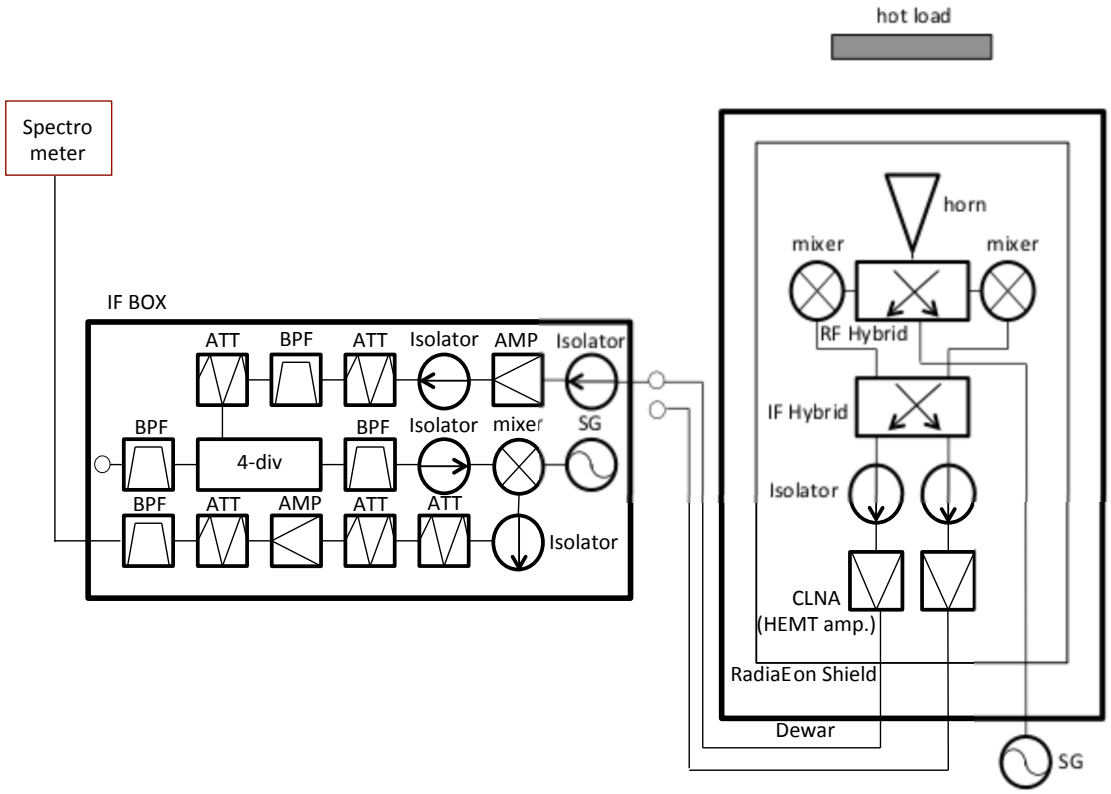

Figure 4.35: Block diagram of Allan variance measurement system

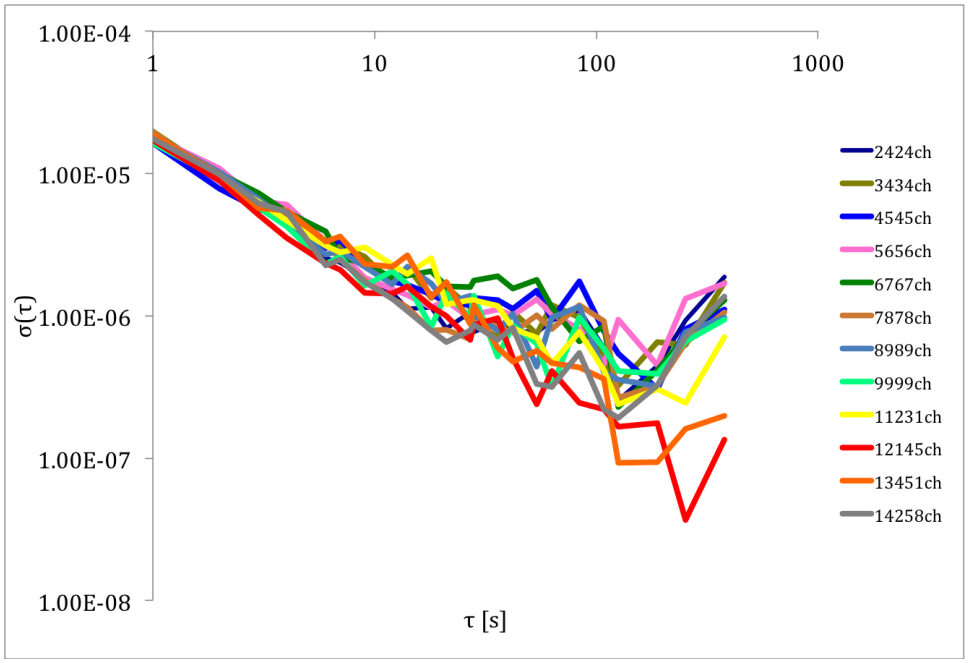

Figure 4.36: Allan-variance of 461 GHz DSB tuning way

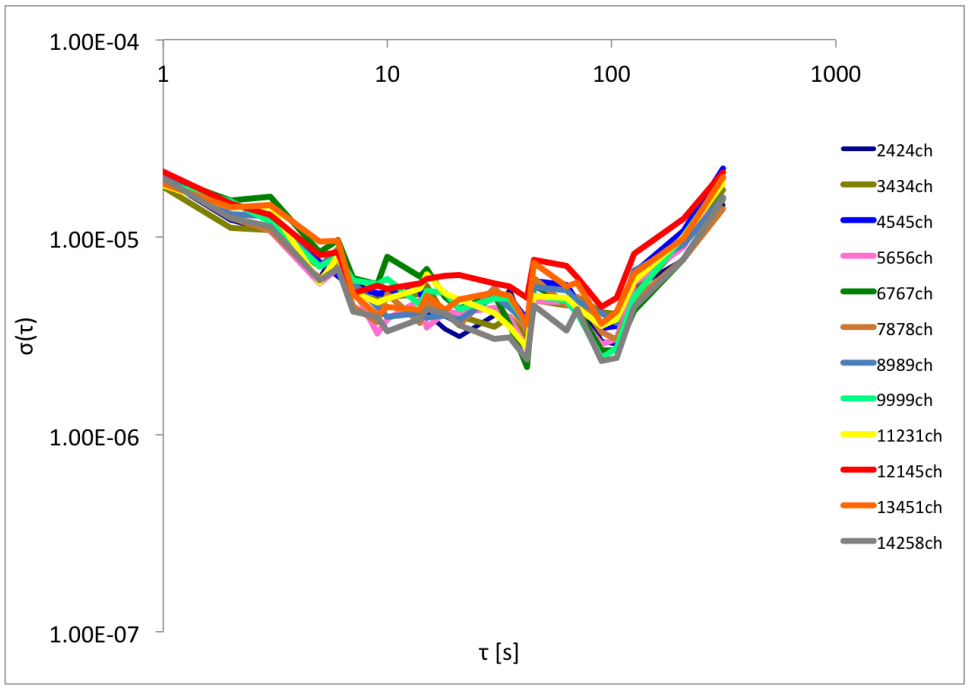

Figure 4.37: Allan-variance of 461 GHz SSB tuning way for mixer1

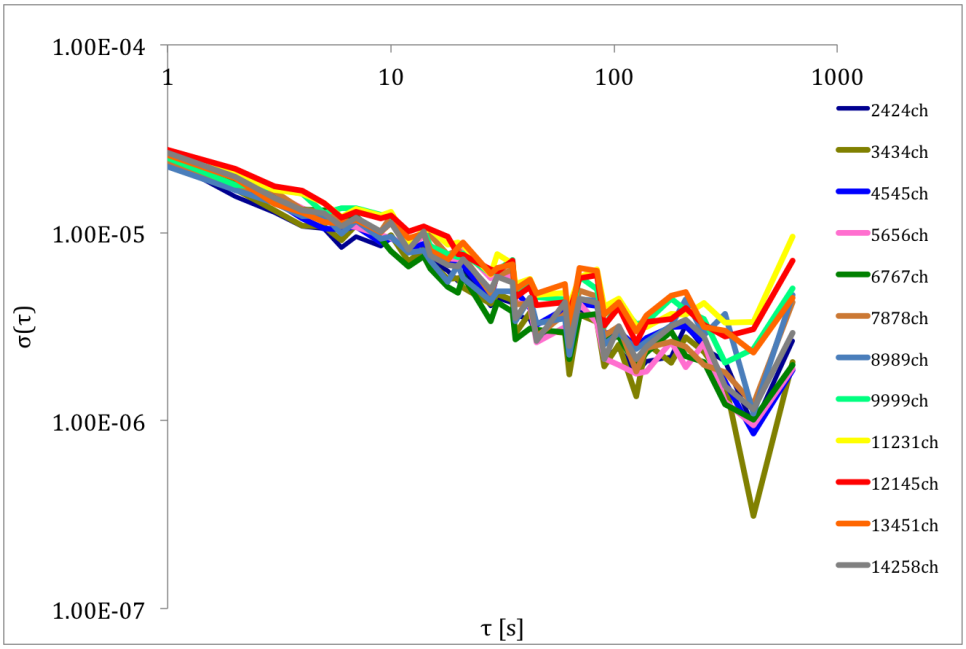

Figure 4.38: Allan-variance of 461 GHz SSB tuning way for mixer2

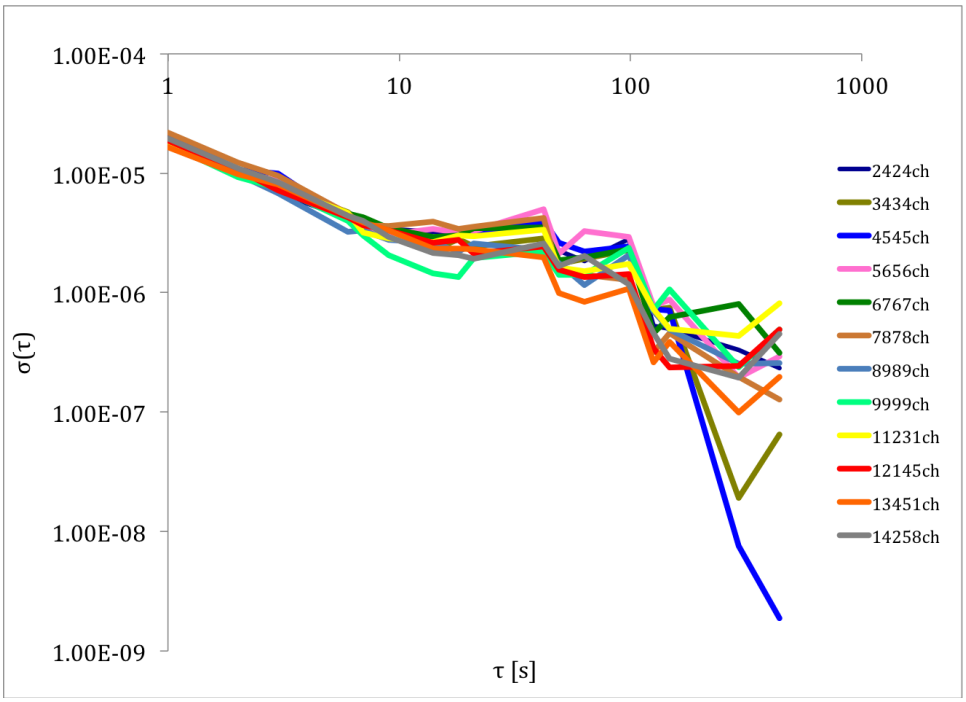

Figure 4.39: Allan-variance of 492 GHz DBS tuning way

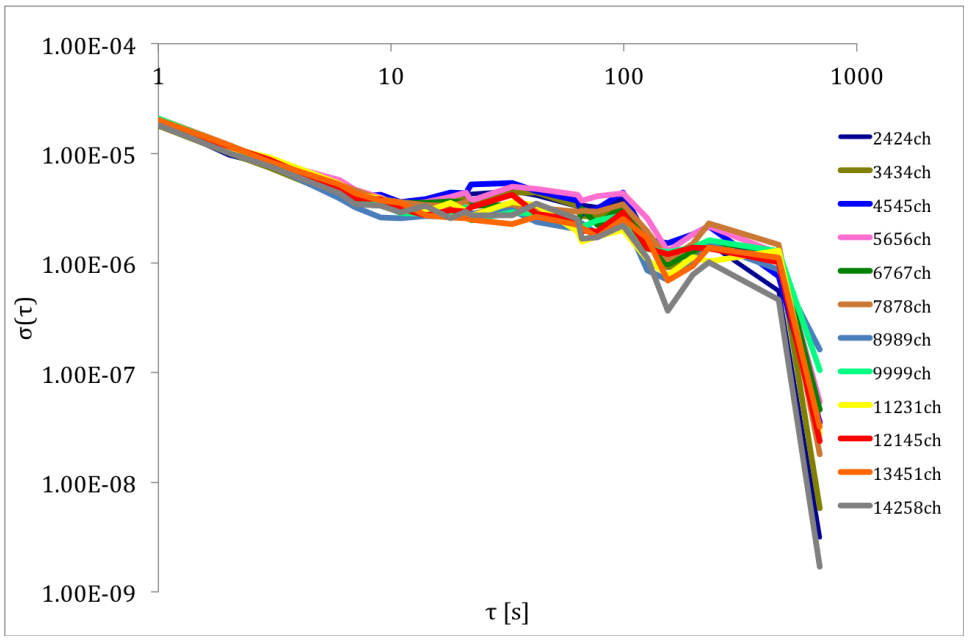

Figure 4.40: Allan-variance of 492 GHz SSB tuning way for mixer1

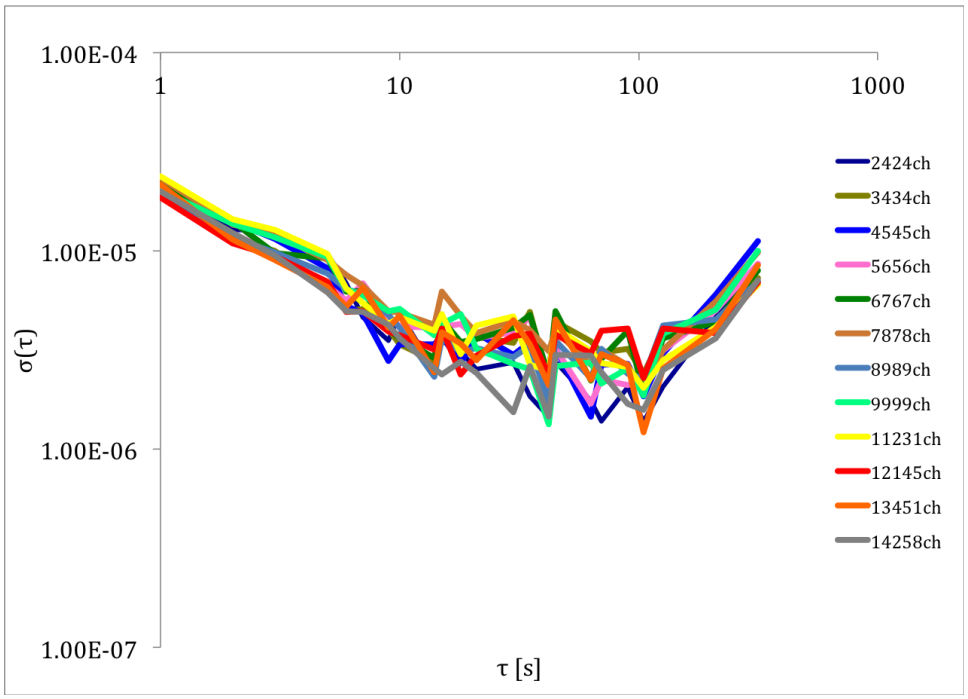

Figure 4.41: Allan-variance of 492 GHz SSB tuning way for mixer2

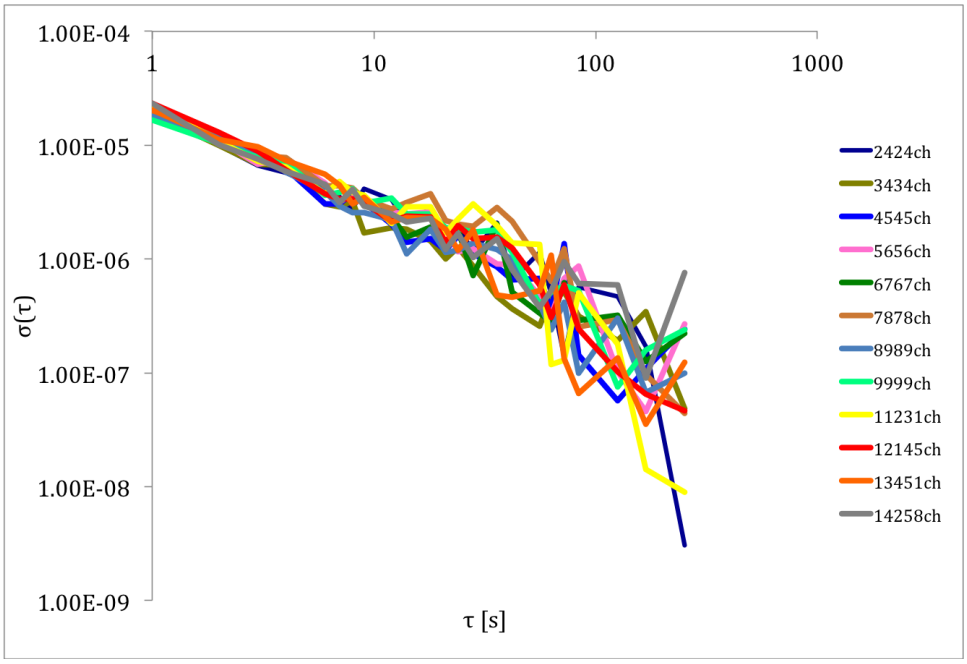

Figure 4.42: Allan-variance of 475 GHz DSB tuning way

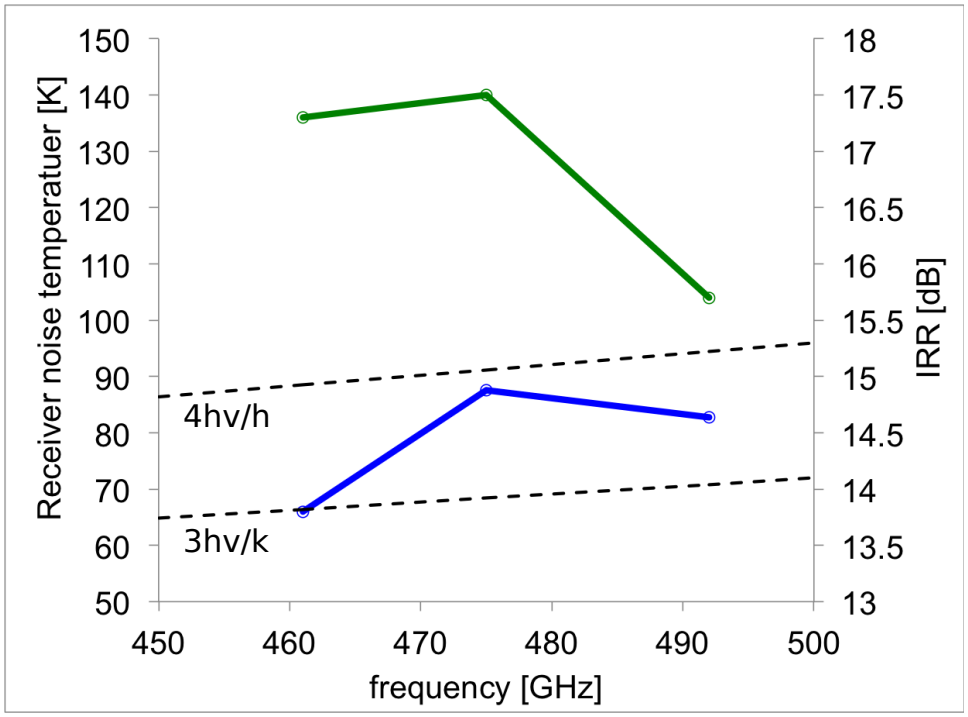

Figure 4.43: Trx and IRR of 461, 475 and 492 GHz. Blue line is T_{RX}, green line is IRR and two broken lines are quantum noise of few-times.

Conclution

We developed low thermal load cryo-receiver and low noise 500 GHz receiver. The receiver performance of 461, 475 and 492 GHz is showed in Figure 4.43. Both frequencies, receiver noise temperature are less than 4 times of quantum noise. In particular, noise temperature of 461 GHz is less than 3 times of quantum noise. These noise temperate are most low temperature at the world. Furthermore, IRR are more than 14 dB and Allan variance is more than 100 s at all frequencies. This receiver' performance is enough to observe at Antarctica.

5

Observation

5.1 Test observation

5.1.1 Performance

We had operated new 500G Hz receiver at the northern desert area of Chile where altitude is 4400-m and pressure is 600 hPa from September 2012 to November 2012. The lowest system noise temperate of 492 GHz was about 600 K.

Noise temperature

The receiver noise temperature was estimated from measurement of the atmospheric optical depth and the system noise temperature of 461 GHz and 492 GHz. The optical depth is measured by tapping way and measured points are $\sec$ z (z is angle between azimuth and zenith) from 1.0 to 3.0 per 0.1. When we measured system noise temperature, optical depths are $\tau_{461}\approx$0.67 and τ_{492} $\approx$0.76. This result are equal to data at lab each frequencies. The system noise temperature was 840 K for 461 GHz. We derive receiver noise temperature assuming loss in the optics of 0.61 dB and optical depth of 0.67.

Allan variance

We evaluated the Allan variance of the system to be over 60 seconds when input signal was terminated by ambient temperature black body.

Angular resolution

The angular resolution of the beam was measured by cross scanning of the Sun. The output power of IF frequency of 7.2 GHz is recorded while scanning the Sun. It fitting by Gaussian-shape beam. Figure 5.1 and 5.1 are showed the result of cross scanning of the Sun. The green cross is output power and red line is fitting line. The fitting law is written as

$$f(x) = a\frac{\left[elf\left(\frac{((x-c)+b)}{\sqrt{2\left(\frac{e}{2\times 1.1774}\right)^2}}\right) - elf\left(\frac{((x-c)-b)}{\sqrt{2\left(\frac{e}{2\times 1.1774}\right)^2}}\right)\right]}{2} + d \tag{5.1}$$

where a, b, c, d and e are variable number and e is HPBW.

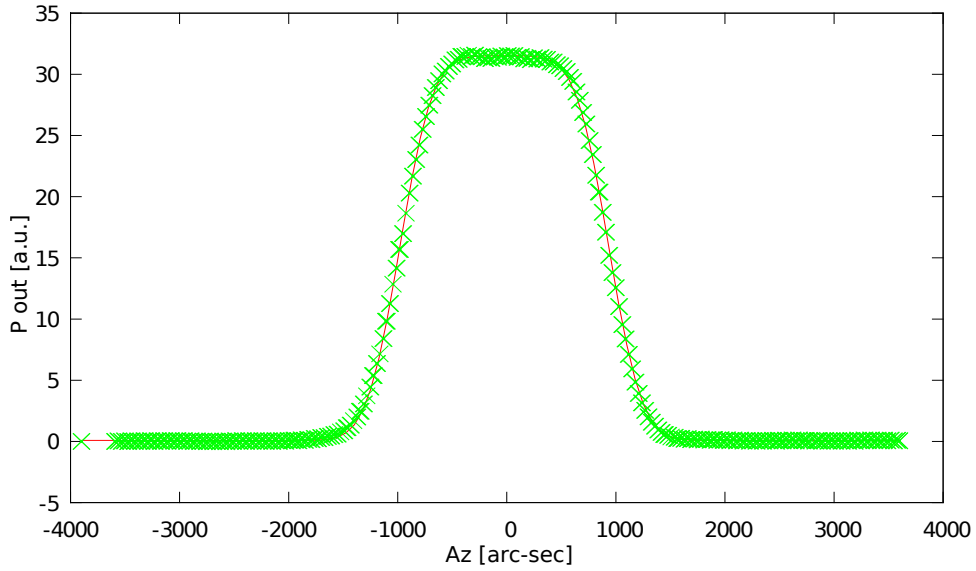

Figure 5.1: Total IF output power during a one-directional Azimuth scan of the Sun

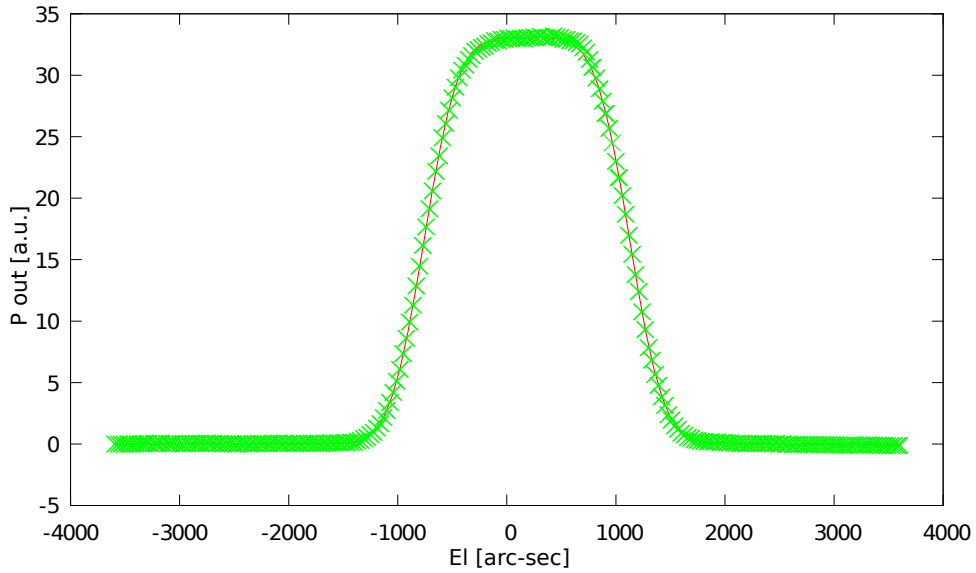

Figure 5.2: Total IF output power during a one-directional Elevation scan of the Sun

The half power beam width (HPBW) of the telescope at 461 GHz is calculated to be $9'.22 \pm 0.02$ at Azimuth and $9'.36 \pm 0.02$ at Elevation.

Beam efficiency

We conformed main-beam efficiency by compared to old 500 GHz receiver in 30-cm telescope. The main-beam efficiency of old 500 GHz receiver is estimated by the moon efficiency, η_{moon} that is measured as follows,

$$I_{30cm} = \frac{\int_{\Omega mb} P(\theta,\phi) d\Omega}{\int_{\Omega moon} P(\theta,\phi) d\Omega} = \frac{T_A^*}{T_S} \tag{5.2}$$

where $P(\theta,\phi)$ is the beam pattern of the telescope, T_A^* is the antenna temperature of the new moon, T_S is brightness temperature of the new moon. The aperture efficiency of new receiver is estimated by comparing T_a^* of Orion-KL with old one and corrected the difference. Therefore, aperture efficiency is calculated to be 85 $\pm$ 5 % of 461 GHz.

Pointing

The pointing was estimated by observation of bright stars taken by CCD camera, which on the 30-cm telescope. We repeated optical pointing four times and root mean squared error along azimuth and elevation were 0′.2 and 0′.1 respectively. Radio pointing was adjusted by observation of compact CO ($J = 4 - 3$) source which are Orion-KL, M17 and Carina molecular cloud. The radio pointing model should be expressed by following equation with six parameters that was propounded for 60-cm telescope Taku. NAKAJIMA & NOGUCHI (2007)

$$dAz = C_1 \sin(Az - El) + C_2 \cos(Az - El) + D_1 + E_1 \cos(El) - E_2 \sin(El) + \delta Az(sourece, t) \tag{5.3}$$

and

$$dEl = C_1 \sin(Az - El) - C_2 \cos(Az - El) + D_2 + E_1 \cos(El) + E_2 \sin(El) + \delta El(sourece, t) \tag{5.4}$$

Radio pointing accuracy's root mean squared error along azimuth and elevation were 1′.2 and 0′.8.

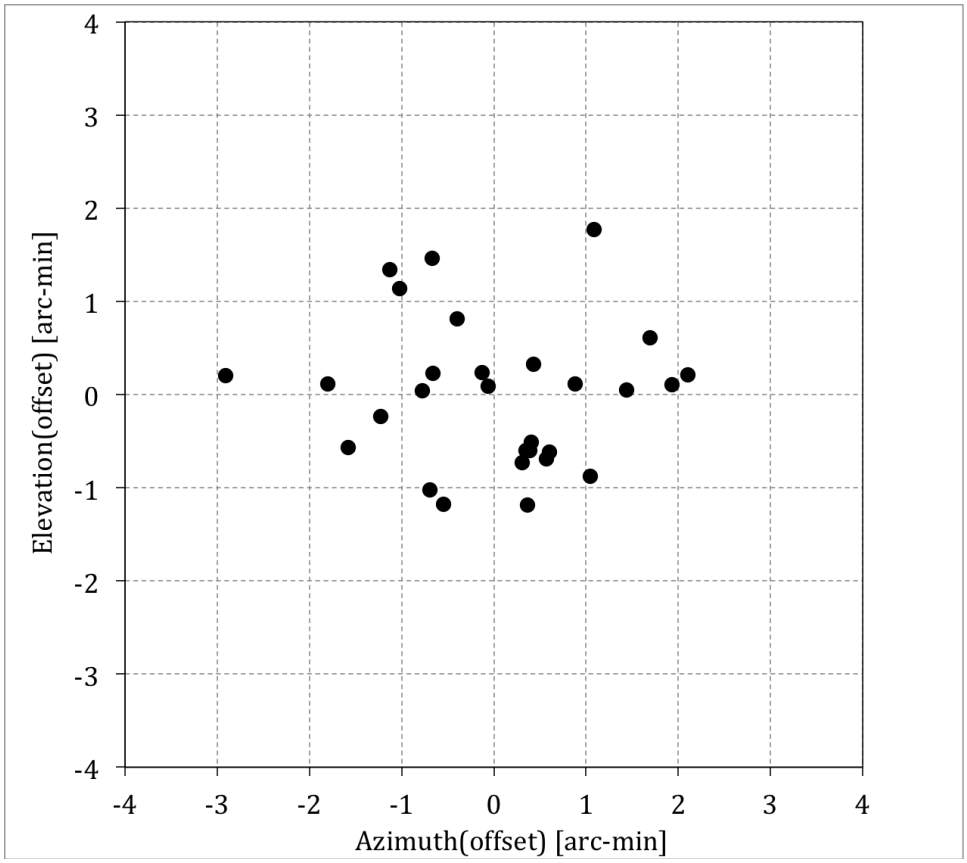

Figure 5.3: Scatter plots of the radio pointing residuals.

5.1.2 Observation

We observed the point α(1950) = $5^h32^m46^2.5$ and δ(1950)=$-5°24'14".0$ in CO and [CI] (figure 5.4 and 5.5). The peak temperature of CO is 26.1 $\pm$ 0.2 K and integrated intensity is 129.6 $\pm$ 0.2 K km s^{-1} with smoothed to 0.4 km s^{-1}. The peak velocity is 9.7 $\pm$ 0.4 km s^{-1} and velocity width at half power (FWHM) is 4.6 $\pm$ 0.4 km s^{-1}. The peak temperature of [CI] is 3.2 $\pm$ 0.2 K and integrated intensity is 12.4 $\pm$ 0.2 K km s^{-1} with smoothed to 0.4 km s^{-1}. The peak velocity is 8.9 $\pm$ 0.4 km s^{-1} and velocity width at half power (FWHM) is 3.7 $\pm$ 0.4 km s^{-1}. Figure (5.4) and (5.5) are showed spectrum of CO and CI toward Orion-KL.

After the first light in CO ($J = 4 - 3$) and CI ($^3P_1 -^3 P_0$) lines toward Orion-KL, we succeed in mapping Orion Molecular Cloud A in CI ($^3P_1 -^3 P_0$) line. The observation mode is position swatting mode with a 6′.5 grid spacing and total observation points are 138. The integration time is 50 s and typical r.m.s (root mean square) noise fluctuation

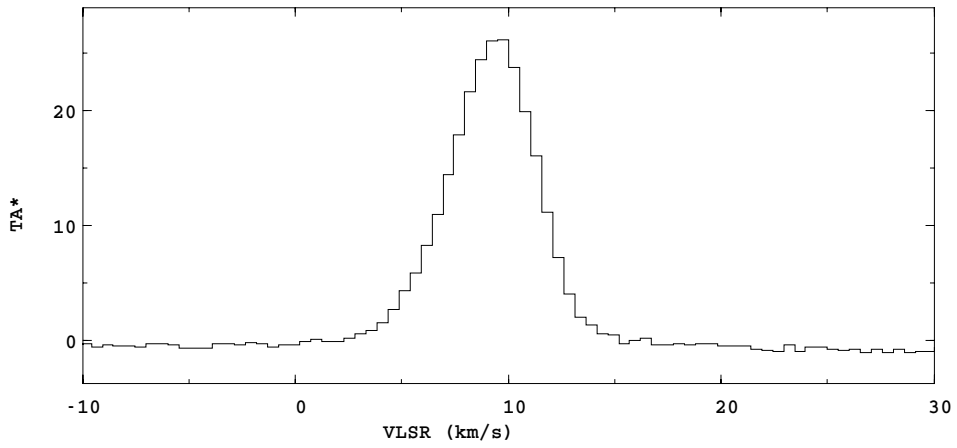

Figure 5.4: Spectrum of CO toward Orion-KL.

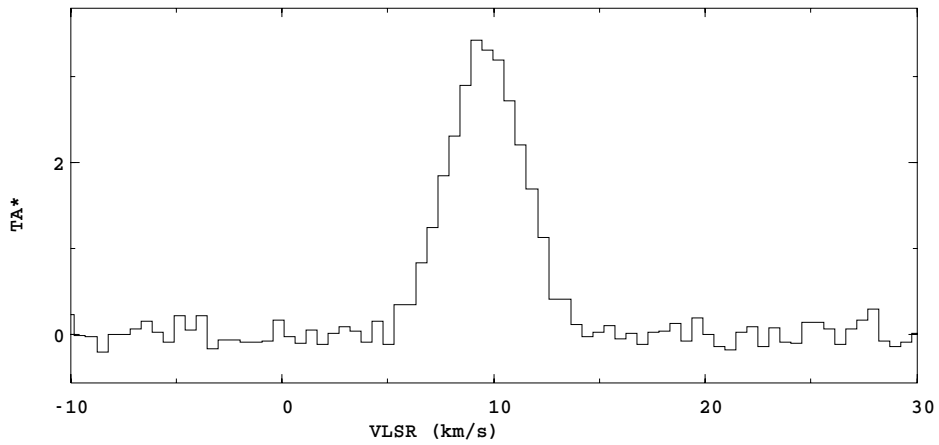

Figure 5.5: Spectrum of CI toward Orion-KL.

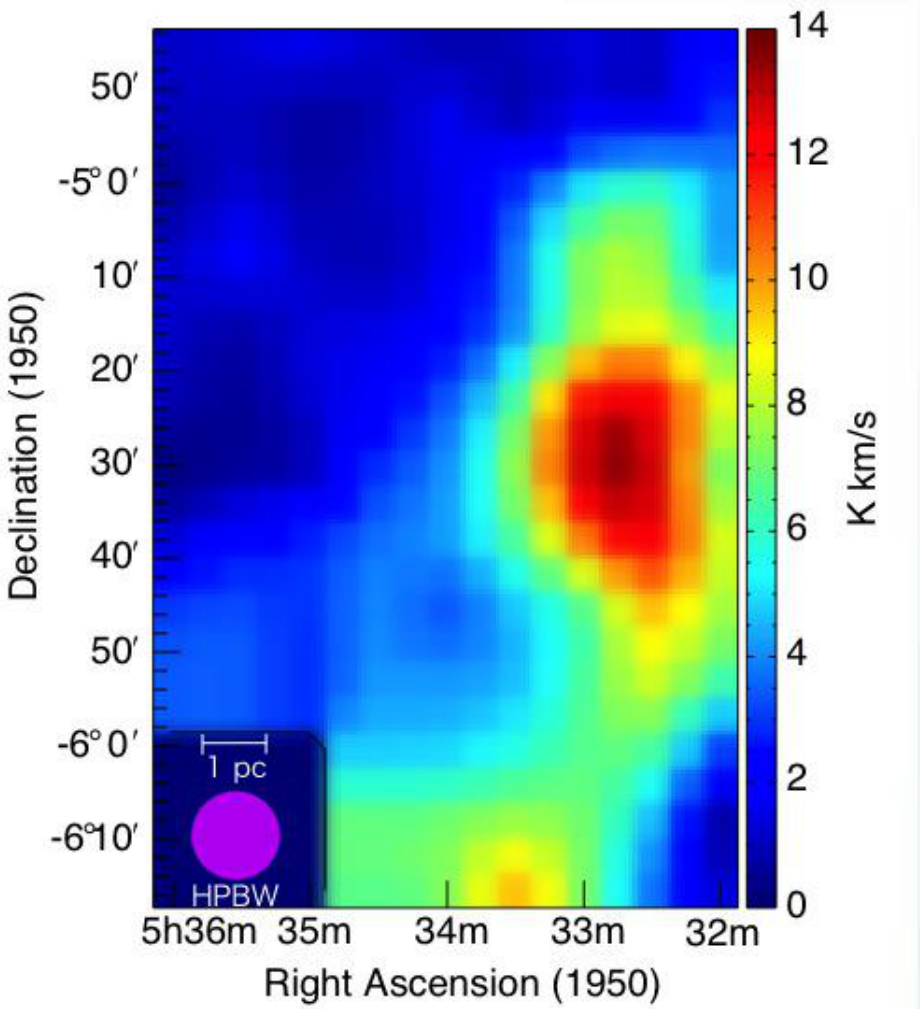

Figure 5.6: The map of [CI] at the Orion molecular cloud.

of 0.2 K were achieved at a velocity resolution of 0.67 km s^{-1}. Figure 5.6 is showed integration map of [CI] at Orion molecular cloud.

6

Summary

We have developed a low noise 500 GHz heterodyne receiver for antarctic telescopes. This receiver is designed to be installed in a transportable 30 cm submillimeter-wave telescope. It would be used as a receiver for a 10 m Terahertz Telescope. Results of this thesis are summarized as follows

1. The 500 GHz receiver was cooled down by a low cooling power GM-cooler that electric consumption is 1.2 kW. The new 500 GHz receiver uses sideband-separate (2SB) system that consists of are corrugate horn, RF hybrid, two DSB mixers, IF hybrid and two cryogenic IF amplifiers. This receiver observes 460-493 GHz and down-converted IF frequency is 4-8 GHz. The frequency resolution of the spectrometer is 61 kHz with 1 GHz band width centered at 7.2 GHz of the IF. The mixer unit and amplifiers are installed at 3 K stage connected by very short length cables to reduce signal loss between the mixer and amplifies. Capton film is used as a RF window of the cryostat. Local signal is transported by WR-6 type waveguide from cryostat bottom stage to the RF hybrid. Weight of this receiver is less than 30 kg and is handled by few person's hands in antarctica.

2. In design, total receiver noise temperature of 461 GHz is 70 K in SSB evaluated at input window of the cryo-receiver assuming loss in the window system of 0.63 dB, mixer unit noise of 30 K, loss in cable between the mixer conversion loss of 0.1 dB, between mixer and HEMT of 0.7 dB and HEMT noise of 7.4 K. This noise temperature is equal to three times of quantum noise limit.

3. In design, thermal load is 54 mW at 3 K stage and 1.3 W at radiation shield stage. It is crucial to reduce physical temperature of the mixer unit less than 3.5 K for realizing this low receiver noise temperature of 70 K. At IF cables and waveguide, we put thermal anchors on these from radiation shield stage to control thermal load to the mixer. We modeled thermal resistance of the waveguide and IF cables including thermal anchors and we selected the positions that thermal load is minimum to the mixer. The waveguide anchor reduced 1.8 K of mixer temperature and that corresponds to reduction of 100 K in receiver noise temperature. The multi layer insulator (MLI) is placed between the 60 K shielding and the inner surface of the cryostat that reduces the thermal load to the radiation shield stage. As the IR blocking filters, we selected Zitex G115 and inserted two filters under the windows. One

is placed at the 60 K radiation shield stage, and the other one is placed at the 200 K holder.

4. We succeeded in cooling down the SIS mixer to 3.2 K using the compact GM cooler. We checked cooling capacity of the cooler in advance by additional thermal load on the 3 K and the 60 K radiation shield stages. We derived a thermal load-temperature diagram from which we can estimate the thermal load form the measured temperature of the stages. We confirmed our designed thermal load for 3 K and 60 K radiation shield stage of 60 mW and 1.5 W respectively from measured temperature.

5. We evaluated receiver noise temperature, Image Rejection Ratio (IRR) and receiver stability by changing. Receiver parameters such as SIS voltage, intensity of magnetic field and intensity of local signal. We optimized receiver parameters for achieving lowest noise, receiver noise temperature in SSB at the front of RF window is less than 70 K and 90 K at 461 GHz and 492 GHz respectively. This result is most low receive noise temperature at all of the world's 500 GHz receiver. We conformed IRR is grater than 14 dB and receiver stability τ is longer than 100 s at spectrometer.

6. New 500 GHz receiver is installed on 30 cm telescope and conducted experimental operation at a site (4400 m altitude) in northern Chile from September 2012 to November 2012. We succeed in first light toward Orion-KL with ^{12}CO $(J = 4 - 3)$ and [CI] ($^3P_1 -^3 P_0$) lines. Receiver noise temperature is calculated from measured system noise temperature of 840 K assuming loss in the optics of 0.61 dB and measured optical depth 0.67 of at 461 GHz. It is equal to the result at laboratory. Angular resolution (HPBW) of the beam is estimated to be 9′.4 at 461 GHz by cross scanning of the Sun. Aperture efficiency is calculated to be 85 $\pm$ 5 % at 461-GHz by brightness temperature of Orion-KL. We succeed over 138 points mapping at Orion Molecular Cloud with CI ($^3P_1 -^3 P_0$) line. Receiver is operated for one month continuously.

A

The way to measure Image Rejection Ratio

Image rejection ratio(IRR) is one of the quantity to describe receiver performance at sideband separate receiver(2SB). This receiver is able to observe SSB signal that LSB signal and USB signal at one. RF signal is separated to control of signal phase with path length. Therefore, there is signal leaked leakage to the other output at real. To operate 2SB receiver, it is necessary signal leakage is few to describe physical quantity. It is used IRR to show signal ratio between image signal and real signal (Taku. NAKAJIMA & KAWABE (2008)).

The way to estimate IRR at laboratory is written following

$$R_1 = M_U \frac{M_L M_{DSB} - 1}{M_U - M_{DSB}} \tag{A.1}$$

and

$$R_2 = M_L \frac{M_U - M_{DSB}}{M_L M_{DSB} - 1} \tag{A.2}$$

where R_1 is IRR at USB signal, R_2 is IRR at LSB signal. M_{DSB} is

$$M_{DSB} = \frac{\Delta P_1}{\Delta P_2} \tag{A.3}$$

where $\Delta P11$ is Y-factor at USB and ΔP_2 is Y-factor at LSB. M_U is

$$M_U = \frac{P_{1U}}{P_{2U}} \tag{A.4}$$

where P_{1U} is signal power at USB output with CW signal of USB frequency and P_{2U} is output power at LSB. M_L is

$$M_L = \frac{P_{2L}}{P_{1L}} \tag{A.5}$$

where P_{2L} is signal power at LSB output with CW signal of LSB frequency and P_{1L} is output power at USB.

B

Fundamental of down convert at mixer

In this captor, we explain the fundamental of down convert at mixer like SIS mixer. It called coherent receiver that receiver down converts RF frequency to few GHz frequency and typical observation way at radio telescope receiver. Mixer has characteristic of non-line shape attribute between current and voltage and down converts RF frequency. RF signal and local signal are determined as $\sin$ wave and written by voltage, voltage at mixer is written as follow

$$V = V_{RF}\sin(\omega_{RF}t) + VLO\sin(\omega_{LO}t) \tag{B.1}$$

From the non-line shape attribute between current and voltage, output current is written as

$$\begin{aligned} I &= aV^2 \\ &= a(V_{RF}\sin(\omega_{RF}t) + VLO\sin(\omega_{LO}t))^2 \\ &= a(V_{RF}^2\sin^2(\omega_{RF}t) + 2V_{RF}V_{LO}\sin(\omega_{RF}t)\sin(\omega_{LO}t) + V_{LO}^2\sin^2(\omega_{LO}t)) \end{aligned} \tag{B.2}$$

The second section is written by addition theorem as

$$\begin{aligned} 2nd - section &= a2V_{RF}V_{LO}\sin(\omega_{RF}t)\sin(\omega_{LO}t) \\ &= a(V_{RF}V_{LO}\cos(\omega_{RF} - \omega_{LO})t - \cos(\omega_{RF} + \omega_{LO})t) \\ &= a(V_{RF}V_{LO}\cos 2\pi(f_{RF} - f_{LO})t - \cos 2\pi(f_{RF} + f_{LO})t) \end{aligned} \tag{B.3}$$

And first section is written as

$$\begin{aligned} f_{IF} &= |f_{RF} - F_{LO}| \\ &= \pm(f_{RF} - F_{LO}) \\ f_{RF} &= f_{LO} - f_{IF} \qquad \text{(B.4)} \\ f_{RF} &= f_{LO} + f_{IF} \qquad \text{(B.5)} \end{aligned}$$

where f_{IF} means IF frequency and f_{RF} has two areas that $f_{RF} = f_{LO} - f_{IF}$ is lower side band and $f_{RF} = f_{LO} + f_{IF}$ is upper side band. Of course, there are another frequencies of down converted signal like $2f_{LO}$, $2f_{RF}$, f_{RF}+f_{LO} and others. The components of frequencies that we don't want to observe are cut by filters like isolator which is installed between mixer and HEMT at receiver.

C

Measurement Way of Atmospheric Transparency

The atmospheric transparency is explained in the framework of the radiative transfer and written as follow

$$T_{sky} = T_b \exp(-\tau) + T_{atm}[1 - \exp(-\tau)] \tag{C.1}$$

where T_{sky} is brightness temperature of the sky ,τ is the optical depth of the atmosphere, T_b is brightness temperature of object and T_{atm} is physical temperature of the atmosphere. The signal of the object is blinded by atmosphere and pulsed radiation from atmosphere.

When telescope observes the blank sky, T_b means the cosmic background radiation, T_b=2.7 K. Therefore, equation (C.1) is written as

$$T_{sky} \approx T_{atm}[1 - \exp(-\tau)] \tag{C.2}$$

The optical depth is depended on the path length of the atmosphere in the line of sight. When atmosphere is modeled as plane-parallel, the path length is written as follow

$$\tau(Z) = \tau_0 \sec Z \tag{C.3}$$

where τ_0 is optical depth of zenith and Z is zenith angle.

The input at each Z is given in the temperature as

$$T(Z) = T_{atm}[1 - \exp(-\tau_0 \sec Z)] + T_{RX} \tag{C.4}$$

where T_{RX} is the system noise temperature. And output power is

$$P(Z) = k_B B G T_{atm}[1 - \exp(-\tau_0 \sec Z)] + T_{RX} \tag{C.5}$$

where k_B is the Boltzmann's constant, B is the frequency bandwidth and G is the gain

of telescope. When the telescope is terminated by a load at load at ambient temperature T_{amb}, the output is

$$P_{ref} = k_B BGT_{atm}[T_{amb} + T_{RX}] \tag{C.6}$$

We assume T_{atm} is approximated as T_{amy} and calculate $P_{ref} - R(Z)$.

$$P_{ref} - P(Z) = k_B BGT_{amb} \exp(-\tau_0 \sec Z) \tag{C.7}$$

$$\ln[\mathrm{P_{ref}} - \mathrm{P(Z)}] = \ln[\mathrm{k_B BGT_{amb}}] - \tau_0 \sec \mathrm{Z} \tag{C.8}$$

Therefore, we are able to obtain the optical depth of the atmosphere by fitting of this eqation.

Bibliography

A. R. Kerr, S.-K. Pan, J. E. Effland. 2001, ALMA Memo 357

Burton. W. B., Gordon. M. A.. 1975, Bulletin of the American Astronomical Society, 7, 614

Cohen. R. S, Thaddeus. P. 1977, Astrophysical Journal, Part 2 - Letters to the Editor,, 217, 155

DAMA, T. M.., UNGRECHTS, H.., COHNE, R. S.., GEUS, E. J.., GRENIER, I. A.., J. WAY, D. C. MURPHY., NYMAN, L. A.., & THADDEUS, P.. 1987, THE ASTROPHYSICAL JOURNAL, 322, 706

Ishii, Shun., Seta, Masumichi., Nakai, Naomasa., Miyamoto, Yusuke., Nagai, Makoto., Maezawa, Hiroyuki., Nagasaki, Taketo., Miyagawa, Naoki., Motoyama, Hideaki., Sekimoto, Yutaro., & Bronfman, Leonardo. 2011, Terahertz Science and Technology, IEEE, 3, 15

Lamb, J. W.., Baryshev, A.., Carter, M. C.., D ' Addario, L. R.., Ellison, B. N.., Grammer, W.., Lazareff, B.., Sekimoto, Y.., & Tham, C. Y.. 2001, 1

Nakajima, Taku., Sakai, Takeshi., Kuno, Nario., & Ogawa, Hideo. 2010, Journal of Infrared, Millimeter, and Terahertz Waves, 31, 143

Pardo, J.R.., Serabyn, E.., & Cernicharo, J.. 2001, Journal of Quantitative Spectroscopy and Radiative Transfer, 68, 419

phillips, T. G.., Kwan, John., & Huggins, P. J.. 1980, International Astronomical Union, 21

R. Hohn, W. Ruehe., & Jewell, C.. 2004, AIP pulishing, 710, 505

R. R. Monje, V. Belitsky, V. Vassilev A. Pavolotsky I. Lapkin V. Desmaris D. Meledin D. Henke., & Dochev, D.. 2008, 19th International Symposium on Space Terahertz Tecnology

SATOU, Naohisa., SEKIMOTO, Yutaro., IIZUKA, Yoshizou., ITO, Tetsuya., SHAN, Wen-Lei., KAMBA, Toshiaki., KUMAGAI, Kazuyoshi., KAMIKURA, Mamoru., TOMIMURA, Yu., SERIZAWA, Yasutaka., ASAYAMA, Shin ' ichiro., & SUGIMOTO, Masahiro. 2008, Publ. Astron. Soc. Japan, 60, 1199

Scoville. N. Z, Solomon. O. M. 1975, Astrophysical Journal, 199, 105

Sozo YOKOGAWA, Yutaro SEKIMOTO, Masahiro SUGIMOTO Takeshi OKUDA Tomohiko SEKIGUCHI Toshiaki KAMBA Ken ' ichi TATEMATSU Tetsuo NISHINO Hideo OGAWA Kimihiro KIMURA Kazufusa NODA., & NARASAKI, Katsuhiro. 2003, PASJ, 55, 519

T. M. DAME, DAP. HARTMANN, P. THADDEUS. 2001, THE ASTROPHYSICAL JURNAL, 547, 792

Taku. NAKAJIMA, Masahiro. KAIDEN, Jun. KOROGI Kimihiro. KIMURA Yoshinori. YONEKURA Hideo. OGAWA Shingo NISHIMURA Kazuhito. DOBASHI Toshihiro. HANDA Kotaro. KOHNO Jun-Ichi. MORINO Shin'ichiro. ASAYAMA., & NOGUCHI, Takashi. 2007, Astronomical Society of Japan, 59, 1005

Taku. NAKAJIMA, Takeshi. SAKAI, Shin'ichiro. ASAYAMA Kimihiro. KIMURA Masayuki. KAWAMURA Yoshinori. YONEKURA Hideo. OGAWA Nario. KUNO Takashi NOGUCHI Masato. TSUBOI., & KAWABE, Ryohei.. 2008, Astronomical Society of Japan, 60, 435

Tatibana, F.. 1952, The Japan Society of Mechanical Engineers

Tomoharu Oka, Kazuhisa Kamegai, Masaaki Hayashida Makoto Nagai Masafumi Ikeda Nobuyuki Kuboi Kunihiko Tanaka Leonardo Bronfman., & Yamamoto, Satoshi. 2005, THE ASTROPHYSICAL JOURNAL, 623, 889

Tomoya, Hirota., Satoshi, Yamamoto., Yutaro, Sekimoto., Kotaro, Kohno., Naomasa, Nakai., & Ryohei, Kawabe. 1998, Publications of the Astronomical Society of Japan, 50, 155

Toshikazu ONISHI, Atsushi NISHIMURA, Yuya OTA Akio HASHIZUME Yoshiharu KOJIMA Akihito MINAMI Kazuki TOKUDA Shiori TOUGA Yasuhiro ABE Masahiro KAIDEN Kimihiro KIMURA Kazuyuki MURAOKA Hiroyuki MAEZAWA Hideo OGAWA Kazuhito DOBASHI Tomomi SHIMOIKURA Yoshinori YONEKURA Shin ' ichiro ASAYAMA Toshihiro HANDA Taku NAKAJIMA Takashi NOGUCHI., & KUNO, Nario. 2013, Astronomical Society of Japan, 65, 78

Tucker, John R.. 1985, Rev. Mod. Phys., 57, 1055

Wenlei Shan, Shinichiro Asayama, Mamoru Kamikura Takashi Noguchi Shengcai Shi., & Sekimoto, Yutaro. 2005, 16th International Symposium on Space Terahertz Technology